INVESTIGATING THE MAGNETIC SUCEPTIBILITY SIGNATURES OF A PARTIALLY REMEDIATED SITE CONTAMINATED BY GASOLINE IN ENID, OKLAHOMA.

By

DANIEL K. MORSE

Bachelor of Science in Geology

Oklahoma State University

Stillwater, Oklahoma

2011

Submitted to the Faculty of the
Graduate College of the
Oklahoma State University
in partial fulfillment of
the requirements for
the Degree of
MASTER OF SCIENCE
December, 2015

INVESTIGATING THE MAGNETIC SUCEPTIBILITY SIGNATURES OF A PARTIALLY REMEDIATED SITE CONTAMINATED BY GASOLINE IN ENID, OKLAHOMA.

Thesis Approved:

Dr. Estella Atekwana

Thesis Adviser

Dr. Todd Halihan

Committee Member

Dr. Jim Puckette

Committee Member

ACKNOWLEDGEMENTS

Special thanks to my advisor, Dr. Estella Atekwana, whose patience, funding, and insight allowed for this thesis's completion. To my committee members Dr. Todd Halihan and Dr. Jim Puckette, thank you for your mentoring, and technical contributions. Their help was pivotal to acquisition, interpretation, and correlation of data.

Thanks to Oklahoma State University's Boone Pickens School of Geology. Their facilities and instruments assisted greatly throughout this process.

I appreciate the Oklahoma Corporation Commission for allowing us to use their 8th and Broadway site in Enid, Oklahoma, and their employee, Margarita Mendivelso's contractor updates on this site.

A special thanks to all the others who assisted in my research, Dr. Eliot Atekwana, Dr. Gamal Abdel Aal, Dr. Farag Mewafy, Preston Baker, Kyle Spears, and especially Dr. Pride Abongwa for his guidance, knowledge, and friendship. Also for my encouraging cast of friends and family who have constantly hounded me throughout my extended experience here, Keith Rivera, Erin Roehrig, Morgan Ostroski, Jason Hanzel, my mother Jonnie Morse, Aunt and Uncle Toni and Jonny Payne, my intern mentors Christa Steeklenberg and Paul Griffith, and all of my other peers. Without these people contributing in their own way and driving me towards my goals I would not have been able to make it where I am today, for all of your help I am truly thankful.

Name: DANIEL MORSE

Date of Degree: December, 2015

Title of Study: INVESTIGATING THE MAGNETIC SUCEPTIBILITY SIGNATURES OF A PARTIALLY REMEDIATED SITE CONTAMINATED BY GASOLINE IN ENID, OKLAHOMA.

Major Field: GEOLOGY

Abstract:

Magnetic susceptibility measurements have been traditionally used in paleoclimate studies, as a tool for oil exploration, and for mapping heavy metal contaminated soils. Recently, it has been suggested that magnetic susceptibility can be used as a tool for investigating hydrocarbon contaminated sites where iron reduction is the dominant terminal electron process. Here the dominant magnetic mineral, typically magnetite forms as a secondary byproduct of iron reduction. Therefore magnetic susceptibility can be used as a proxy for assessing locations where iron reducing microbially mediated remediation is occurring. This study extends the work of previous authors and investigates the variability of magnetic susceptibility at a hydrocarbon contaminated site in Enid, OK. Here a leaky underground storage tank resulted in the release of gasoline into the subsurface aquifer. The objectives of this study are to: (1) investigate the relationship between magnetic susceptibility and the water table fluctuation zone and (2) determine the relationship between the magnetic susceptibility variation and the contaminant phase (free, dissolved, and vapor phase) distribution. Magnetic susceptibility and electrical resistivity were measured along 3 contaminated cores retrieved from the study site. In addition, magnetic susceptibility data were acquired down 20 boreholes within contaminated and uncontaminated locations. Water samples were also retrieved for geochemical analyses to test for the presence of terminal electron acceptors indicative of biodegration. Geochemical measurements suggest that nitrate and iron reduction was the dominant terminal electron acceptor process ongoing at the site. In addition, we observed that magnetic susceptibility measurements were elevated within contaminated areas; and highest within the water table fluctuation zone, with peaks associated with the highest water level tapering down across this zone. Unlike other studies, the magnetic susceptibility measurements were not directly correlative to plume thickness, but coincides with the steepest hydrologic gradients. This observation suggests that magnetite is favorably produced along steep hydrologic and redox gradients. We conclude that magnetic susceptibility is a viable geophysical tool for investigating hydrocarbon contaminated sites, especially where steep hydrologic and redox gradients exist.

TABLE OF CONTENTS

LIST OF TABLES

Table Page

LIST OF FIGURES

Figure Page

CHAPTER I

INTRODUCTION

Magnetic susceptibility (MS) is a physical property measurement of a substance and determines the substance's ability to be magnetized. Several minerals have varying MS as seen in Table 1. The mineral magnetite (Fe_3O_4) has one of the highest magnetic susceptibilities and is one of the most a common minerals in crustal rocks. Magnetite can be formed biotically by using iron as an electron acceptor in metabolic pathways, or abiotically through mineral precipitation as magnetite is particularly stable at typical surface conditions. Magnetic susceptibility has proven useful in a variety of different geologic investigations. Cioppa (1997) used magnetic measurements to illustrate changes in paleoclimate and erosional patterns. Magnetic signatures have also been observed to be associated with hydrocarbon migration within oil fields (Liu, et al., 2006). Additionally magnetic susceptibility has been used to monitor heavy metal contamination and aided in plume designation (Perez, et al., 2014).

Table 1. Magnetic Susceptibility of various minerals (Modified from Gibson, et al., 1998)

Type	Susceptibility Range (κ)	x10^4 SI average	Type	Susceptibility Range (κ)	x10^4 SI average
Graphite		-100	Siderite	100-310	
Quartz		-12	Pyrite	1256-5277	1366
Rock Salt		-12	Limonite		2764

Anhydrite		-12	Arsenopyrite		3016
Gypsum					
Calcite	-7 to -12	-12	Hematite	502-37699	6912
Coal		25	Chromite	3015 - 1 x 10^5	7540
Clays		251	Franklinite		4.5 x 10^5
Chalcopyrite		402	Pyrrhotite	1.2 x 10^3 to	1.5 x 10^6
				6.3 x 10^6	
Sphalerite		754	Ilmenite	2.5 x 10^5	
Cassiterite		1130		To 3.8 x 10^6	1.2 - 6.3 x 10^6
			Magnetite	1.2 x 10^6 to 2	6.3 x 10^6
				x 10^7	

Recently magnetic susceptibility has also been found useful in mapping hydrocarbon contamination due to magnetite formation during biodegradation. For example, at a former air force base in Hradcany, Czech Republic, Rijal et al. (2010) investigated magnetic susceptibility variations within sediments. In this study, the authors observed higher magnetic susceptibility values within the water table fluctuation zone (WTFZ). At this site air sparrging caused the water table to fluctuate approximately 1m. The highest measurements of MS were found at the top of the WTFZ and decreased towards the bottom. Furthermore these trends of higher readings were predominantly contained within the contamination plume. This suggests that the magnetite formed secondarily to contamination rather than being intrinsic to the local sediment.

In another study by Rijal et al. (2012) , hydrocarbon-contaminated site in Hänigsen, Germany was investigated to compare with their former findings. Here they again observed that higher MS readings were associated with the WTFZ within the contaminated area. However, there was a significantly higher magnetic response associated with the test area containing more

contaminants and higher total bioavailable iron content despite the fact that iron redox microorganisms were found throughout the test area. Temperature dependent MS, anhysteretic remnant magnetization and isothermal remnant magnetization revealed that magnetite was the dominant contributor to MS results. Following these measurements Rijal et al. (2012) concluded that magnetic susceptibility is a function of contamination concentration and available iron in the presence of appropriate iron metabolizing organisms that produces magnetite.

Mewafy et al. (2011) investigated a site in Bemidji, Minnesota, USA where an oil pipeline ruptured spilling over a million liters into the environment. The results were similar to those of Rijal et al. (2010, 2012); higher MS values were associated with the WTFZ within the confines of the contaminated soils, which were attributed to iron metabolizing organisms. Elevated MS was also observed within the vadose zone overlying the free-product plume. The elevated MS in the vadose zone was attributed to anaerobic/aerobic oxidation of methane linked to iron reduction resulting in the precipitation of magnetite. Mewafy et al. (2011) concluded that MS can be used as a proxy of intrinsic bioremediation of contaminants.

Atekwana et al. (2014) extended the Mewafy et al. (2011) study and investigated the variability of magnetic susceptibility at the Bemidji, Minnisota, USA site. They observed higher MS measurements within the WTFZ within the free-product zone. The magnitude of the MS decreased from the free product plume to the dissolved-product plume. X-Ray diffraction (XRD) and scanning electron microscope (SEM) analyses suggested that nano scale magnetite particles were responsible for the increased MS and that variable groundwater fluctuation, the state of the oil dissolved or free phase, and iron availability dictated the MS response pattern illustrated in Figure 1.

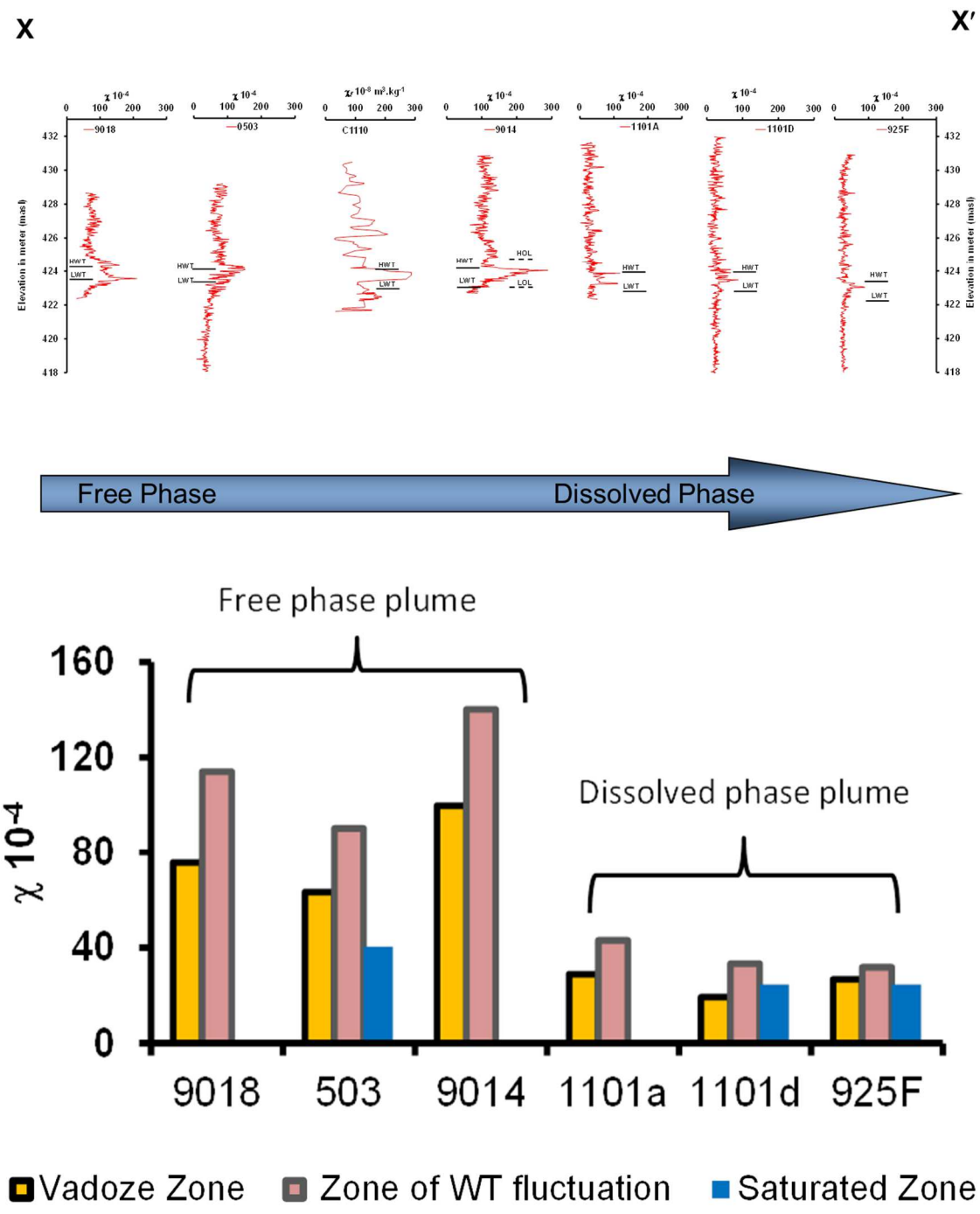

Figure 1. (Top) Variability of borehole magnetic susceptibility along the axis of a hydrocarbon contaminated plume. (Bottom) Variability in magnetic susceptibility in relation to different phases of oil. Modified from Atekwana et al. (2014).

Hypothesis

This study will test the hypothesis that elevated magnetic susceptibility occurs within the smear zone of hydrocarbon contaminated sites defined by the WTFZ.

The above sited studies suggest that MS in addition to other geophysical techniques has the potential to be used as a tool to not only delineate the contaminant plume but also as a proxy to iron reduction in the contaminated aquifer. Nonetheless apart from the above studies MS has not been widely applied at hydrocarbon impacted sites.

Objectives

This site represents a natural setting similar to previously mentioned hydrocarbon impacted sites where magnetic susceptibility has proven useful for delineating plume locations and remediation state (Rijal et al. 2010; 2012, Mewafy et al., 2011; and Atekwana et al., 2014). The objectives of this study are to (1) investigate the relationship between the intensity of magnetic susceptibility and the WTFZ at a hydrocarbon contaminated site and to (2) determine if magnetic susceptibility is limited to the source location or if it is

associated with the free product plume.

CHAPTER II

SITE HISTORY

The study site is an gasoline station in Enid, Oklahoma at the intersection of 8th and Broadway Street that has a leaky underground storage tank (LUST) (Figure 2). This location, which is cataloged as Environmental Protection Agency's (EPA) site 064-2182, provides an excellent natural laboratory to study the relationship between hydrocarbon contamination and MS variation. The underground storage tank found to be leaking gasoline into the subsurface was excavated 1996 to address the LUST, however hundreds of gallons of fuel had already percolated into the groundwater (McSorely, 2003). In 2002 the EPA had an air sparge remediation system installed on this site. This in situ system introduces air into the subsurface to assist natural biotic remediation. Air Sparging causes aqueous phase contaminants to become volatile and diffuse through the vadose zone. Studies documenting lithology, contamination, hydrology, and remediation at this site include Mc Phail (2003), McSorely (2003), Halihan et al. (2005), and Jefferies (2011).

The stratigraphy of the study site is described in Table 2 and includes 12.8 meters of soil and Quaternary alluvium that varies in total thickness by less than a meter across the suite. The unconsolidated alluvium overlies the Permian Hennessey Group bedrock, which acts as an aquitard (McPhail, 2003; McSorely, 2003). Unit A, which lies above the bedrock, is a sandy pebble section that fines upward ranging from 2.5-10.5 feet in thickness. A thin 50cm organic soil horizon containing grassy balls and roots was observed at ME-08's Unit A. The abrupt contact between Units A and B is marked by a gley unit. Unit B is made up of sandy clay that varies in

thickness from 29-34 feet. Gley formation is caused by interaction with the sandy clay and the water table. The extended amount of time this type of soil is saturated below the water table causes it to become cemented by calcite. Unit C is the upper most unit and is silty clay with minor sand content. This silty clay is approximately 3 to 7 feet in thickness. As Unit C creates the ground surface it, contains an abundance of organic materials and some manganese nodules.

McPhail (2003) constructed cross sections from core description that illustrate these minor changes, an example of which is shown in figure 3 along wells ME-15, ME-13, ME-14, and ME-16. McPhail (2003) models the site geology as alluvium approximately 15m thick underlain by a bedrock aquitard, the Permian Hennessy Group. The alluvium is divided into three sub units. Unit A is 3.2-7.62 m thick sand coarsening downward. Unit B is 8.84-10.36m thick with sandy clay topping gley. Unit A is .92- 2.13m thick organic rich silty clay with sand.

Table 2: Generalized description of the soil column to the bedrock at the Enid site (Modified from McPhail, 2003).

Unit	Unit Name		Thickness (ft)	Thickness (m)	Approximate Depth (m)
C	Alluvium	Silty clay with sand	3-7	0.92-2.13	1
B		Sandy clay	25-29	7.62-8.84	9
		Gley	4-5	1.22-1.52	10
A		Sand-gravel	2.5-10.5	3.2-7.62	12
	Permian Hennessey Group		**Bedrock Aquitard**		

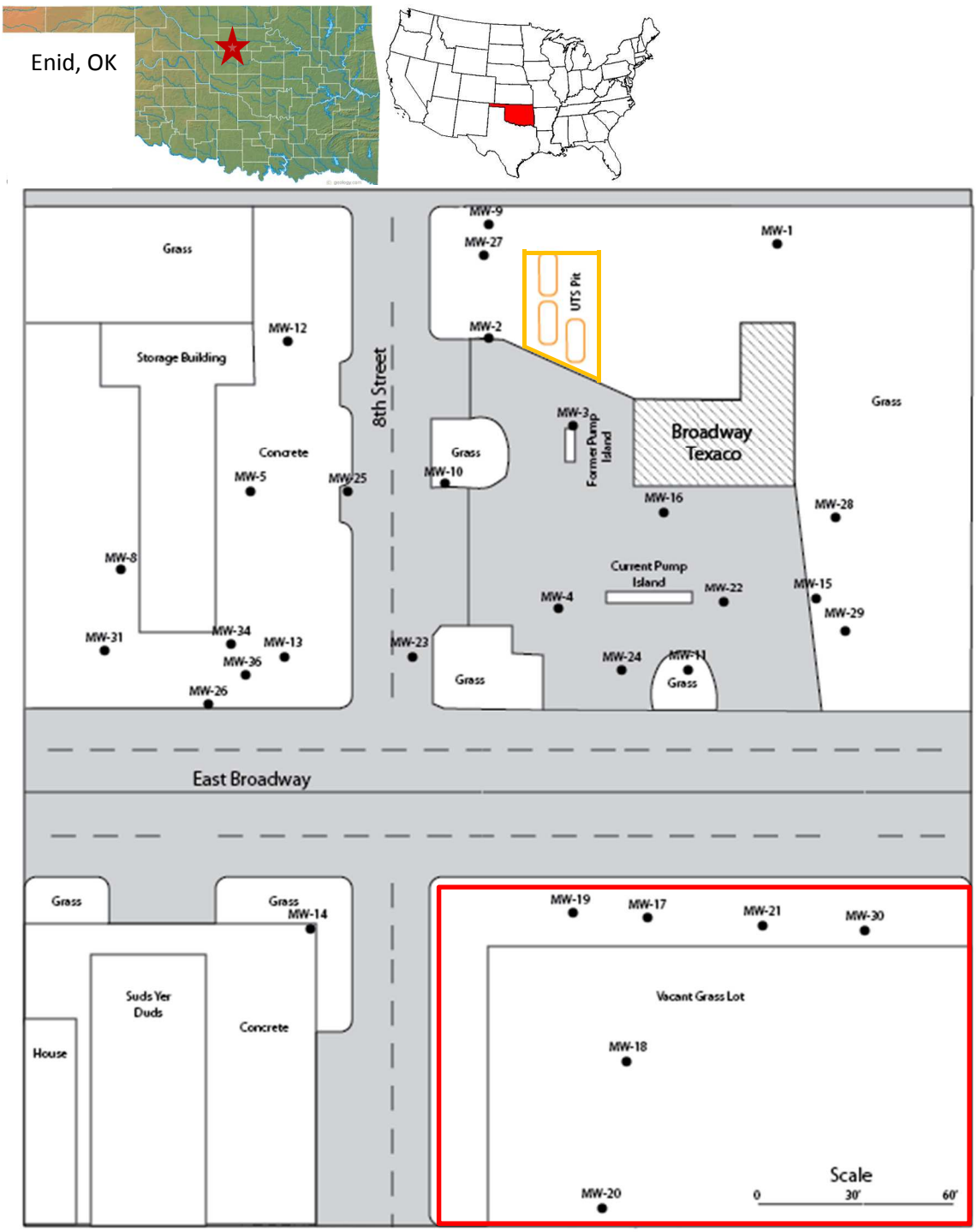

Figure 2. 8th and Broadway study site location in Enid, Oklahoma indicating surrounding infrastructure and borehole locations utilized in investigations. Orange outline identifies contaminant source. Red outline indicates area shown in figure 6.

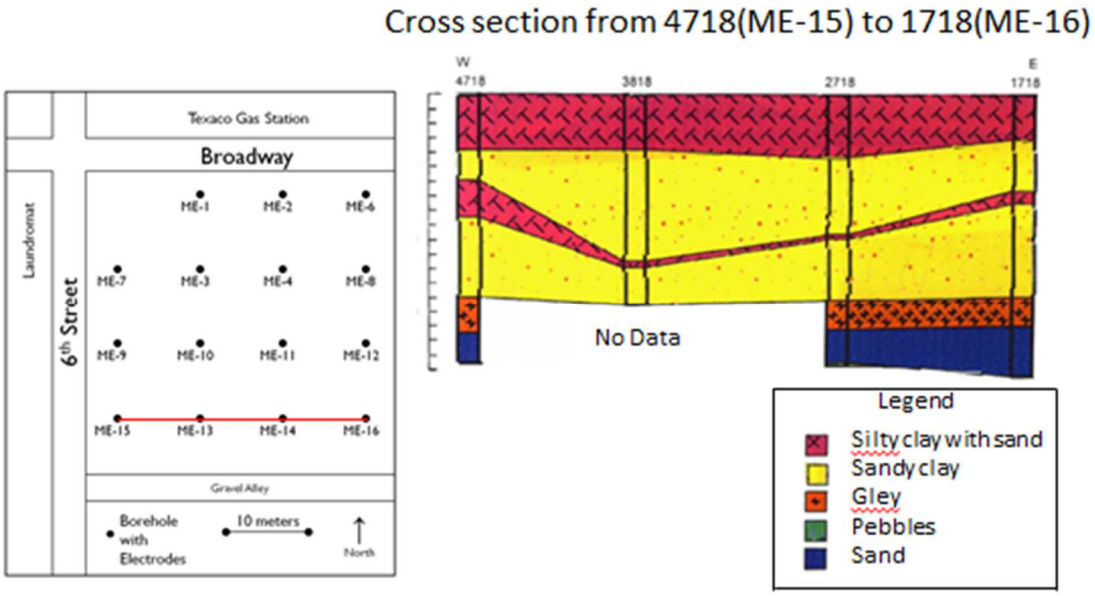

Figure 3. Cross section along the southern end of the study site showing variability of sediment stratigraphy. Cross section construction using wells ME-15, ME-13, ME-14, and ME-16 from west to east (Jeffreis, 2011)

Continuous measurements of the light nonaqueous phase liquids (LNAPL) presence from 2001 to the present were taken using noninvasive geophysical techniques, extracting cores, and sampling monitoring wells around the source. From these measurements it was determined that the LNAPL plume had migrated to the southeast and continued to broaden in width (Jeffries, 2011). It was found that the contaminant free product, measuring up to 3ft in thickness, followed the groundwater flow direction to the southeast. These measurements have led to the conclusion that this site has become stagnate with little progression towards complete remediation as the thickness of free product has not significantly reduced (Jefferies, 2011).

The free product monitoring of the subsurface that occurred over time from 2001-2009 indicates a broadening of free product with a southward migration (Figures 4-6). The gley and clay act as confining guides for the LNAPL plume migration as they are less permeable (Jefferies,

2011). McPhail (2003) collected 16 cores covering the complete alluvium section. The generalized subsurface stratification seen in table 2 was derived from these core analyses.

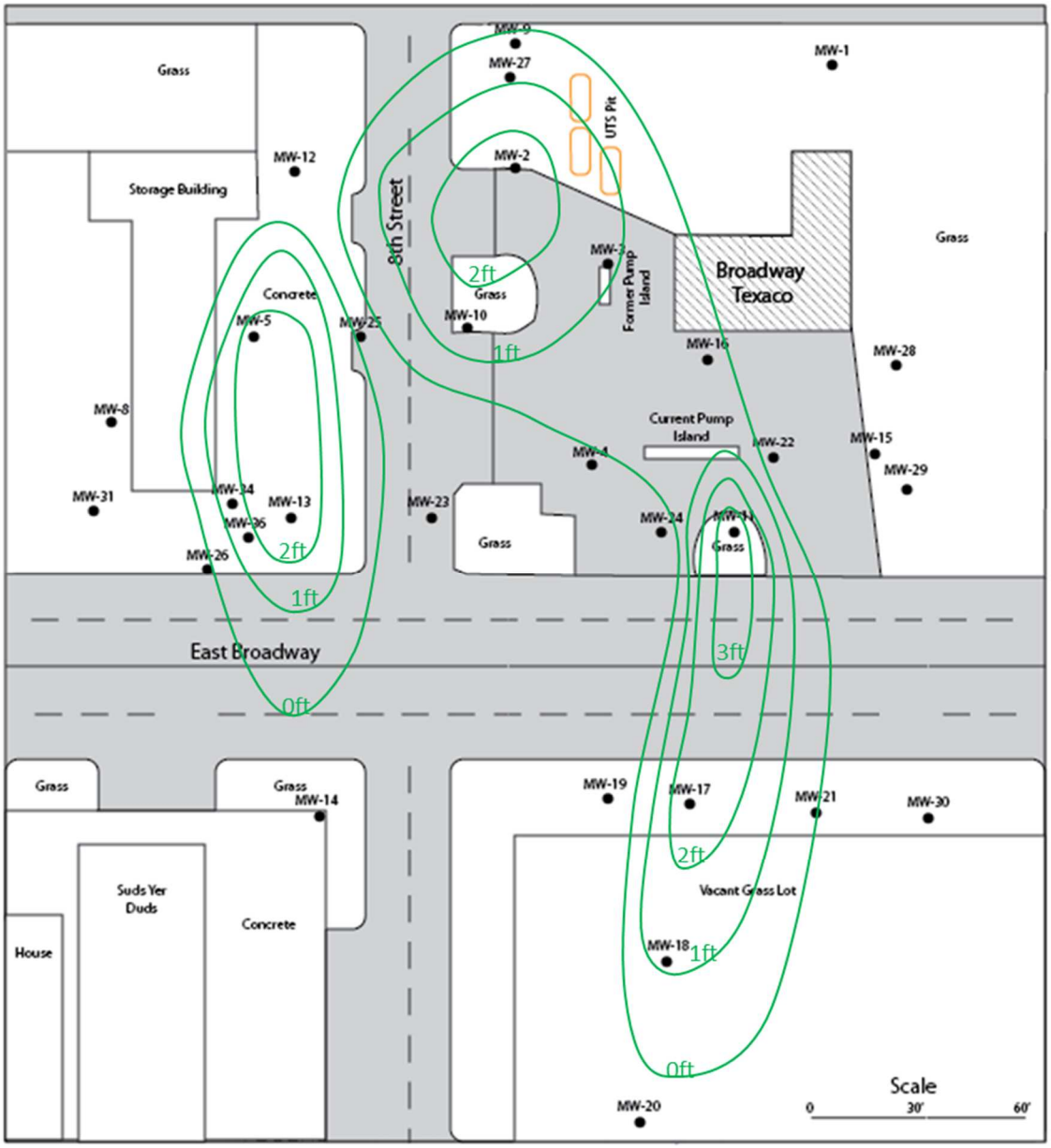

Figure 4. Map indicating the free product thickness in July 2001. Monitoring wells are indicated by MW. Green lines are in 1 foot contours. Modified from Jeffries (2011).

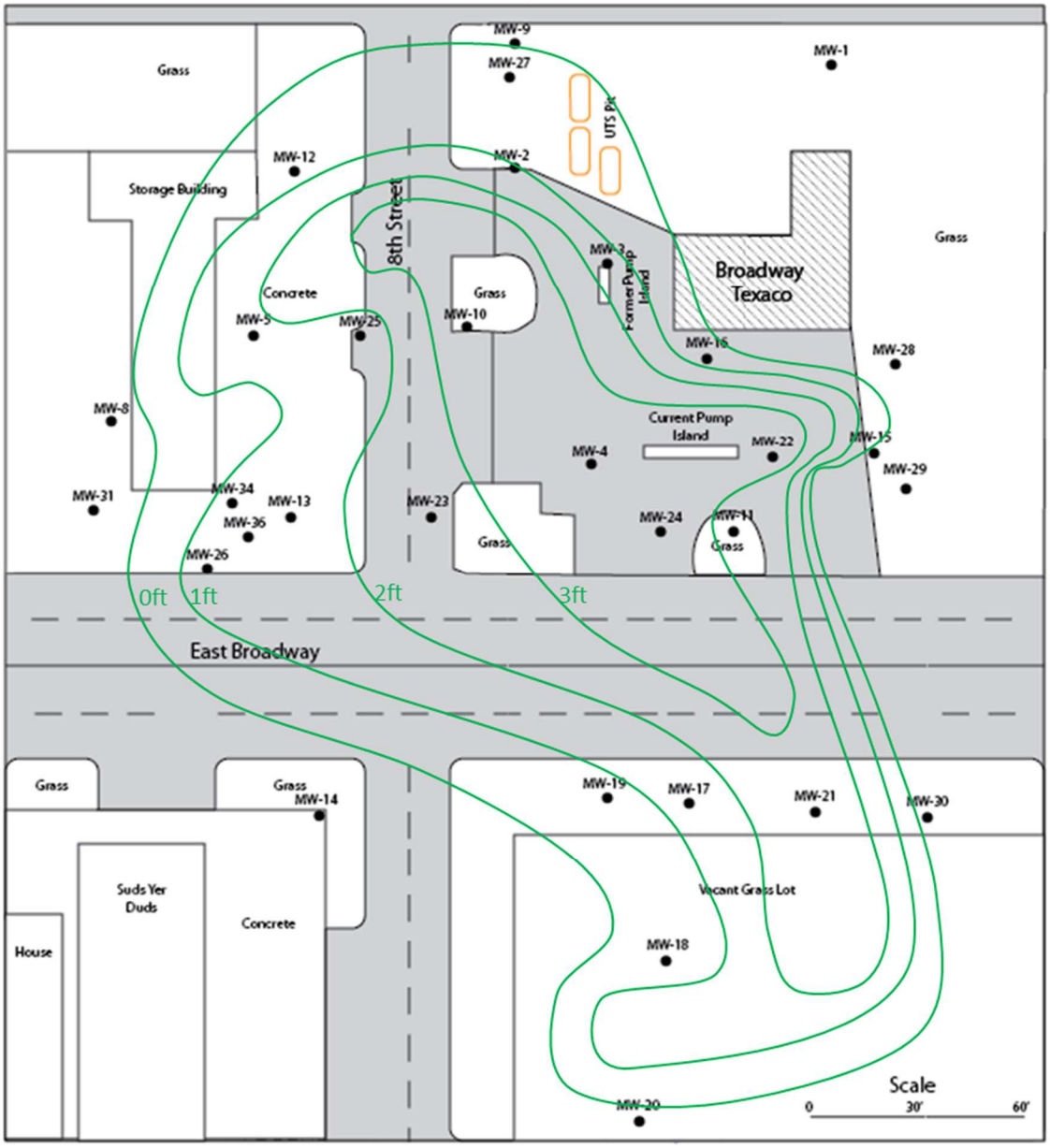

Figure 5. Map indicating the free product thickness in July 2007. Monitoring wells are indicated by MW. Green lines are in 1 foot contours. Modified from Jeffries (2011).

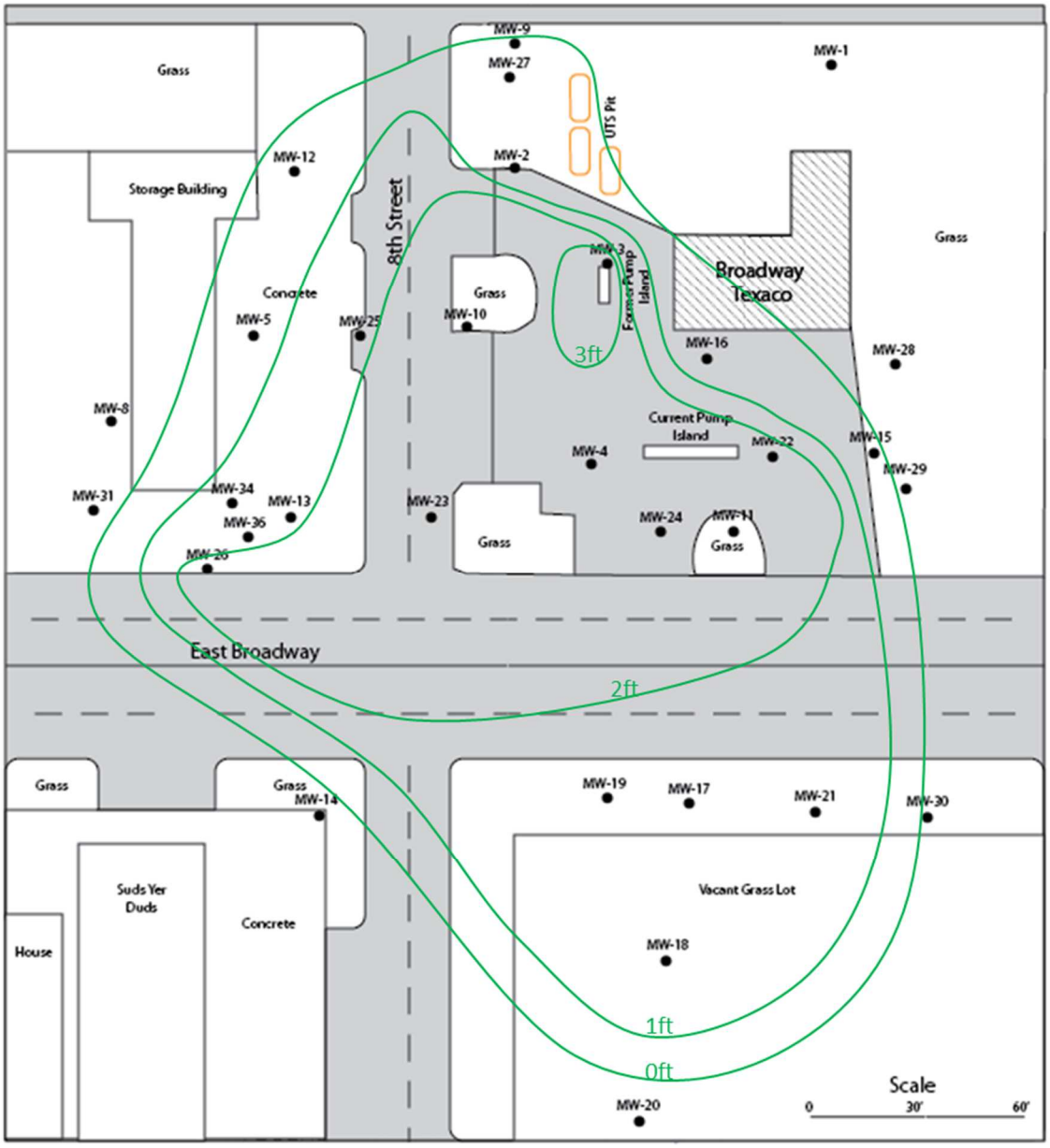

Figure 6. Map indicating the free product thickness in August 2009. Monitoring wells are indicated by MW. Green lines are in 1 foot contours. Modified from Jeffries (2011).

Hydrology

Previous hydrologic studies were conducted at this site prior to and after the installment of the air sparging remediation system (Halihan, et al., 2005). The findings of the study are shown in figure 7 where the water table elevations upwards from site's datum range from 89.7 to 90.2 feet or 8.5-10.5 meters below the surface with a seasonal variation of ± 1 meter. This figure also shows that the groundwater preferentially flows to the southwest, carrying the LNAPL. Also note the steep gradients in the vicinity of the gasoline station in the northeast quadrant of the study area were water tends to pool around MW-11 where it is recharged from the north, west, and southerly directions, while the water gradient dips to the southeast (Halihan et al., 2005).

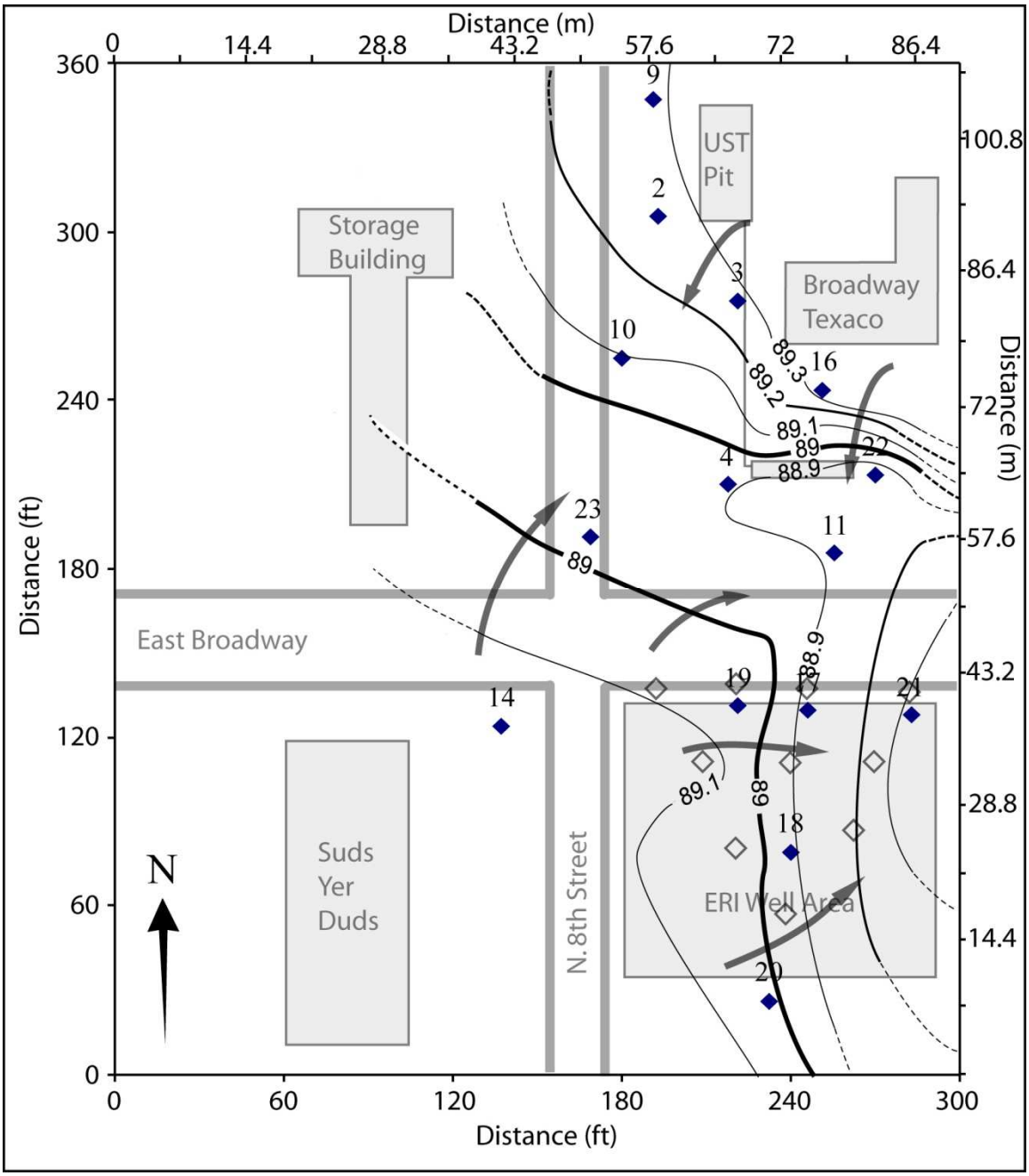

Figure 7. Water table elevation above datum at the Enid, OK site. Contour intervals are .1ft. Filled diamonds are monitoring wells and open diamonds are previously planned remediation monitoring wells. Notice that groundwater flow pools to south of the gas station and flows to the southeast. Modified from Jeffries (2011)

CHAPTER III

METHODOLOGY

This chapter presents the methods used in data acquisition, processing, and interpretation for core description, electrical resistivity, magnetic susceptibility, and geochemical sampling. Core samples utilized in this study as well as monitoring wells used in the magnetic investigation locations are highlighted in figure 8.

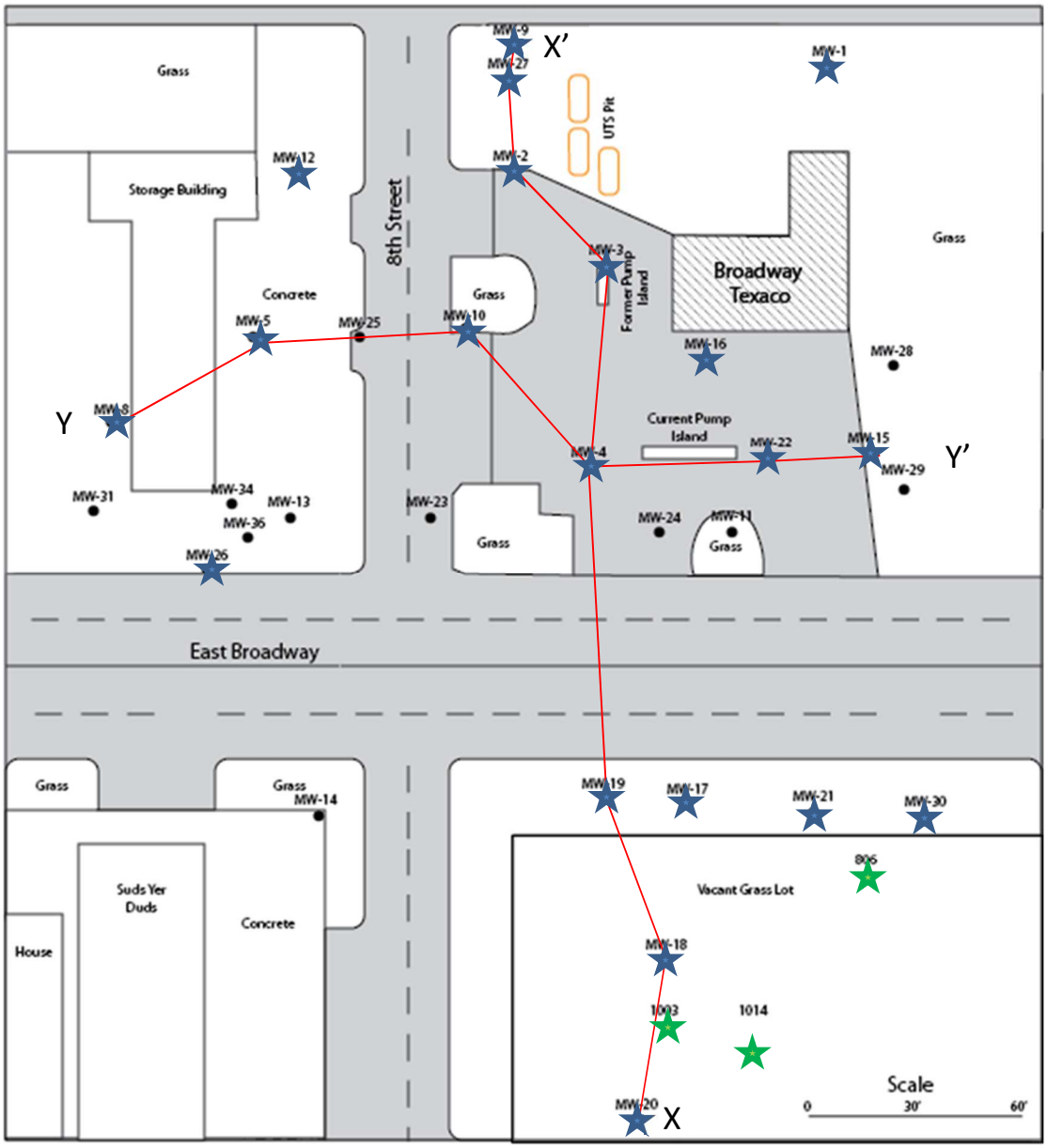

Figure 8. Locations of cores used for stratigraphic correlation, resistivity and magnetic measurements (green), as well as monitoring well locations utilized in the borehole magnetic susceptibility measurements (blue). Red line illustrates wells included in cross section X -X' and Y-Y' of figure 12.

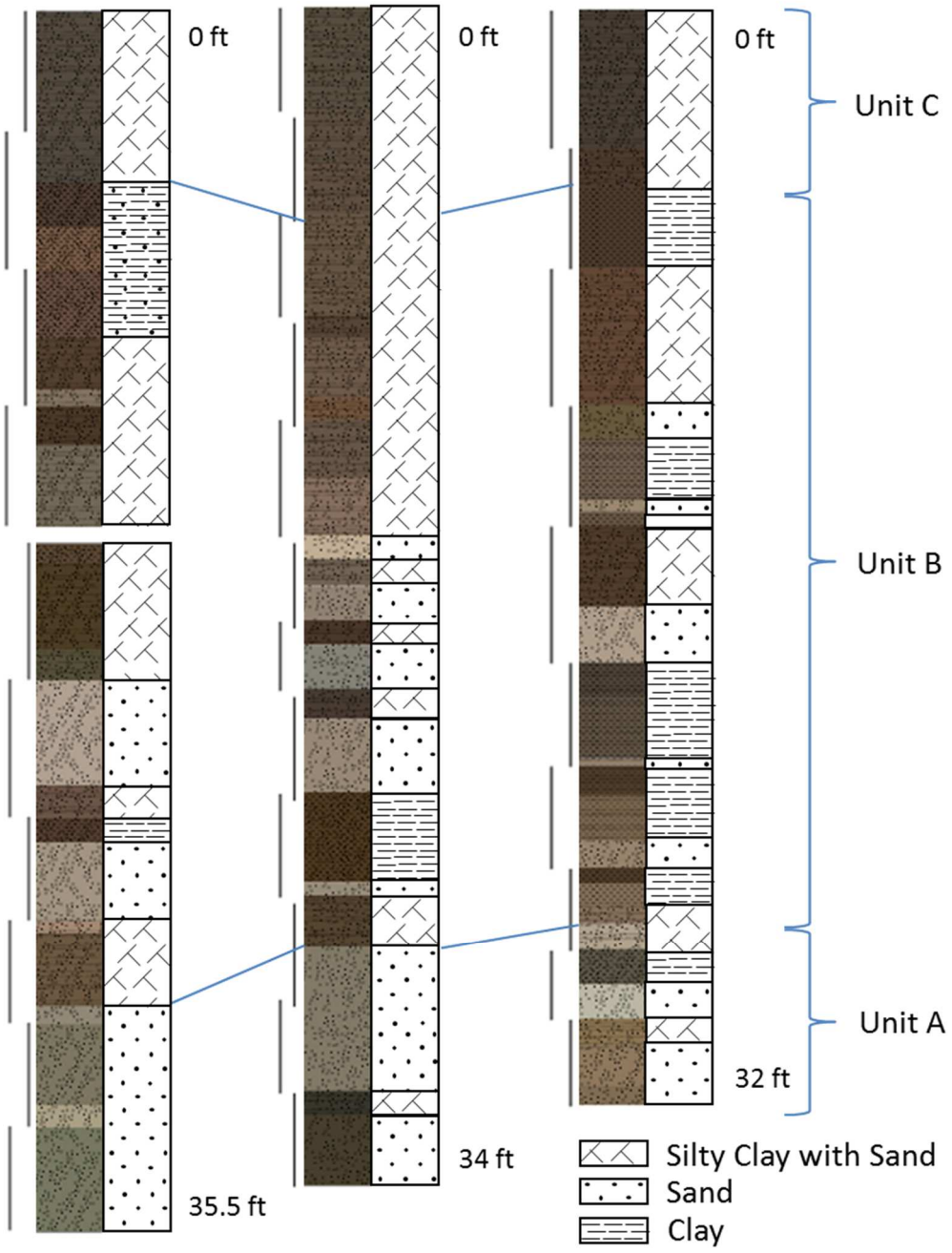

Figure 9. Simplified stratigraphy observed in cores 806, 1003, and 1014. Lines next to cores indicate core segments.

CORE MEASURMENTS

Electrical resistivity, magnetic susceptibility, and photoionization detection (PID) measurements were made on three core samples extracted from the southern portion of thesite used in this thesis. These cores are named for their respective locations between numbered electrodes found in Jefferies (2011) and are identified as: 806, 1003, and 1014 (figure 8). Core 806 extended from the surface (0) to 10.82m; core 1003 from 0 to 10.36m, and core 1014 from 0 to 8.99m. Cored samples were stored in a refrigerator at 3 °C to prevent chemical and biological reactions that might alter the samples.

Core Electrical Resistivity

Resistivity measurements were collected for the three cores using 4 electrodes arranged in a Wenner Array, which consist of two current electrodes on the outside and two potential electrodes between them, all in a linear fashion equal distance apart. Current flows between the current electrodes where the potential electrodes quantify how much the current flow is inhibited. For these measurements an electrode spacing of 3 cm was chosen to cover the length of all three cores. Detailed sediment core descriptions from McPhail (2003) suggest that the 3cm spacing was adequate to capture any lithological or contaminant influences. Resistivity data were collected using the IRIS Syscal Pro system by attaching clamps to imbedded non-reactive galvanized nails that served as electrodes. Because this Wenner array requires a total distance of 9cm per measurement, the ends of core sections could not be measured. The resistivity values were then

plotted against their measured core length in excel to produce visual 1D resistivity representations.

Core Magnetic Susceptibility

Magnetic susceptibility measurements were collected in two separate experiments. The core measurements were made using a Bartington MS2C magnetic susceptibility meter. This instrument is able to detect low frequency magnetic susceptibility of variable ferromagnetic, paramagnetic, and diamagnetic minerals. The principle of operations are as follow per the Bartington operating system manual. The magnetic state of a specimen is generally described by the following equation:

$$B = \mu_0 (H+M)$$

Where:

B is the flux density of the specimen in T (Tesla).

μ_0 is the permeability of free space in. This is a constant ($4\pi * 10^{-7}$)

H is the applied field strength in Am^{-1}.

M is the magnetization of the specimen in Am^{-1} .

Dividing through by H: $\mu = \mu_0 + \mu_0\kappa$

Where:

μ is the permeability of the specimen (dimensionless)

κ is the volume magnetic susceptibility of the specimen (dimensionless)

Rearranging:

$$\mu_0\kappa = \mu - \mu_0$$

The sensor is a very high thermal stability oscillator for which a wound inductor is the principle frequency-determining component. When the inductor contains only air the value of μ_0 determines the frequency of oscillation. When the inductor is placed within the influence of the specimen to be measured, the value of μ determines the frequency of oscillation. The meter to which the sensor is connected digitizes the μ_0 and μ dependent frequency values with a resolution of better than one part in a million and computes the value of magnetic susceptibility.

Delivery of core samples through the opening in the Bartington MS2C sensor was achieved by erecting a polyvinyl chloride (PVC) chute that had no effect on the sample measurement yet held it center of the screening sensor. Core diameters were within the constraints of the operating manuals suggested size, therefore did not call for adjustment of collected values. Measurements were made every 3cm as to prevent overlapping magnetic influence from adjacent measurements per suggestion of operating manual (Bartington, 2015). Measurements at the end of core sections were discarded as they were consistently low due to airspace influence. Zero drift was observed at the end of the experiment, eliminating the need for a value adjustment. Magnetic susceptibility measurement values in cgs10^{-4} were then input into excel and plotted against measured core depth to emulate 1D representations of core samples.

BOREHOLE MAGNETIC SUSCEPTIBILITY

Borehole MS measurements were collected using a low frequency Bartington Magnetic Susceptibility Borehole Sonde MS2B. The operating principles behind borehole measurements are similar to those previously documented in the section on core sampling.. Bartington sonde measurements were made in the field down the boreholes of previously built monitoring wells. These wells are cased with PVC of various diameters that do not effect magnetic susceptibility measurements. The sonde is lowered down the well and mechanically lifted through the borehole taking measurements with a minimum sensitivity of cgs10^{-5} every 16 cm with a resolution of 25 cm (full width half maximum). After measurements are taken they are multiplied by a factor according to their specific borehole diameter to compensate for loss of response due to air space (1 for 5 cm diameter,1.3333 for 7 cm diameter, 3.6363 for 8 cm diameter, and 11.1111 for 10 cm diameter boreholes). The MS measurements were input into Petrel software for interpretation.

GEOCHEMICAL SAMPLING

Multiple geochemical measurements were taken in the field and laboratory. Groundwater from monitoring wells was extracted using a peristaltic pump. This water was then flushed through a flow cell into a Yellowstone Instrument (YSI) multi-paramenter probe for measuring water temperature, specific conductance (SPC), pH, alkalinity, dissolved oxygen (DO), conductivity, total dissolved solids (TDS) and oxidation reduction potential (ORP). Water samples were filtered through a 0.45 μm pore size filter for iron sampling. Lab measurements for aqueous phase Fe^{2+}, and Fe^{3+} using a photo detector were performed. Due to the vast majority of samples being below the instruments sensitivity threshold, another experiment was employed measuring total iron using another photo detector following the Ferrozine method utilized in

Viollier, et al. (2000). A small amount of nitric acid (HNO^3) was added to each sample to return any iron to its aqueous state that might have oxidized out of solution during storage.

Chemical analyses performed at an earlier date were also used in this study that observed water levels, temperature, pH, specific conductance, TDS, dissolved oxygen, chlorine, NO_3, SO_4, PO_4, alkalinity, CO_2 yield, dissolved inorganic carbons (DIC), carbon ^{13}, dissolved oxygen ^{18}, sodium, magnesium, and calcium following similar procedures. The ionic composition was measured by storing 0.45 μm filtered samples in polyethylene bottles (pre-acidified for cations) and analyzed by ion chromatography. Carbon isotope ratio ($\delta^{13}C$) was measured using a technique described by Atekwana and Krishnamrthy (1998).

The PID measurements used in this study were collected by Jefferies (2011), using a handheld PID device with a one-half foot frequency. Data illustrated in this study was digitized from Jeffries (2011) as the spreadsheet was not available.

CHAPTER IV

RESULTS

CORE MEASURMENT RESULTS

Electrical Resistivity

Figures 10, 11, and 12 show the results of the resistivity measurements parallel to MS and PID for cores 806, 1003, and 1014. The results show that the resistivity values fall into 4 different geoelectrical layers. The uppermost 200 cm of measured core depth shows significantly higher values that are erratic, ranging from 200-800 Ω·m that decreases with depth. The second section from 200 cm to approximately 600 cm generally maintains a lower electrical resistivity profile around 60 Ω·m. The third layer extends from approximately 600 cm to 750 cm. Here the profile exhibits large peaks in electrical resistivity up to 425 Ω·m. The lowermost portion of the measured cores in the WTFZ from 750 cm to the base is topped with lower resistivity measurements around 100 Ω·m and changes differently with depth between the separate core samples until the end of the sample.

Magnetic Susceptibility

The MS measurements seen in figures 10, 11, and 12 relate to the measurements obtained using the Bartington MS2C along the core samples 806, 1003, and 1014. Readings reflect 4 distinct layers of differing MS characteristics. The uppermost, measured from the surface to around 150 cm shows a dramatic increase from the magnetic baseline up to 280*10^-6 SI and then slowly drops to the baseline. The second portion between 150 cm down to somewhere

between 775 cm and 850 cm pending the sample. Here the MS maintains a low baseline reading around 15*10^-6 SI with some small sporadic readings where the measurement increases as high as 113*10^-6 SI. The third thinner section lies below the previous marker and continues for about 75 cm. Here at the top of the WTFZ MS reaches its higher readings and begins to taper down back to the baseline: Core 806, 130*10^-6 SI; Core 1003, 1613*10^-6 SI; Core 1014, 340*10^-6 SI. Below this drop in MS, the fourth layer continues similarly to the second layer maintaining near baseline values where data is available.

PID

The PID measurements in ppm vary for each well in figures 10, 11, and 12. They do maintain a baseline of 0 until reaching depths of 800mm for core 806, 700 mm for core 1003 and 1014. Here around the WTFZ PID measurements become erratic reaching their highest.

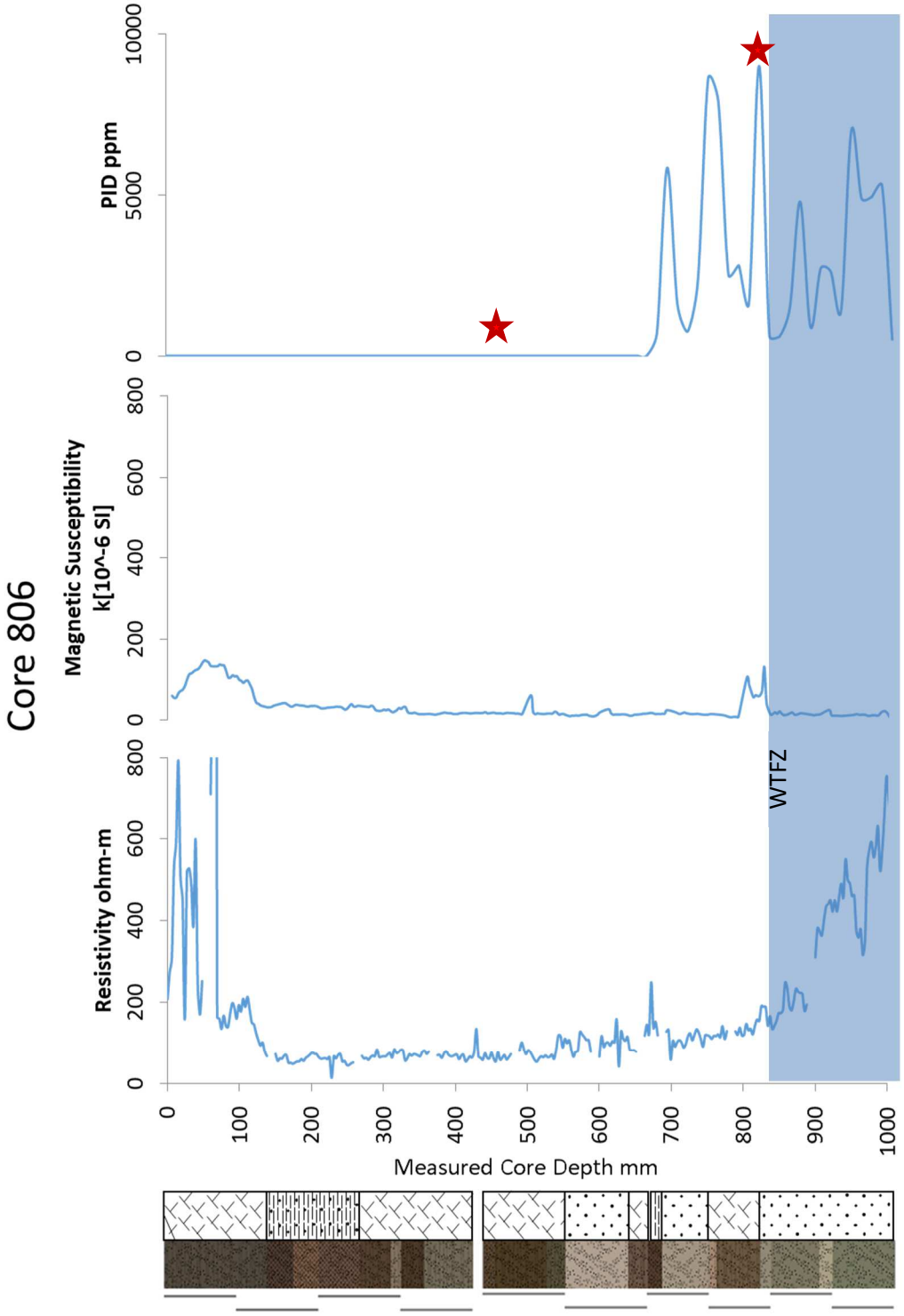
Core 806
PID ppm
0
5000
10000
Magnetic Susceptibility
k[10^-6 SI]
0
200
400
600
800
Resistivity ohm-m
0
200
400
600
800
WTFZ
0
100
200
300
400
500
600
700
800
900
1000
Measured Core Depth mm

Figure 10. Stratigraphy, electrical Resistivity, magnetic susceptibility and PID values for core 806. See figure 8 for core location. Red stars illustrate BTEX sampling locations. Blue box indicates WTFZ.

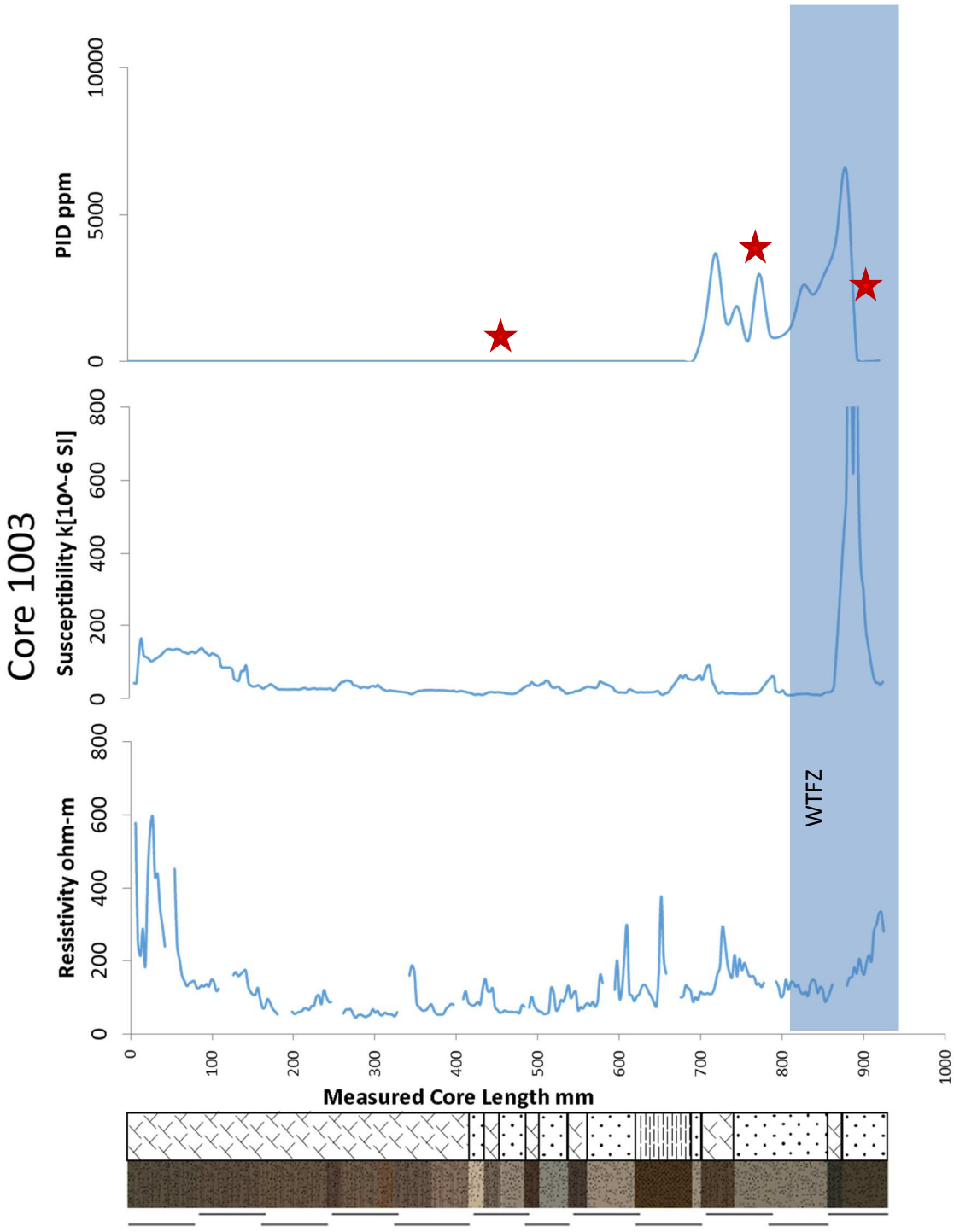
Core 1003
PID ppm
0
5000
10000
Susceptibility k[10^-6 SI]
0
200
400
600
800
Resistivity ohm-m
0
200
400
600
800
WTFZ
0
100
200
300
400
500
600
700
800
900
1000
Measured Core Length mm

Figure 11. Stratigraphy, electrical resistivity, magnetic susceptibility and PID values for core 1003. See figure 8 for core location. Red stars illustrate BTEX sampling locations. Blue box indicates WTFZ.

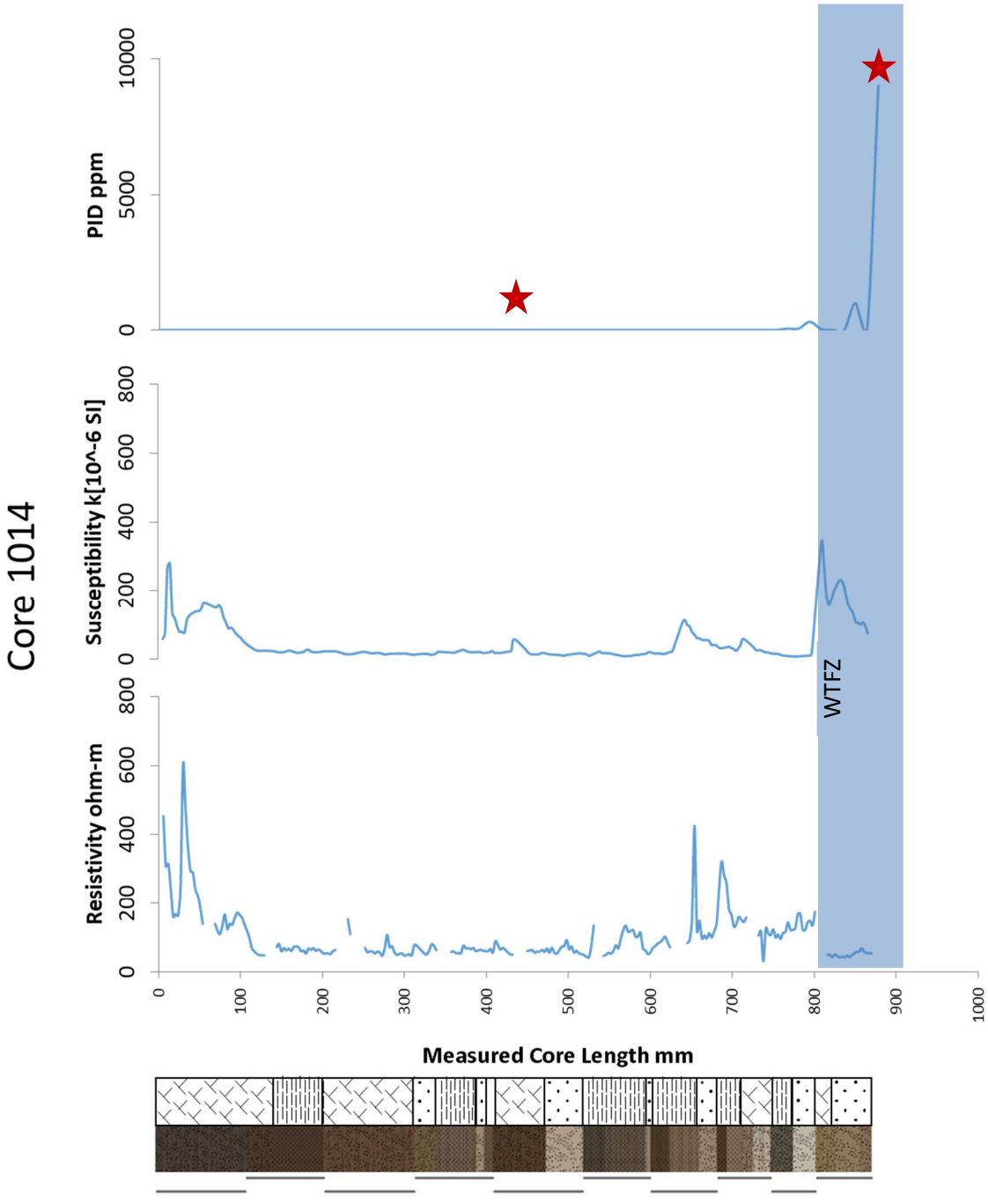
Core 1014
PID ppm
0
5000
10000
Susceptibility k[10^-6 SI]
0
200
400
600
800
Resistivity ohm-m
0
200
400
600
800
WTFZ
0
100
200
300
400
500
600
700
800
900
1000
Measured Core Length mm

Figure 12. Stratigraphy, electrical resistivity, magnetic susceptibility, and PID values for core 1014. See figure 8 for core location. Red stars illustrate BTEX sampling locations. Blue box indicates WTFZ.

BOREHOLE MAGNETIC SUSCEPTIBILITY

Individual measurements that were made along the depth of monitoring wells are presented in Appendix A. An example of the MS measurements along profile X-X' is shown in figure 13 and Y-Y' in figure 14. Zone 1extends from the surface to a depth of 6 m and shows elevated MS values around 1040*10^-6cgs. Zone 2 extends from 6 m to 9.5 m where there is an approximate baseline low maintained around 1030*10^-6cgs, with small periodic increases. Zone 3 measures from 9.5 m to 10.5 m within the WTFZ and exhibits a significant increase in magnetic response within some wells with variable shape depending the well location. Zone 4 is within the saturated zone below 10m and extends to the bottom of the measured section. Here magnetic susceptibility measurements return to baseline values similar to those for zone 2.

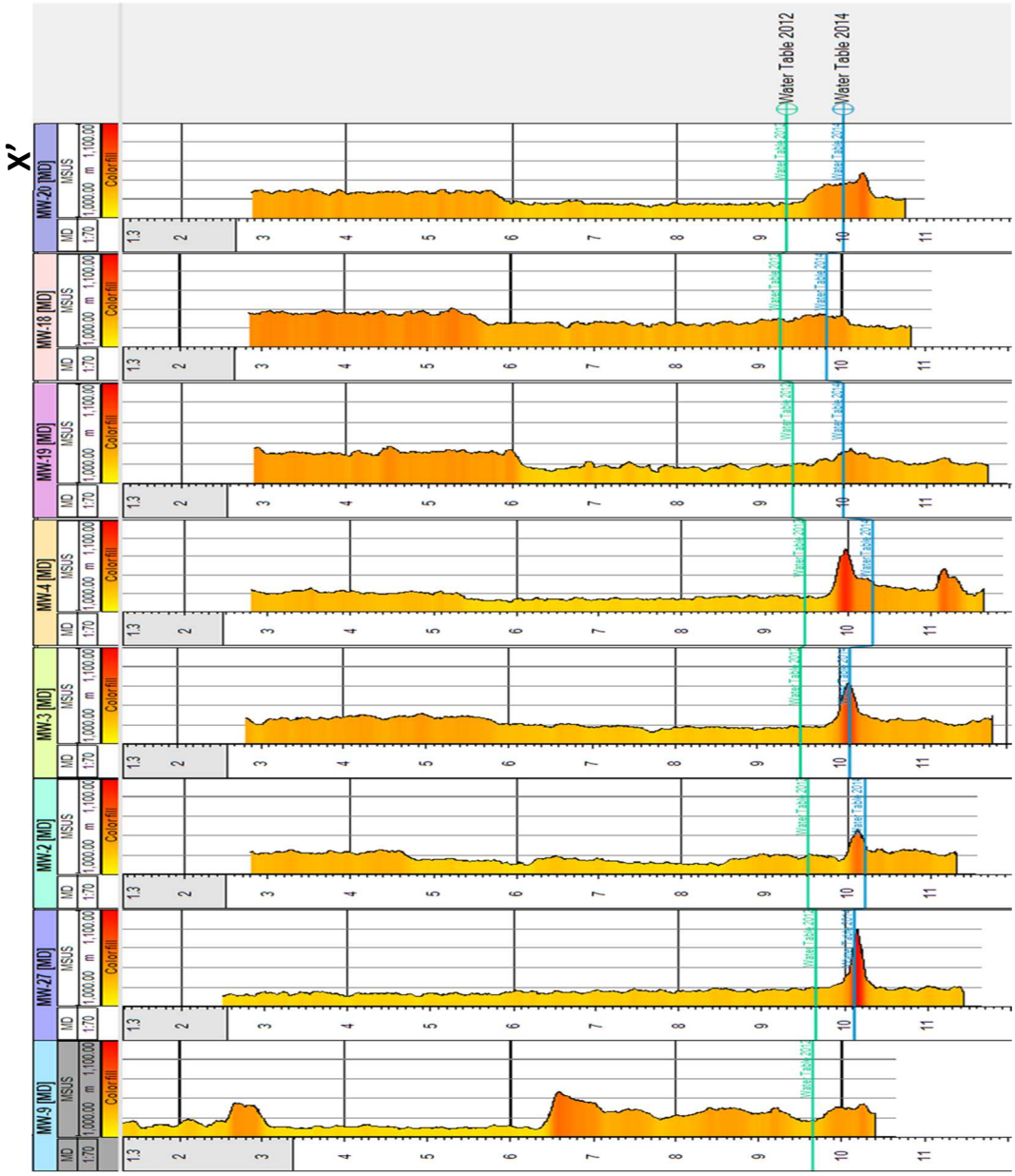

Figure 13. Cross section illustrating variability in borehole magnetic susceptibility along cross section X – X'. Blue line shows depth of water table during February 2015. Teal line shows water table depth in January 2005. Cross section location is shown in figure 8.

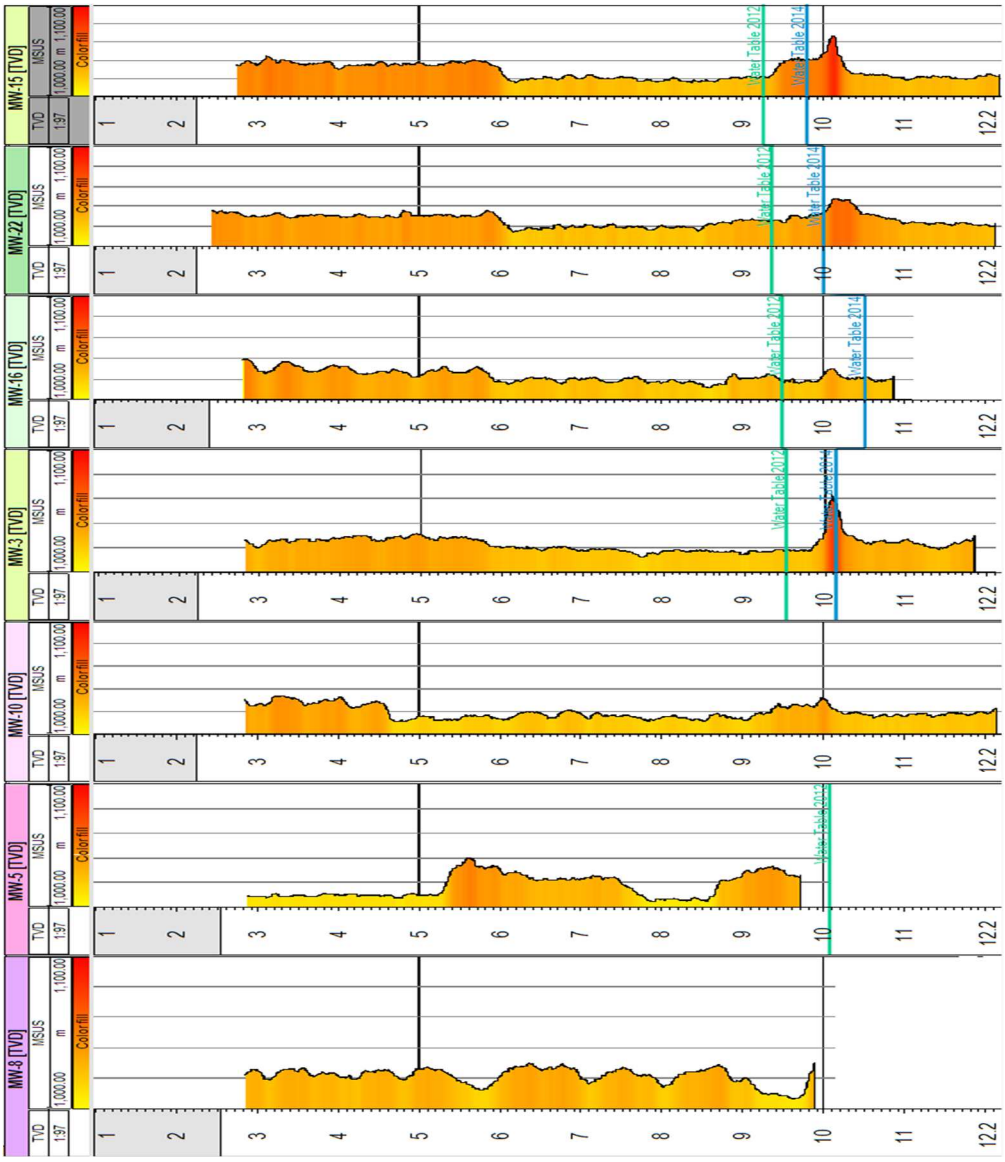

Figure 14. Cross section of variability of borehole magnetic susceptibility Y – Y'. Blue line shows depth of water table during February 2015. Teal line shoes water table depth in January 2005. Cross section location can be seen in figure 8.

GEOCHEMICAL ANALYSIS

PID data digitized from Jeffries (2011) shown in figures 10, 11, and 12 are values from core samples 806, 1003, and 1014. PID measurements were made approximately every 6 inches and plotted against depth. Areas of interest and highest PID values were subject to BTEX testing; results can be seen in table 3. Water samples from MW-2, MW-10, MW-18, MW-19, and MW-20 were also measured for benzene, toluene, ethylbenzene, and xylenes (BTEX) composition seen in table 4.

Geochemical values previously collected in 2011 at monitoring wells MW-2, MW-10, MW-18, MW-19, and MW-20 on presented on table 5. Geochemical data presented in tables 6 and 7 were input into Geosoft Oasis Montage, producing aerial maps using minimum curvature as the contouring algorithm. This data is presented in Appendix B.

Table 3. Numerical values of BTEX concentrations from extracted soils in cores 806, 1003, and 1014.

Core	Core Depth (feet)	Benzene (mg/Kg)	Toluene (mg/Kg)	Ethylbenzene (mg/Kg)	Xylene (mg/Kg)
0806	15–15.5	<0.025	<0.025	<0.025	<0.025
	29–29.5	1.92	5.61	5.14	28.9
1003	15–15.5	<0.025	<0.025	<0.025	<0.025
	29–29.5	0.484	5.52	4.99	29.2
	34–35	0.683	0.676	0.121	0.57
1014	15–15.5	<0.025	<0.025	<0.025	<0.025
	31.5–32	0.734	2.17	4.55	20.4

Table 4. Numerical values of BTEX concentrations from water samples from monitoring wells MW-2, MW-10, MW-18, MW-19, and MW-20.

Well	MTBE (mg/L)	Benzene (mg/L)	Toluene (mg/L)	Ethylbenzene (mg/L)	Xylene (mg/L)
MW-02	0.093	0.54	0.109	0.005	0.225
MW-10	0.5	5.76	12.9	1.88	20
MW-18	0.363	3.41	9.53	2.33	17.4
MW-19	0.027	0.738	0.006	0.005	0.055
MW-20	4.56	8.79	0.05	0.063	0.122

Table 5. Previously collected data from February 2011 for monitoring wells MW-2, MW-10, MW-18, MW-19, MW-20

Well	Water Level FEB 2001	Temp	SpC	TDS	DO	pH	ORP	Cl	SO4	NO3	ALK	NA	K	Mg	Ca
	m	°C	µS/m	g/L	mg/L		mV	mg/L	mg/L	mg/L	mg/L (CaCO3)	mg/L	mg/L	mg/L	mg/L
MW-20	9.13	17.48	1413	0.919	0.31	5.7	-1328	48.5	0.5			678	195.2	24.4	134.6
MW-19	9.28	19.23	1455	0.946	0.86	6.15	737.1	117.4	97.6	19.3		457	165.2	25.7	144.3
MW-18	9.21	17.26	1477	0.949	0.62	6.23	22	16.8	1		0.4	830	282.5	20	110.4
MW-20	0.31	17.85	1020	0.696	4.09	5.98	-110.5	22.7	5.3			359	79.7	15	80.2
MW-10	9.313	15.48	1390	0.904	16	5.9	-65	42.7	1.8	1	2.4	600	197.5	21.1	103.1

Table 6. Geochemical data from samples collected in January 2005.

Well	Water Level Feb 2012	Water Level Jan 2005	TEMP	Ph	SpC	TDS	DO	NO3	SO4	PO4	Mg	ALK	DIC	$d^{13}C_{DIC}$
Units	m	m	°C		µS/m	g/L	mg/L	mg/L	mg/L	mg/L	mg/L	mg/L (CaCO3)	mgC/L	Per mill
MW-1	9.16	8.89	19.2	6.46	1.509	0.965	0.97	43.61	115.3		24.99	548	180.9	-20.477
MW-2	9.52												156.7	-17.383
MW-4	9.48							1.58	37.54					
MW-6	10.64	9.19	21.94	6.88	1.283	0.826	3.11	49.39	127.11		18.65	404	103.7	-13.003
MW-8	NA	9.65	20.94	6.52	1.694	1.083	1.32	1.47	1.75	6.81	28.75	769	234.8	-19.529
MW-12	10.48	9.37	26.29	6.74	2.313	1.485	0.57	3.08	3.43	8.42	32.7	1073	309.3	-17.879
MW-14	NA	9.21	23.51	6.69	1.695	1.087	0.37	0.45	177.08		18.71	604	187.8	-19.022
MW-15	9.25	8.84	19.95	6.51	1.56	0.999	0.41	2.31	2.07	7.92	27.84	550	164.9	-18.489
MW-16	9.48	9.56	20.19	6.74	1.589	1.017	0.7	2.14	2.15	6.62	17.22	641	177.5	-18.107
MW-17	9.4	9.51	20.89	6.56	1.358	0.868	1.81	1.74	4.11	5.5	21.19	519	171.9	-18.531
MW-19	9.39	9.64	21.28	6.59	1.572	1.007	2.9	34.63	212.52		25.19	413	106.3	-12.696
MW-20	9.32	9.07	19.25	6.54	1.507	0.965	1.49	2.16	10.68	4.06	19.77	645	188.4	-18.728
MW-22	9.36	9.78	20.18	6.52	1.617	1.033	0.52	8.8	83.48	2.23	24.68	528	149.9	-17.139
MW-23		9.11	20.88	6.72	1.514	0.971	0.83	16.89	118.91		22.6	472	137.1	-15.871
MW-24		9.01	21.28	6.65	1.626	1.041	0.9	29.04	221.64		24.85	409	112.4	-14.412
MW-25		9.26	21.2	6.48	1.854	1.182	2.16	16.23	108.27	0.94	25.76	579	166.6	-17.356
MW-26	9.09	9.1	20.84	6.7	1.754	1.116	0.44	22.37	106.46		23.32	594	176.5	-17.676

Table 7. Geochemical data from samples collected February of 2015.

Well	Water Level FEB 2015	Temp	pH	SpC	TDS	ALK	DO	ORP	Total Fe
Units	m	°C		µS/m	g/L	mg/l (CaCO3)	mg/L	mV	mg/L
MW-1	9.93	14.73	7.19	1415	0.922	46.1	11.34	-39.2	.009
MW-2	10.2	16.9	7.44	1384	0.9	544.4	18.2	-71.1	.278
MW-3	10.12	15.43	6.91	1130	0.735	280	2.65	-84.4	.383
MW-4	10.3	15.54	7.16	1428	0.93	51.5	23.31	-112.9	.094
MW-11	10.2	16.55	6.86	1475	0.959	180	10.04	-140	.048
MW-13	10.12	17.2	7.42	1558	1.014	180.3	10.95	-37.2	.042
MW-14	10.14	15.88	7.6	1418	0.922	377.1	23.32	-84	.363
MW-16	10.5	12.62	7.44	1376	0.895	728.5	21.8	-119.1	.046
MW-17	9.8	14.94	6.75	1265	0.822	487.5	8.64	-84.9	.096
MW-18	9.8	13.1	6.89	1559	1.014	60.8	27.23	-93.2	.146
MW-19	10	11.15	6.7	1625	1.056	477	2.24	-216.7	.052
MW-20	10	7.2	6.62	1531	0.995	665.3	4.94	-95.9	.044
MW-21	9.84	14.32	6.45	1037	0.674	500.5	6.57	-48.5	.12
MW-22	9.98	15.45	6.94	1346	0.876	55.1	10.45	-95.6	.067
MW-24	9.84	16.13	6.83	1448	0.942	31.9	10.05	-117.4	.224
MW-25	9.42	14.84	6.84	1429	0.926	143.4	12.75	-91.4	.842
MW-26	9.89	17.67	7.95	1601	1.042	344.2	17.67	-136.4	.843
MW-27	10.12	16.29	8.03	1472	0.957	533.7	6.64	-139.9	.106
MW-29	9.8	13.82	6.81	1504	0.518	600.1	23.65	-93.7	.073
MW-30	9.92	14.29	7.01	1177	0.754	601	18.13	-94.1	.096
MW-34	10.34	16.93	7.39	1696	1.102	288.6	12.78	-122.7	1.136
MW-36	10.24	17.25	7.62	1557	1.012	400.4	13.72	-36.2	.007

CHAPTER V

DISCUSSION

In similar studies correlations between MS and contamination prevalence have been observed. (Rijal et al., 2010) Furthermore strongest MS measurements have been correlated with the WTFZ within contaminated areas as a result of authigenic magnetite production (Rijal et al., 2012, Atekwana et al., 2014). Attenuation of MS values have been observed to decrease distally from the thickest portions of contaminates as it degrades from free-phase to dissolved phase as seen in figure 1 (Atekwana et al., 2014). Magnetite is readily produced by a variety of different bacteria as an end result of iron metabolic pathways and is associated with aqueous electron acceptor depletion. Magnetite production can also be inhibited by intrinsic subsurface conditions such as low Fe^{2+}/Fe^{3+} ratios or over abundance (Zachara et al., 2002, Hansel et al., 2005, Atekwana et al., 2014). MS measurements have also been observed as having a strong correlation with degraded hydrocarbon organic carbon availability (Atekwana et al., 2014, Ameen et al., 2014) In all cases presence of magnetitie has been correlated as evidence of biodegration.

Similarly, in this study variability of MS indicates evidence of biodegration of contaminants. Similar investgations at other hydrocarbon impacted sites provide evidence that magnetite is the dominant mineral causing observed changes in MS. Although mineralogical data was not collected, we infer from previous studies that the higher MS readings are associated with secondary magnetite precipitation as magnetite is the only reasonable candidate because of the high MS measurments.

CORE MEASURMENTS

In figure 10, 11, and 12 we observe that the highest MS values measured for core are associated with the WTFZ. Furthermore, core 806 has higher resistivity values than cores 1003 and 1014. This difference is leads to the interpretation that the area around cores 1003 and 1014 were either never contaminated, or experienced biological remediation. The first is unlikely as it is noted that upon extraction the core samples had a pungent hydrocarbon scent, indicative of contamination. Evidence of contamination can also be observed in the appreciable PID measurements. BTEX measuremnts also indicate evidence of biodegration as we see BTEX ratios increase in relative benzene abundance as xylene, ethylbenzene and toluene are metabolized first. The magnetic susceptibility measurements made from the core and monitoring wells are also indirectly related to the same processes that controlled variations in resistivity. As is evident in figure 10 patterns of relating change in magnetic susceptibility and resistivity illustrated in the 4 body model described before.

The uppermost 2 meter section is controlled by organic activity in terms of an increase in both resistivity and magnetic susceptibility. The shallow zone of accumulation, where weathered minerals, atmospheric anthropogenic input, and moisture collect, likely attributes components for bacterial and chemical magnetite production. (Riedinger et al., 2005; Noubactep et al., 2012; Klueglein et al., 2013)

The 2nd layer, where we have lower readings, is the result of water and iron absence. The small increases in magnetic susceptibility observed are likely due to temporary available nutrients created, and volatilization processes of remediation. Another likely candidate are small perched aquifers created by small clay bodies as seen in Fels, et al. (1999) that create niches appropriate

for magnetite production. These observations often result in slight spike in magnetic susceptibility immediately followed by a drop in resistivity typically associated with water retentive clays further suggesting minor collections of perched water.

The larger magnetic responses seen in the 3rd layer are attributed to the abundant resources supplied by the water table, contaminants, and thriving biology likely there. The Iron oxidation-reduction cycle as well as bacterially mediated magnetite production allows for a significant amount of magnetite to be produced here within the WTFZ (Hansel et al., 2003; Liu et al., 2006; Noubactep et al., 2012, Rijal et al.,2010, 2012; Ameen et al., 2014; Atekwana et al., 2014). The slow reduction of magnetic susceptibility at lower depths from peaks seen in this layer is possibly due to either a natural lower secondary production of magnetite due to gradual increase in water table height, or magnetite becoming soluble reducing the iron to an aqueous phase when submerged below the water table.

The lower most 4th layer, where measurements return to a baseline reading, is likely similarly due to solubility of magnetite being consistently exposed to the saturated zone. Another possibility is that magnetite production never occurred because it required oxygen levels or absence of contaminant regimes created by LNAPL buoyancy that is only achievable at the water tables surface allowing for either chemical or biological production. In figure 10 we again observe here a difference between cores 1003 and 1014 against 806, as 806 has the lowest MS value further suggesting lower remediation extent.

BOREHOLE MEASUREMENTS

Magnetite can form both biotically and abiotically as stated in the introduction. Combining borehole MS measurements seen in figure 13 and 14 and Appendix A with the geochemical data in tables 3-7 provides insight to the state of the system at their respective locations and times of acquisition from the Enid site. Returning to figure 3 we see the initial distribution of the free product from the single northern source migrating in two directions to the south. This split is likely caused by some impeding force such as a low permeability clay body causing a bimodal distribution around the intersection. It stands to reason the outermost boundaries are due to a similar lithologic control or that the groundwater preferential flow causes the elongate distribution as suggested in figure 9. Looking at many of the geochemical maps seen in appendix B we see several differences between MW-13 and MW-35. This supports the idea that there is a geologic boundary between these two wells which happen to be the closest two wells in proximity to each other. A further inference of differing regimes was derived from color differences of extracted water samples. Well pairs MW-19 and MW- 17 as well as MW-22 and MW-29 also show several geochemical instances in tables 4-7 of differentiation despite their close proximity that arise suspicion of geologic influence, but further research is needed for confirmation.

As stated previously in figure 7, the hydrology studies of Halihan et al. (2005) suggest that the water table and in turn contaminants pool around the pump island (MW-4, MW-22, MW-11, and MW-24) and the eastern most portion of the vacant lot to the southeast (MW-17, MW-21, and MW-30). This is due to lithology and water table elevations (Jefferies, 2011; McPhail,

2003). It is important to note that the average depth of the water table had fluctuated by nearly a meter since flow regimes have been studied so controls may have varied within the WTFZ.

The WTFZ correlation to magnetic susceptibility observed in figures 15 is similar to the increase in MS response in contaminated documented by Rijal et al. (2010, 2012), Mewafy et al., (2011) and Atekwana et al. (2014), opposed to outside of the plume indicating bioremediation. However in those studies the magnetic susceptibility correlated directly with contaminant plume thickness. Observations in this study suggest a stronger correlation to the initial source contamination locality while still retaining higher readings across the WTFZ as seen in figures 13 and 14. This relationship can by interpreted several ways including:(1) that higher measured magnetic susceptibility is likely associated with the initial source contamination at this particular site, further supporting the idea that this sites remediation is occurring at a very slow rate, or (2) that despite plume thickness being evenly distributed, the area associated with the higher MS readings correlates with free phased contaminants opposed to dissolved phase as in Atekwana et al. (2014), (3) contaminant thickness has no effect on MS measurements but rather contaminant remediation byproducts, such as more elementary organic carbon as seen in Ameen et al., (2014), or possibly (4) a physiological control as there is a strong correlation with the highest WTFZ MS measurements and steeply dipping hydraulic gradient that increases magnetite production via remediation. (figure 16), which coincidentally coincides with the first mentioned possibility. The magnetic susceptibility associated with the south eastern well MW-30 is also likely omissible as it is near an excavated residential infrastructure of an unknown origin, but likely a basement or septic tank given its depth, which could add a multitude of contaminants affecting the geochemistry.

Using magnetic susceptibility as a proxy for remediation there is observed relative MS increases in the contaminated core samples extracted from the south east seen earlier in figure 10. Detection of these increased MS is likely related to the type of tool used. In the borehole, measurements were averaged over 16 in, whereas in the core samples magnetic susceptibility was averaged over 3 cm. However the difference between borehole measurements within the main plume body must be addressed. Analyzing the geochemical data, we notice first there is indications of biologic remediation occurring throughout the plume seen in figure 17 by the increase in δ13 carbon found within the plume. Due to the low magnetic response found throughout we must infer that there is something impeding magnetite production. Furthermore, some of the values of iron shown in figure 19 fall below the critical 1mmol/L (~54ppm) suggested in Atekwana et al. (2012) for minimum concentrations for magnetite precipitation. Comparing the interplume iron measurements to the background measurements in ground water, we can infer that there is a semi closed system associated with the plume that does not allow for the influx of iron. Iron would normally act as a final electron acceptor in iron redox bacteria metabolisms ultimately resulting in both remediation of contaminants and magnetite precipitation. Measurements in table 6 associated with other major electron acceptors can be seen in appendix B. These maps show no trends associated with the plume, MS measurements, or hydraulic gradients, but rather localized usage of nitrate and magnesium. This therefore illustrates that these constituents are not contributing as electron acceptors throughout the system but rather utilized locally to the well by opportunistic microbes in the in remediation process which would normally occur as seen in figure 19.

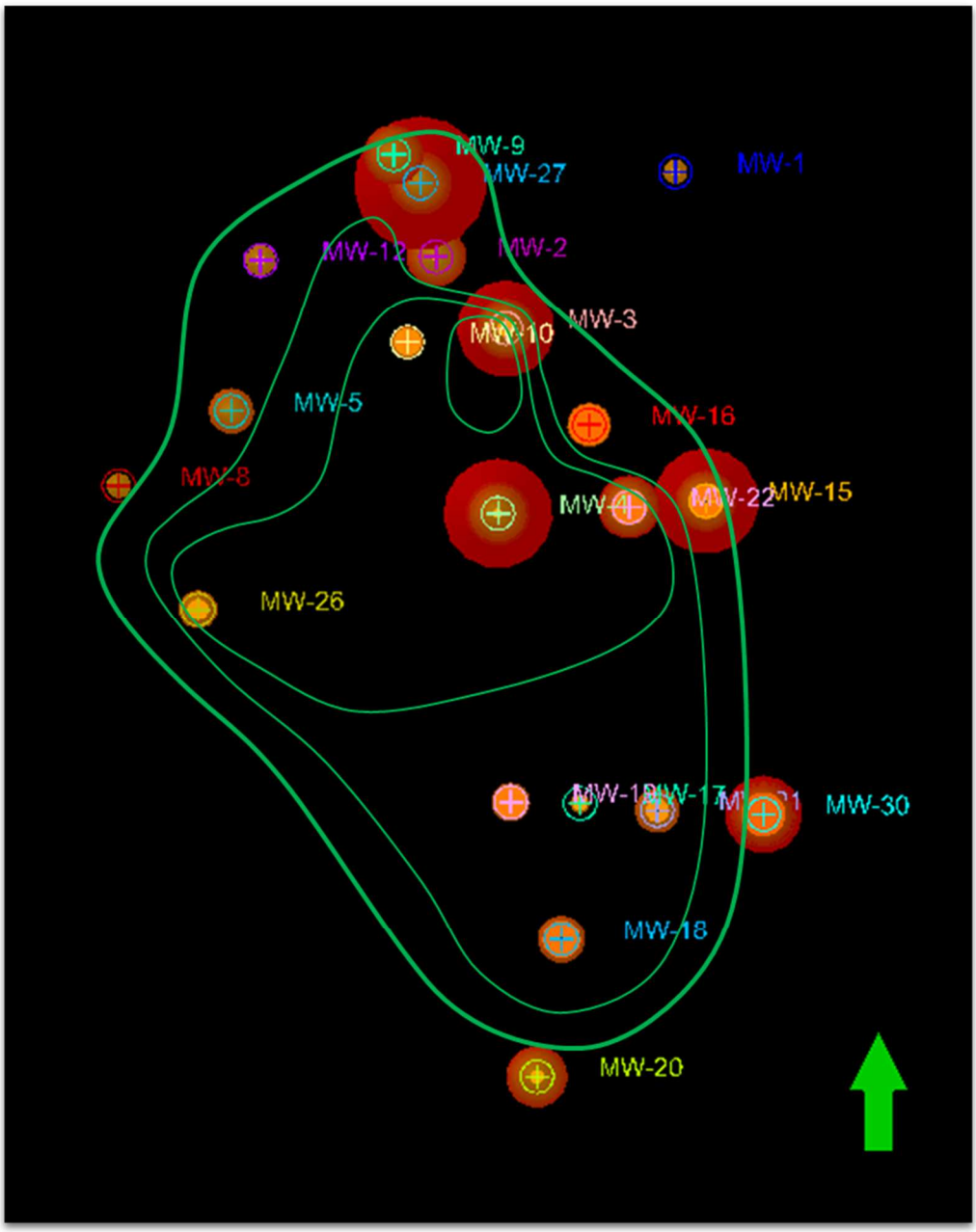

Figure 15 (a) Most recent plume extent (2009) superimposed atop magnetic susceptibility survey (2012). Plume boundary in 1ft contours starting at 0. Magnetic susceptibility strength conveyed through warmer colors and relative size of colored circles.MS scale relative 1000-1100*10^{-6} cgs.

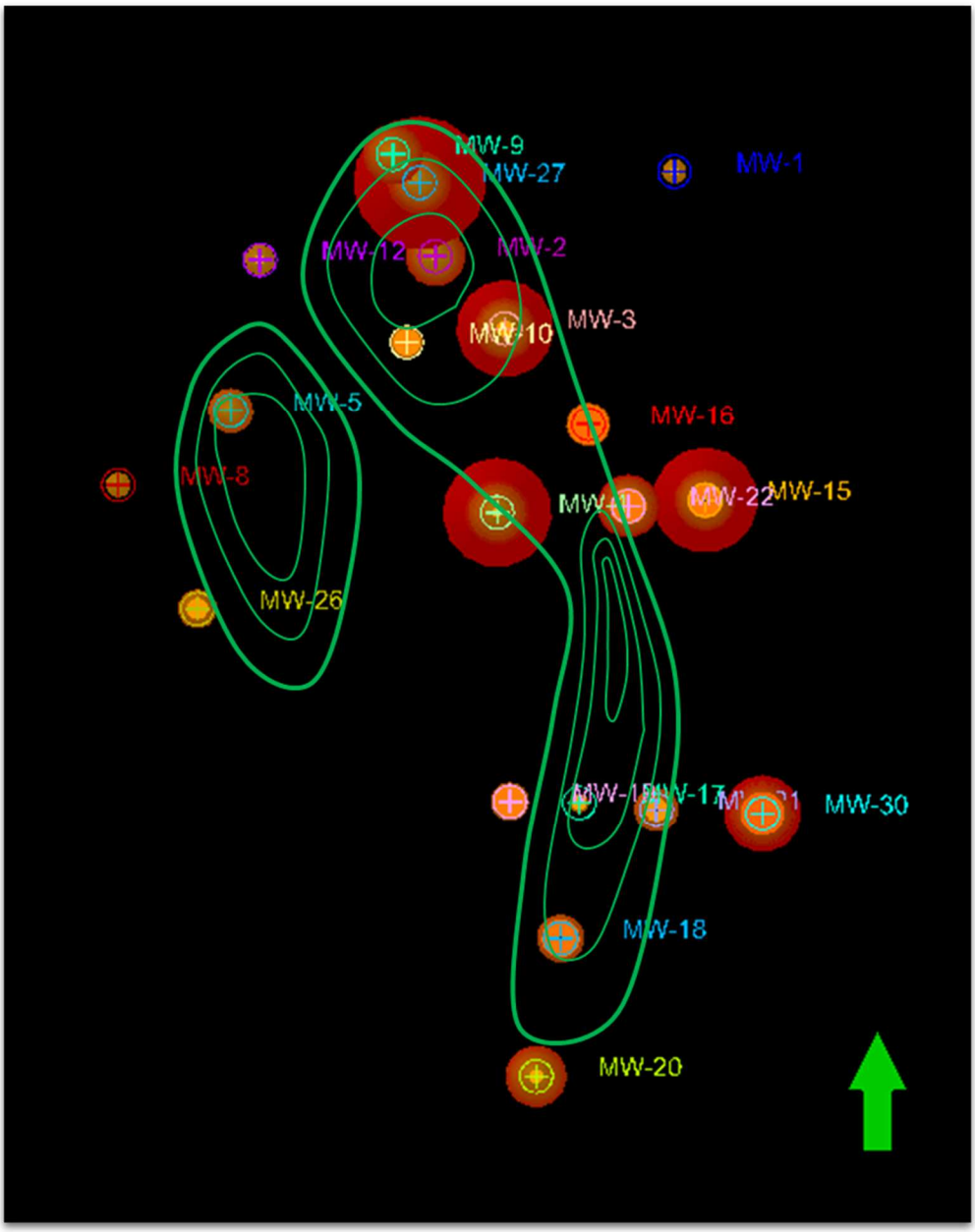

Figure 15 (b) Earliest plume extent (2001) superimposed atop magnetic susceptibility survey (2012). Plume boundary in 1ft contours starting at 0. Magnetic susceptibility strength conveyed through warmer colors and relative size of colored circles. MS scale relative 1000-1100*10^{-6} cgs.

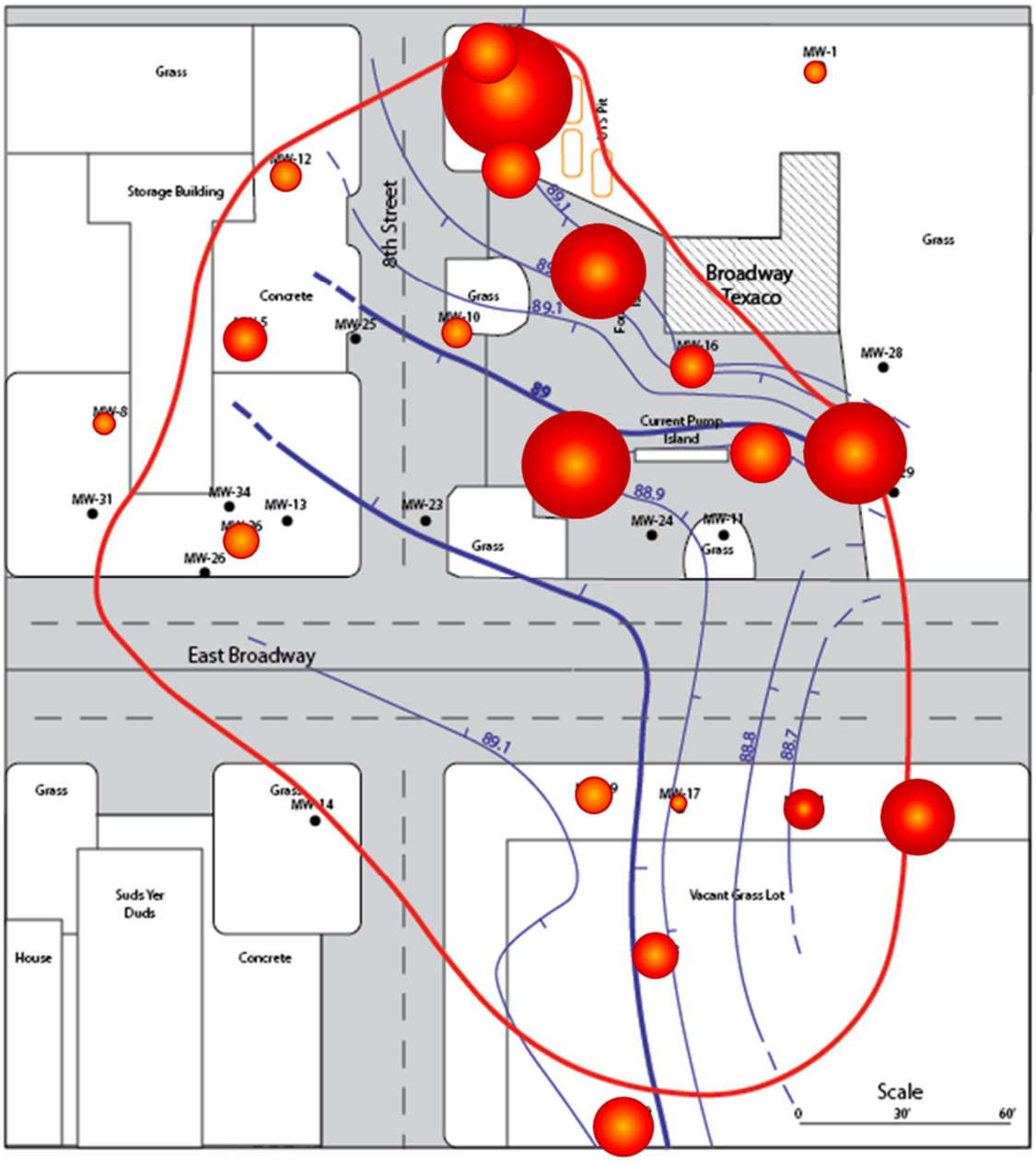

Figure 16. Magnetic susceptibility superimposed on hydraulic gradient map. MS scale relative 1000-1100*10^{-6} cgs.

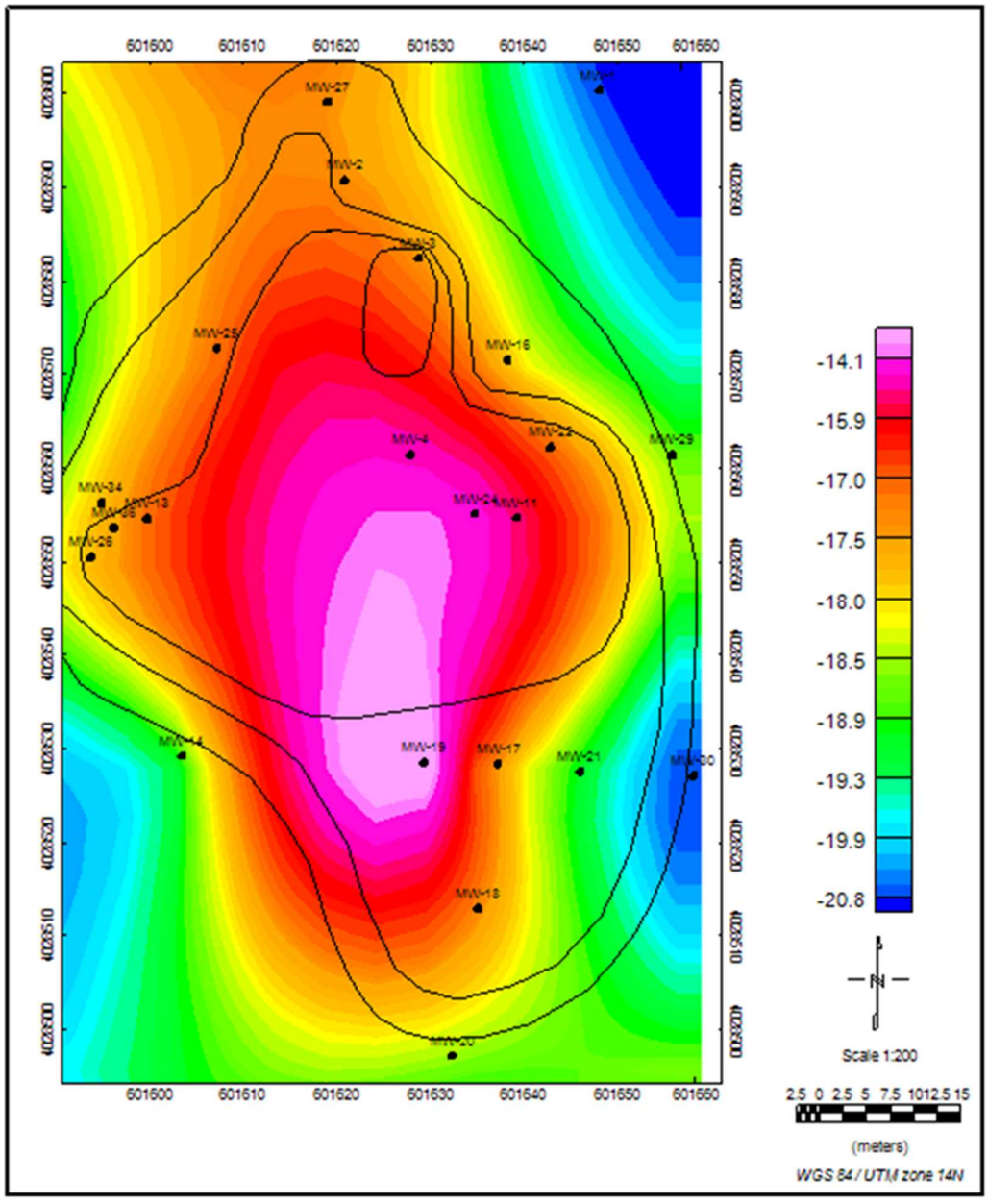

Figure 17. Plume outline superimposed on δ13 Carbon abundance indicating biologic activity associated with hydrocarbon contamination.

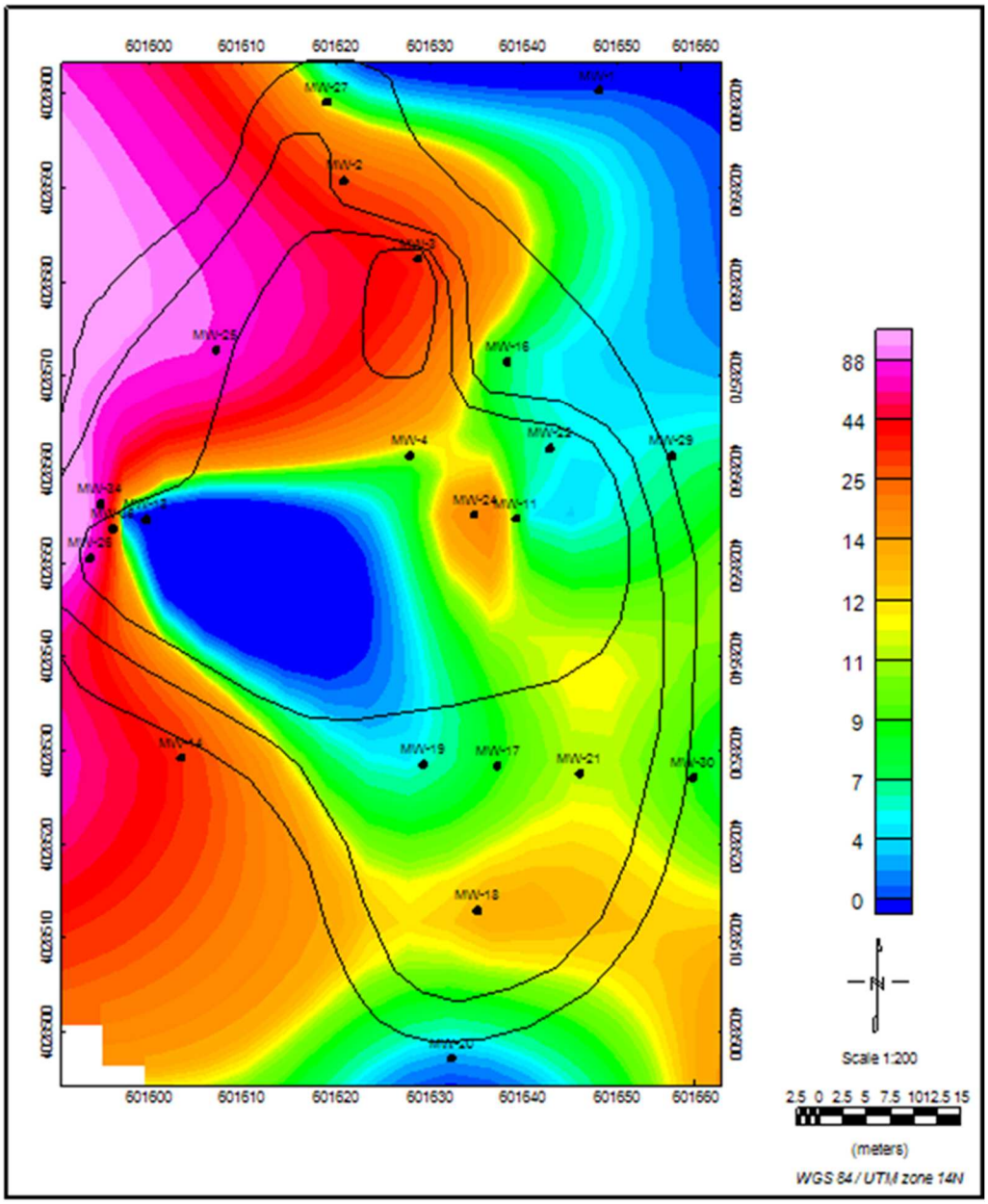

Figure 18. Plume outline super imposed on total iron concentrations in ppm. Note the lack of reds and purples which would be indicative of necessary iron concentrations for magnetite production.

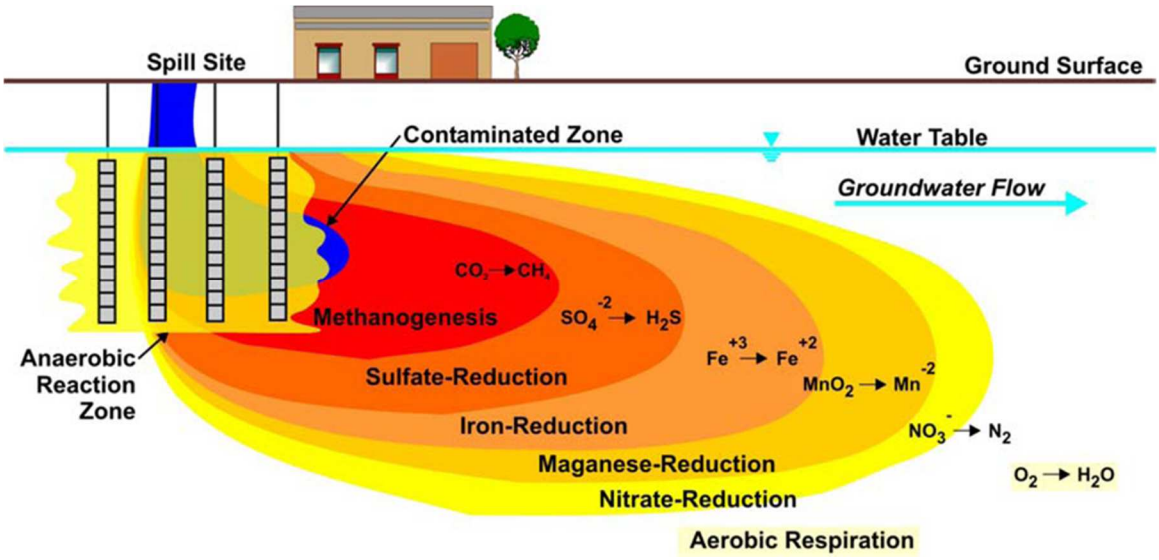

Figure 19. Typical prioritization of major electron acceptors in accordance of contamination proximity. (Modified from Parsons et al., 2005)

Figure 12 is a cross section of magnetic susceptibility cross cutting the thickest portions of the plume. Here we see an increase in in magnetic response across the WTFZ associated with the thickest portions of the plume and a decrease in response as thickness decreases as seen in Atekwana et al. (2012). Another observation is an increase in MS in the the uppermost organic rich portion. Two inferences can be made that cause this upper portions increase in magnetic susceptibility. (1) First since the first half of borehole measurements in this cross section lay beneath thick concrete, there is little anthropogenic atmospheric pollution that can percolate through allowing for iron metabolizing bacteria to produce magnetite. Similarly in the later half of the cross section there is exposed ground near wells allowing for surface input. (2) Second is that the increase in upper borehole measurements is controlled by remediation state. Through methanogenisis or volatilization of contaminants gases escape through the vadose zone. These

volatile gases then collect in the moisture rich organic portion resulting in iron cycle production of magnetite.

CHAPTER VI

CONCLUSION

MS variation across the site contaminated with gasoline in Enid, Oklahoma, show that elevated MS is coincident with zones of contamination. Results also show that the elevated MS occurred within the WTFZ. The above observations are coincident with observations at other hydrocarbon contaminated sites. Differently, our results show that the higher MS was correlated with the source zone in contrast to previous studies that related the MS to higher concentration of organic matter or free product thickness. We conclude that MS is a viable technique for investigating source zone contamination at hydrocarbon contaminated sites.

REFERENCES

Adepelumi, A., Solanke, A., Sanusi, O. B., & Shallangwa, A. M., 2006, Model tank electrical resistivity characterization of LNAPL migration in clayey-sand formation. *Environmental Geology*. Vol. 50 p. 1221-1233.

Archie GE, 1942, The electrical resistivity log as an aid in determining some reservoir characteristics. *T Am Inst Mineral Metall Petrol Eng,* Vol. 146 p. 54–62.

Ameen, N. N., Klueglein, N., Appel, E., Petrovský, E., Kappler, A., & Leven, C., 2014, Effect of hydrocarbon-contaminated fluctuating groundwater on magnetic properties of shallow sediments. *Studia Geophysica Et Geodaetica*, Vol. 58-3 p. 442-460.

Aristodemu E., A. Thomas-Betts., 2000, DC resistivity and induced polarization investigations at a waste disposal site and its environments. *Journal of Applied Geophysics*, Vol. 44, I. 2-3 p. 275–302.

Atekwana, E., Krishnamurthy, R., 1998, Seasonal variations of dissolved inorganic carbon and delta C-13 of surface waters: Application of a modified gas evolution technique, *Journal of Hydrology*, Vol. 205 I. 3-4, p 265-278

Atekwana, E. A, Atekwana E. A., Rowe R. S., Werkema D. D., Legall, F. D., 2004, The relationship of total dissolved solids measurements to bulk electrical conductivity in an aquifer contaminated with hydrocarbon, *Journal of Applied Geophysics*, Vol. 56, I. 4 p. 281-294.

Atekwana, E., Mewafy, F., Abdel Aal, G., Werkema, D., Revil, A., & Slater, L., 2014, High

-resolution magnetic susceptibility measurements for investigating magnetic mineral formation during microbial mediated iron reduction. *Journal of Geophysical Research-Biogeosciences,* I. 119-1 p. 80-94

Atekwana EA, Sauck WA, Werkema DD Jr, 2000, Investigations of geoelectrical signatures at a hydrocarbon contaminated site. *J Appl Geophys*, Vol. 44 p. 167–180.

Bartington Instruments, 2015, Bartington Instruments Operation Manual.

Boudreault, J.,Et. Al., 2010, Geophysical characterization of contaminated urban fills. *Engineering Geo,* Vol 116 I. 3-4 p. 196-206.

Che-Alota, V., 2009, Temporal geophysical and geochemical signatures due to contaminant source reduction at Wurtsmith Airforce Base in Oscoda, Michigan, USA (Order No. 1467180). Available from Dissertations & Theses @ Oklahoma State University – Stillwater

Cioppa, M. T., 1997, Paleo- and environmental magnetic investigations in the Appalachians of Pennsylvania. Order No. 9715034

Clément, R., M. Descloitres, T. Gunther, L. Oxarango, C. Morra, J-P. Laurent, J-P. Gourc, 2009, Improvement of electrical resistivity tomography for leachate injection monitoring. *Waste Management,* Vol. 30 I. 3 p. 452-464

Clément, R., L. Oxarango, M. Descloitres, 2011, Contribution of #-D time-Lapse ERT t the study of leachate recirculation in a landfill. *Waste Management,* Vol. 31 I. 3 p.457-467

Dahlin, T., M.H Loke, 1998, Resolution of 2D Wenner resistivity imaging as assessed by numerical Modelling. *Journal of Applied Geophysics*, Vol. 38 I. 4 p. 237-249

Fels, J. B., 1999, Source-identification investigations of petroleum contaminated groundwater in the Missouri Ozarks, *Engineering Geology*, Vol. 52, I. 1–2 p. 3-13

Garming, J. F. L., Bleil, U., & Riedinger, N., 2005, Alteration of magnetic mineralogy at the sulfate–methane transition: Analysis of sediments from the argentine continental slope. *Physics of the Earth and Planetary Interiors*, Vol. 151 I. 3 p. 290-308.

Gemail, K., 2015, Application of 2D resistivity profiling for mapping and interpretation of geology in a till aquitard near luck lake, southern Saskatchewan, Canada. *Environmental Earth Sciences*, Vol. 73 I. 3 p. 923-935

Gibson, R. I., & P. S. Millegan, 1998, Geologic applications of gravity and magnetics: Case histories. Tulsa, OK: Published jointly by the Society of Exploration Geophysicists and the American Association of Petroleum Geologists.

Halihan, T., S. Paxton, M. McPhail, H. McSorley, and M. Riley, 2005a, Final Report for: Environmental Characterization and Monitoring of LNAPL Using Electrical Resistivity Tomography (ERT) and Hydraulic Push Techniques, Oklahoma Corporation Commission.

Halihan, T.,S. Paxton, I. Graham, T. Fenstemaker, and M. Riley, 2005b, Post-Remediation Evaluation of a LNAPL Site Using Electrical Resistivity Imaging, *Journal of Environmental Monitoring*, Vol. 7, p. 1−6.

Hansel, C. M., S. G. Benner, J. Neiss, A. Dohnalkova, R. K. Kukkadapu, & S. Fendorf, 2003, Secondary mineralization pathways induced by dissimilatory iron reduction of ferrihydrite under advective flow. *Geochimica Et Cosmochimica Acta*, Vol 67 I. 16 p. 2977-2992

Hendry, M., L. Wassenaar, 2004, Transport and geochemical controls on the distribution of solutes and stable isotopes. *Isotopes in Environmental and Health Studies* Vol. 40 I. 1 p. 3-19

Jeffries, S. N.,2011, Transient hydrogeophysical investigation of a gasoline impacted site, Enid,

Oklahoma: Electronic resource. Available from Dissertations & Theses @ Oklahoma State University – Stillwater.

Kaufmann, O., & Deceuster, J., 2007, A 3D resistivity tomography study of a LNAPL plume near a gas station at Brugelette (Belgium). *Journal of Environmental & Engineering Geophysics,* Vol. 12 I. 2 p. 207-219

Klueglein, N., Losekann-Behrens, T., Obst, M., Behrens, S., Appel, E., & Kappler, A., 2013, Magnetite formation by the novel Fe(III)-reducing geothrix fermentans strain HradG1 Isolated from a hydrocarbon-contaminated sediment with increased magnetic susceptibility. *Geomicrobiology Journal*, Vol. 30 I. 10 p. 863-873.

Kuras, O. J. D. Pritchard, P. I. Meldrum, J. E. Chambers, P. B. Wilkinson, R. D. Ogilvy, G. P. Wealthall , 2009, Monitoring hydraulic processes with automated time-lapse electrical resistivity tomography. *Comptes Rendus Geoscience,* Vol. 341 I. 10-11 p. 868-885

Lipson, D., & Siegel, D. I., 2000, Using ternary diagrams to characterize transport and attenuation of BTX. *Ground Water,* Vol. 38 I. 1, p. 106-113.

Liu, Q., Liu, Q., Chan, L., Yang, T., Xia, X., & Cheng, T., 2006, Magnetic enhancement caused by hydrocarbon migration in the Mawangmiao oil field, Jianghan basin, China. *Journal of Petroleum Science and Engineering*, Vol. 53 I. 1, p. 25-33.

McDowell, C. J., Buscheck, T., & Powers, S. E., 2003, Behavior of gasoline pools following a denatured ethanol spill. *Ground Water,* Vol. 41 I. 6, p. 746-757.

McPhail, M. L., 2003, Geological controls on the location and distribution of an LNAPL plume at a site in Enid, Oklahoma. Master of Science thesis, Oklahoma State University, Stillwater Oklahoma

McSorley, J., 2003, Direct Push Electrical Resistivity Tomography to Detect LNAPL, Master of Science Thesis, Oklahoma State University. Stillwater, Oklahoma.

Metwaly, M., M. Khalil, E. Al-Sayed, A. El-Kenawy, 2012, Tracing subsurface oil pollution leakage using 2D electrical resistivity tomography. *Arabian Journal of Geosciences,* 10.1007/s12517-012-0600-z

Mewafy, F., Atekwana, E., Werkema, D., Slater, L., Ntarlagiannis, D., Revil, A., Delin, G., 2011, Magnetic susceptibility as a proxy for investigating microbially mediated iron reduction. Geophysical Research Letters, Vol. 38 I. 21

Ng, G., Bekins, B. A., Cozzarelli, I. M., Baedecker, M. J., Bennett, P. C., & Amos, R. T., 2014, A mass balance approach to investigating geochemical controls on secondary water quality impacts at a crude oil spill site near bemidji, MN. *Journal of Contaminant Hydrology,* Vol. 164, p. 1-15

Noubactep, C., Caré, S., & Crane, R., 2012, Nanoscale metallic iron for environmental remediation: Prospects and limitations. *Water, Air, & Soil Pollution*, Vol. 223 I. 3, p. 1363-1382.

Parsons, 2004, Principles and Practices of Enhanced Anaerobic Bioremediation of Chlorinated Solvents. AFCEE, NFEC, ESTCP p. 457

Perez, I. F. Romero, O. Zamora, and M. Gutierrez-Ruiz, 2014, Magnetic susceptibility and electrical conductivity as a proxy for evaluating soil contaminated with arsenic, cadmium and lead in a metallurgical area in the san luis potosi state, mexico. Environmental Earth sciences, Vol.72 I. 5 p. 1521-1531

Porsch, K., M. L. Rijal, T. Borch, L. D. Troyer, S. Behrens, F. Wehland, E. Appelm A. Kappler,

2013, Impact of Organic Carbon and Iron Bioavailability on the Magnetic Susceptibility of Soils. *Geochimica et Cosmochimica Acta* (accepted manuscript)

Potter, D., 2007, Magnetic susceptibility as a rapid, nondestructive technique for improved petrophysical parameter prediction. *Petrophysics*, Vol. 48 I. 3, p. 191-201.

Riedinger, N., Pfeifer, K., Kasten, S., Garming, J. F. L., Vogt, C., & Hensen, C., 2005, Diagenetic alteration of magnetic signals by anaerobic oxidation of methane related to a change in sedimentation rate. *Geochimica Et Cosmochimica Acta*, Vol. 69 I. 16, p. 4117-4126.

Rijal, M., K. Porsch,E.Appel, and A. Kappler, 2012, Magnetic signature of hydrocarbon-contaminated soils and sediments at the former oil field Hanigsen, Germany, *Stud. Geophys. Geod.*, Vol. 158 I. 5 p. 889-908.

E Viollier, P.W Inglett, K Hunter, A.N Roychoudhury, P Van Cappellen, 2000, The ferrozine method revisited: Fe(II)/Fe(III) determination in natural waters, Applied Geochemistry, Vol. 15, I. 6, p. 785-790

Watts, R. J., Daniel R Haller, Alexander P Jones, Amy L Teel, 2000, A foundation for the risk-based treatment of gasoline-contaminated soils using modified Fenton's reactions, Journal of Hazardous Materials, Vol. 76, I. 1-28, p. 73-89

APPENDICES

APPENDIX A: MAGNETIC SUSCEPTIBILITY OF WELLS

Individual magnetic susceptibility measurements given in the text were all in cgs *10^-6, however measurements for monitoring wells were logged in cgs *10^-5 ranging from 1000-1100.

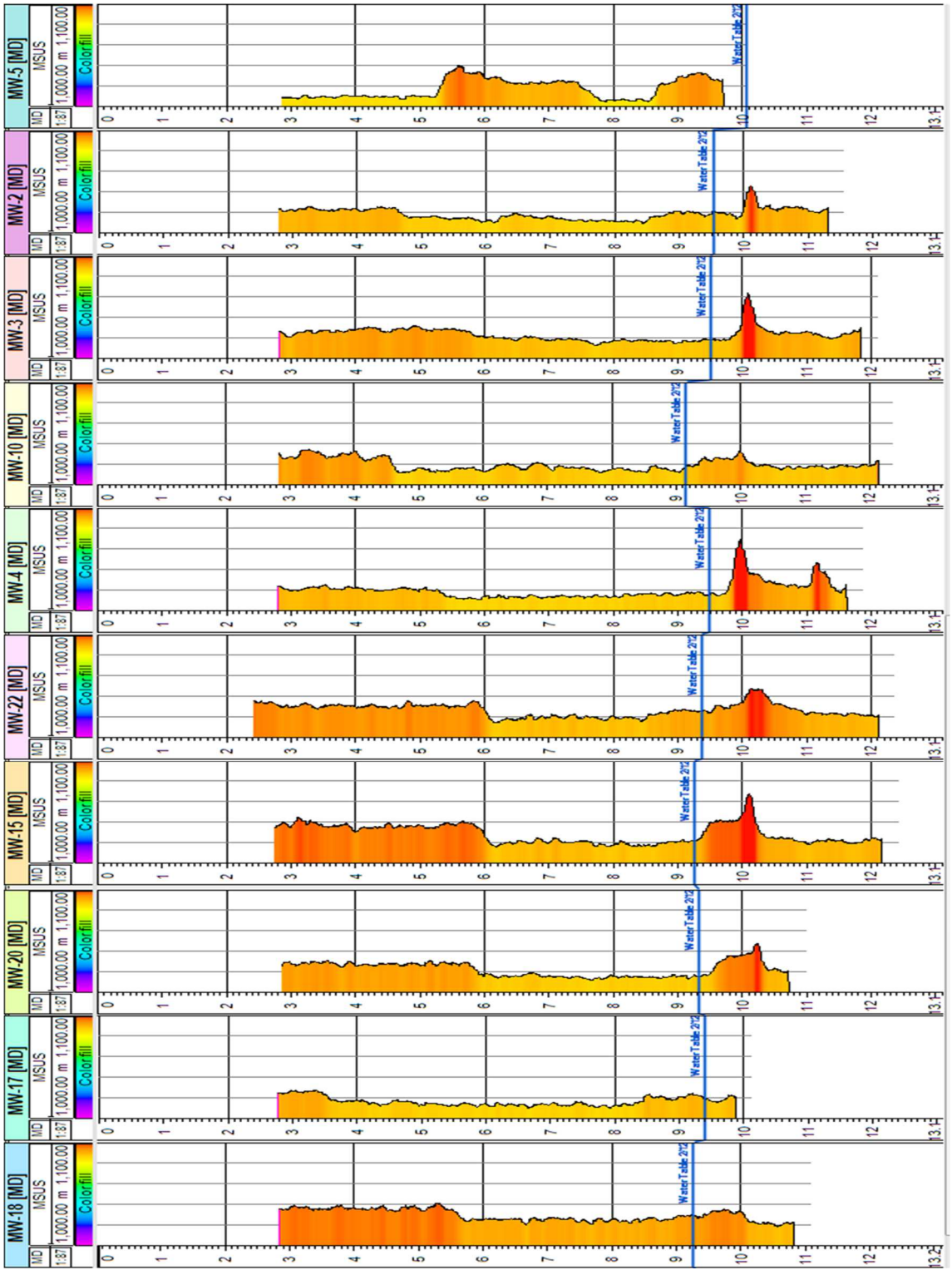
MW-5 [MD]
MW-2 [MD]
MW-3 [MD]
MW-10 [MD]
MW-4 [MD]
MW-22 [MD]
MW-15 [MD]
MW-20 [MD]
MW-17 [MD]
MW-18 [MD]
MD
1:87
MSUS
1,000.00 m 1,100.00
Colorfill
Water Table 2012

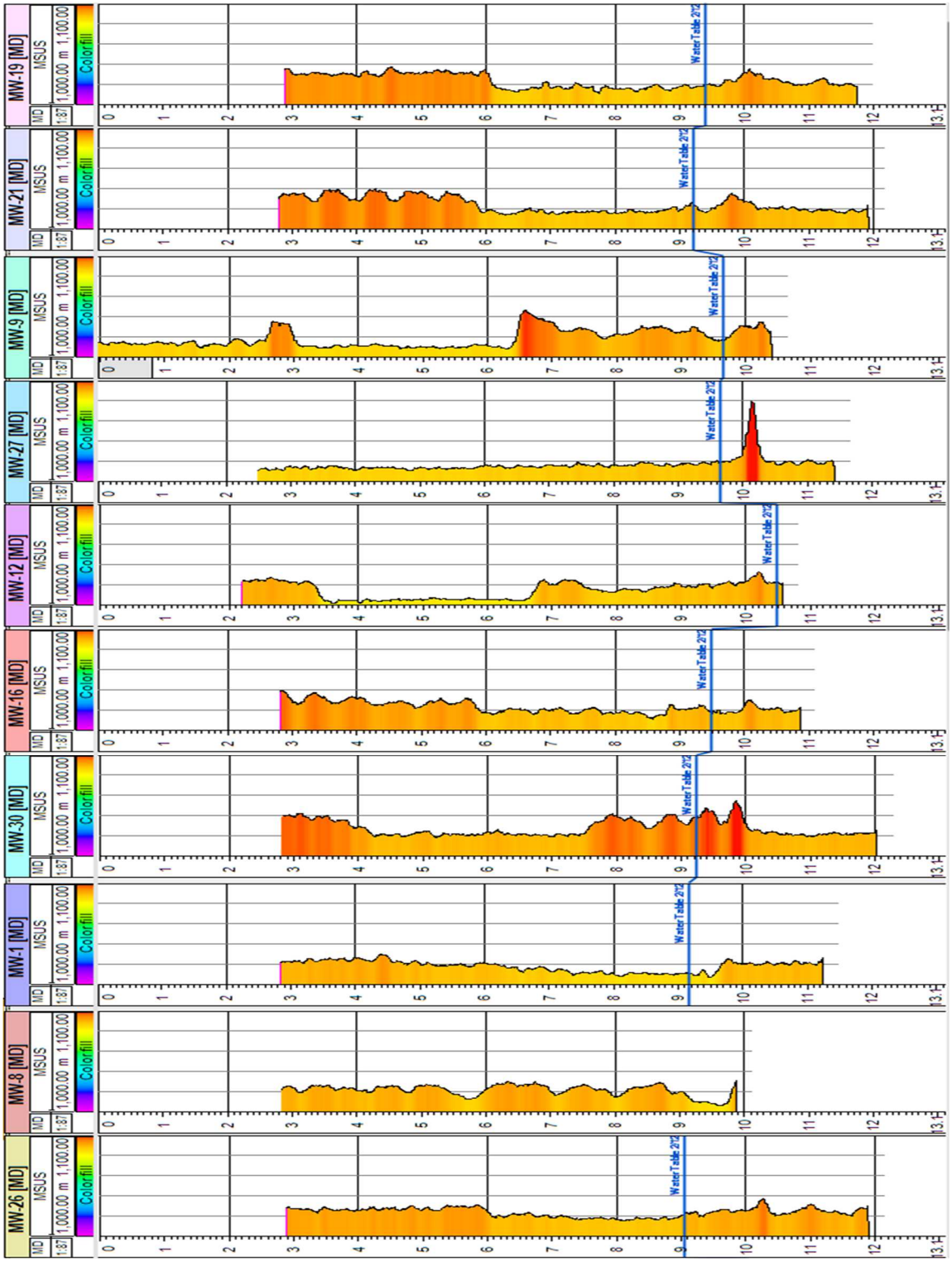
MW-19 [MD]
MW-21 [MD]
MW-9 [MD]
MW-27 [MD]
MW-12 [MD]
MW-16 [MD]
MW-30 [MD]
MW-1 [MD]
MW-8 [MD]
MW-26 [MD]
MD
MSUS
1:87
1,000.00 m 1,100.00
Colorfill
Water Table: 2/12

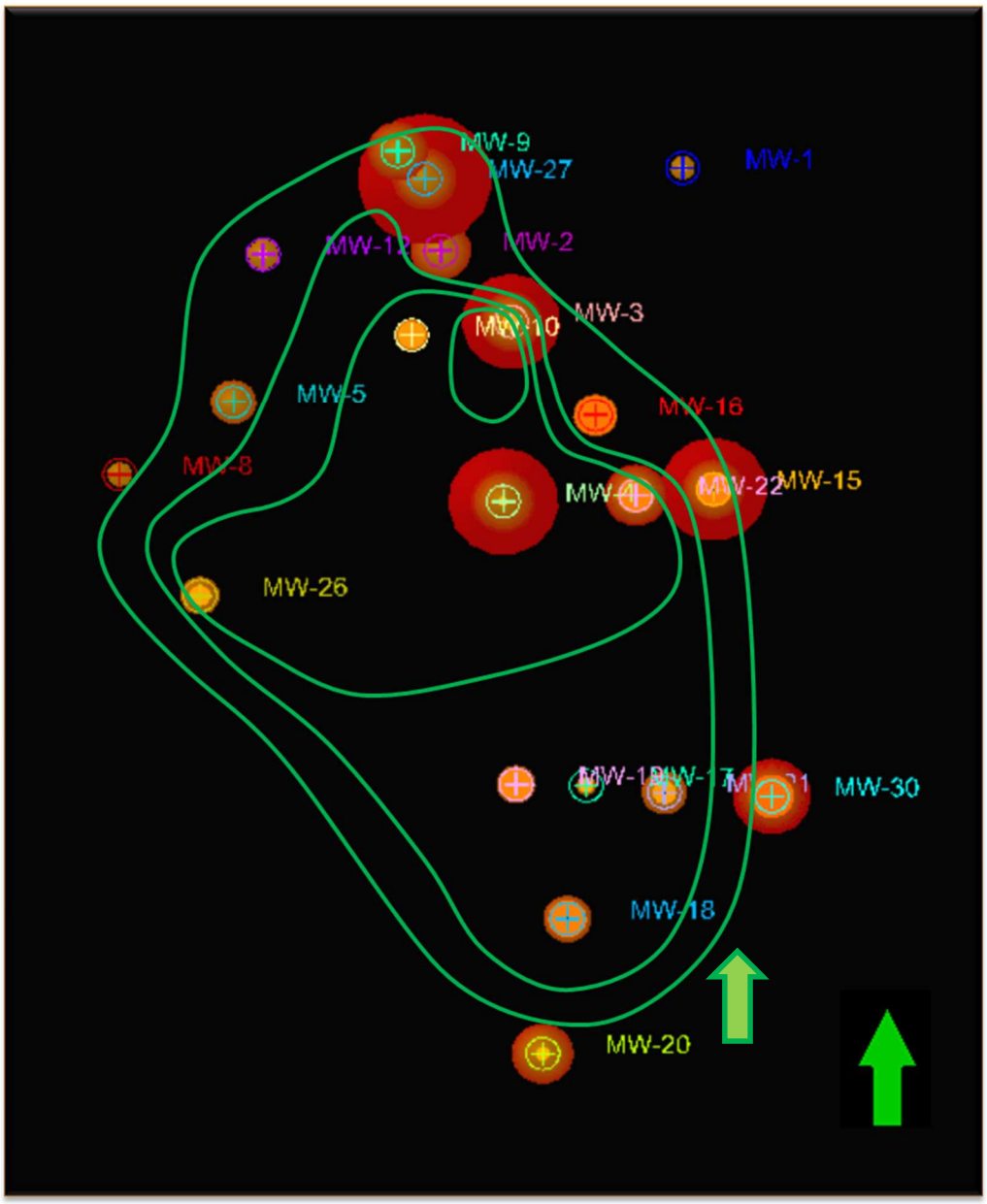

Variable map view of the MS measurments associated with monitoring wells. Width of circles with deeper reds indicate relative higher MS values. Green outline indicates plume edge.

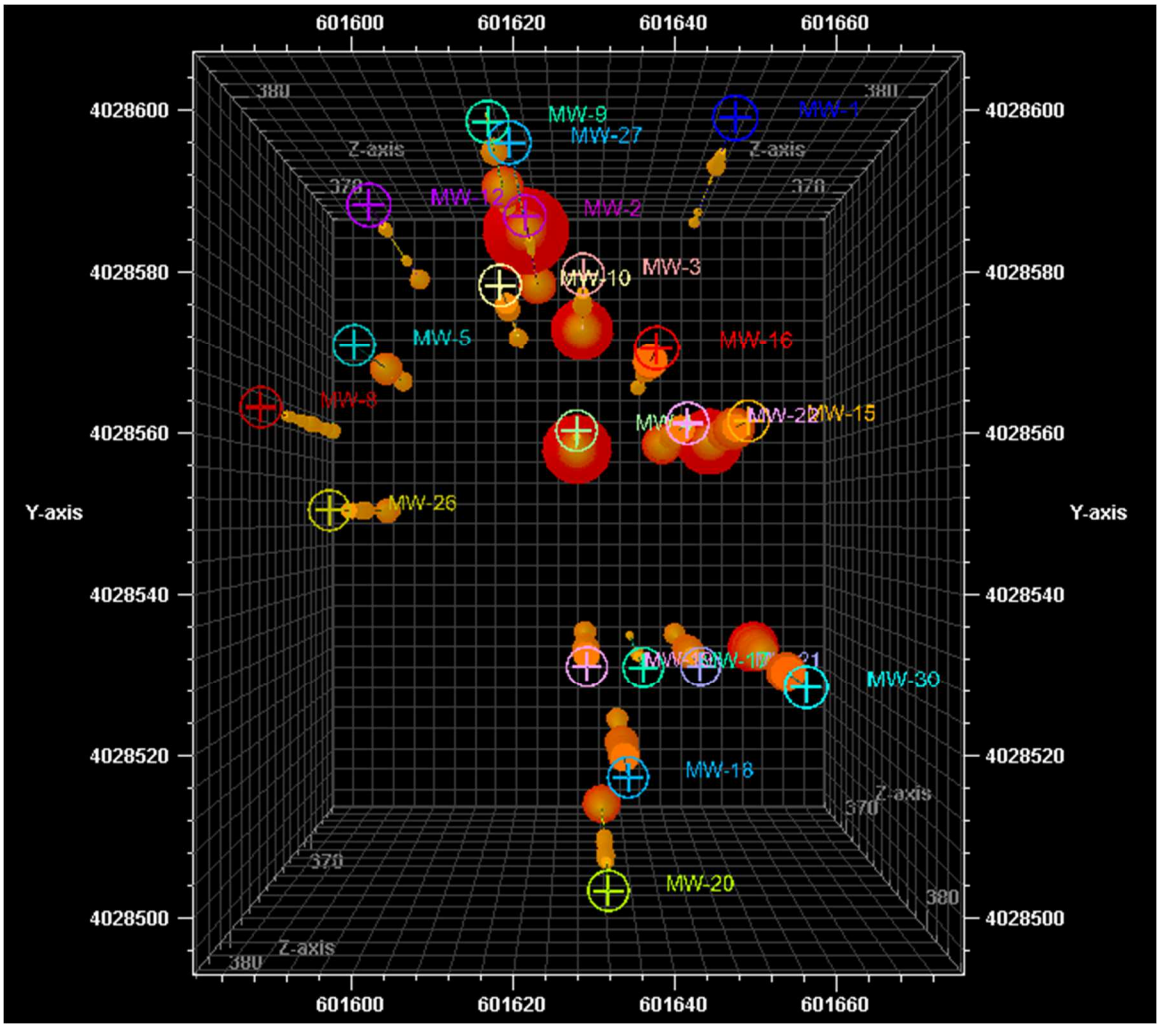

Variable 3D view of the monitoring well MS measurements

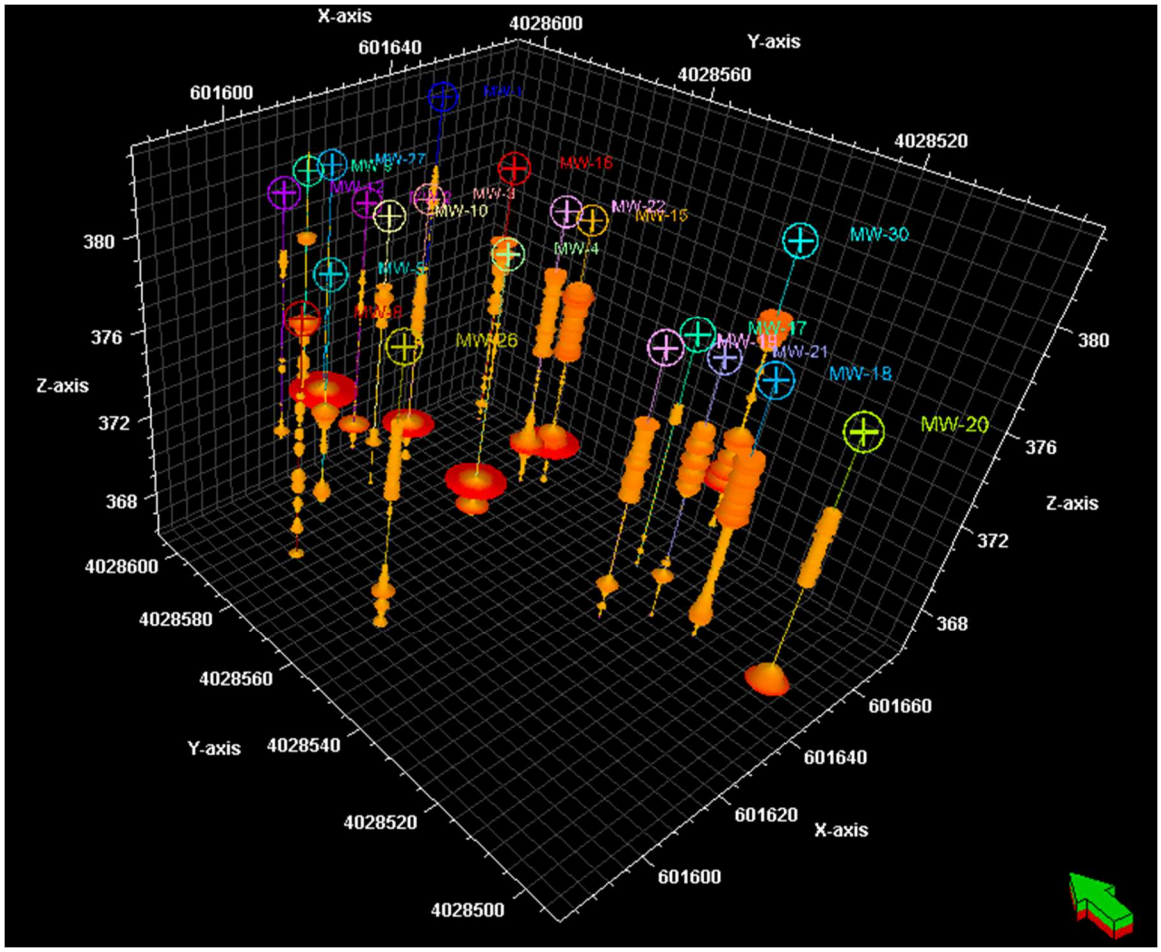

Variable View of the MS measurements of the monitoring wells

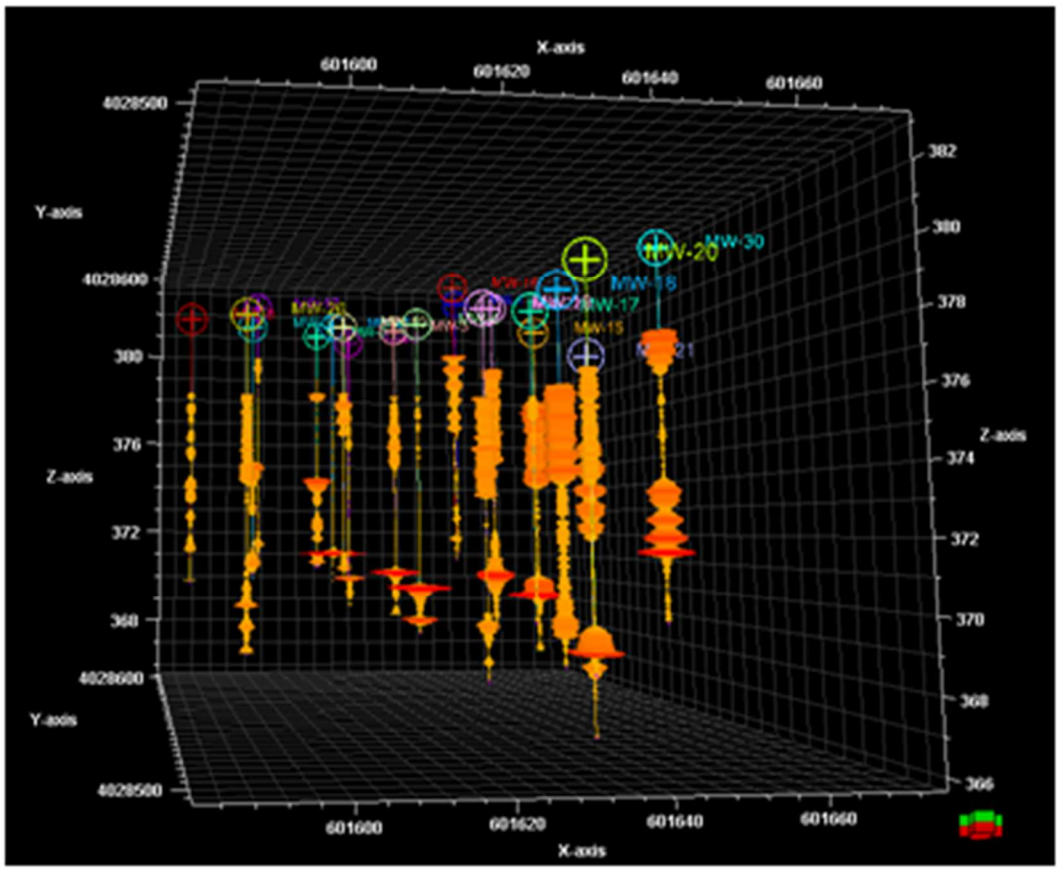

Variable view of the MS measurements of the monitoring wells

APPENDIX B: GEOCHEM MAPS

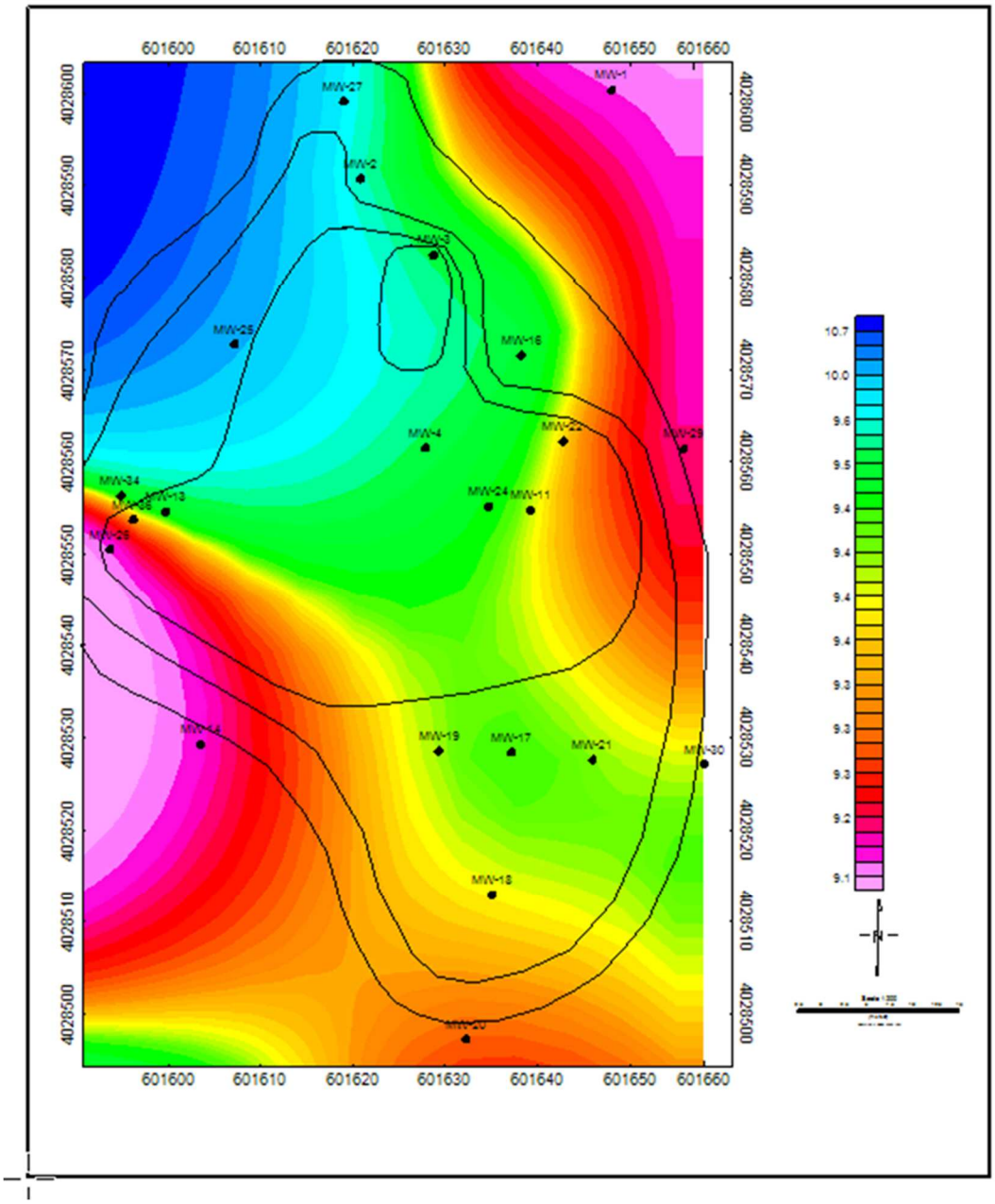

Water table depth (m), February 2012. Outline indicates plume boundary with 1ft contour lines.

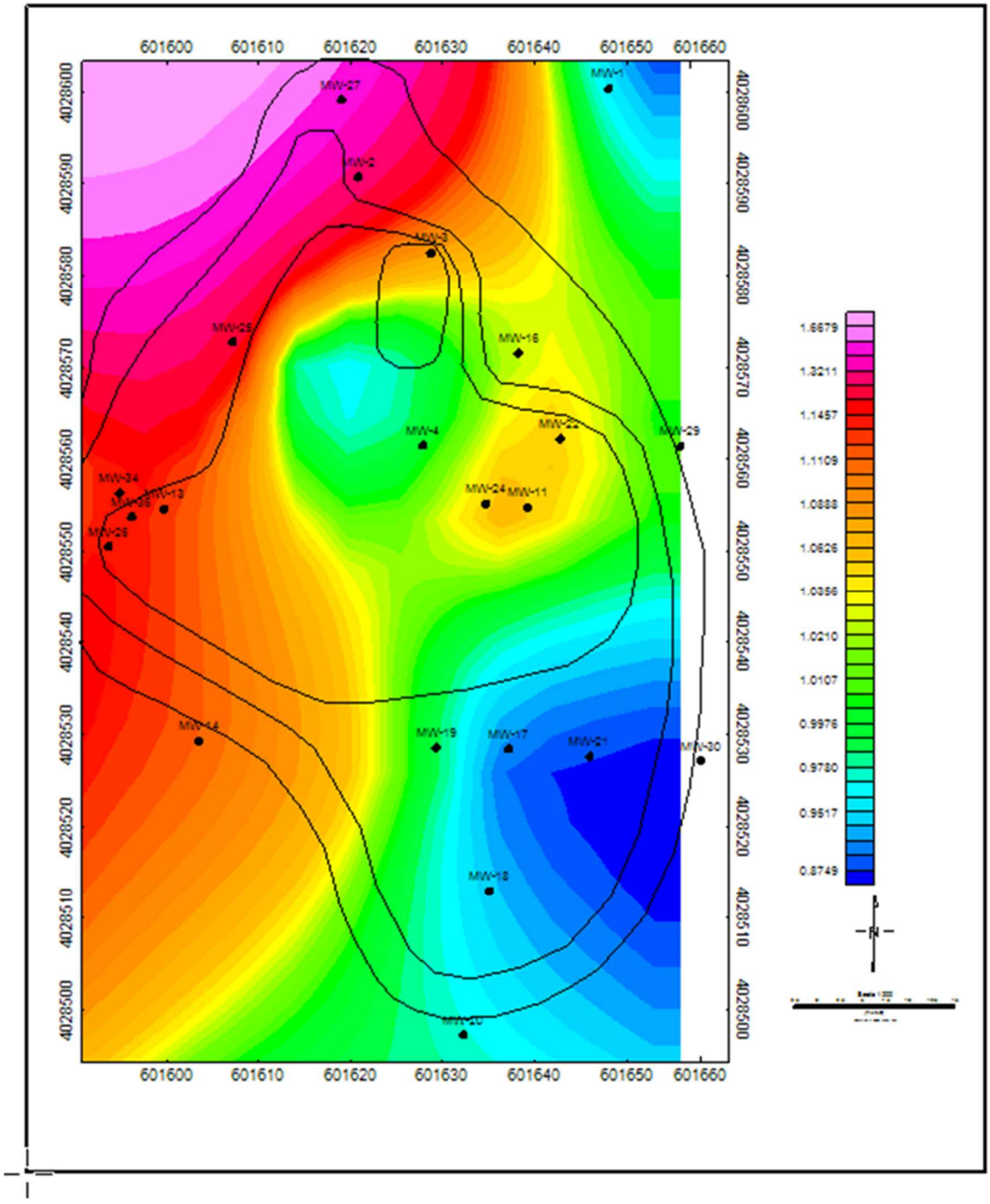

Total Dissolved Solids (g/L), February 2012. Outline indicates plume boundary with 1ft contours.

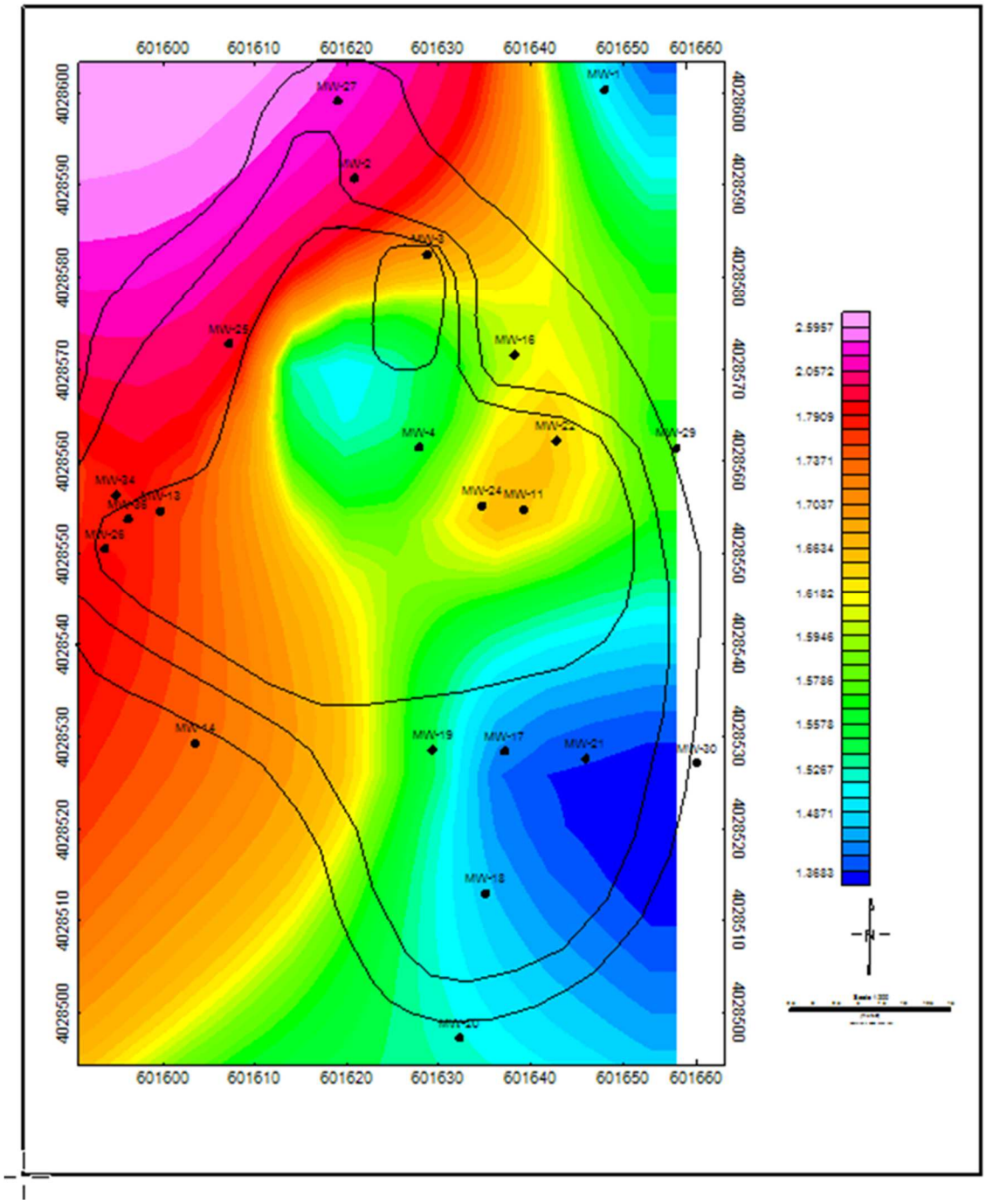

Specific Conductance (µS): February, 2012. Outline indicates plume boundary with 1ft contours.

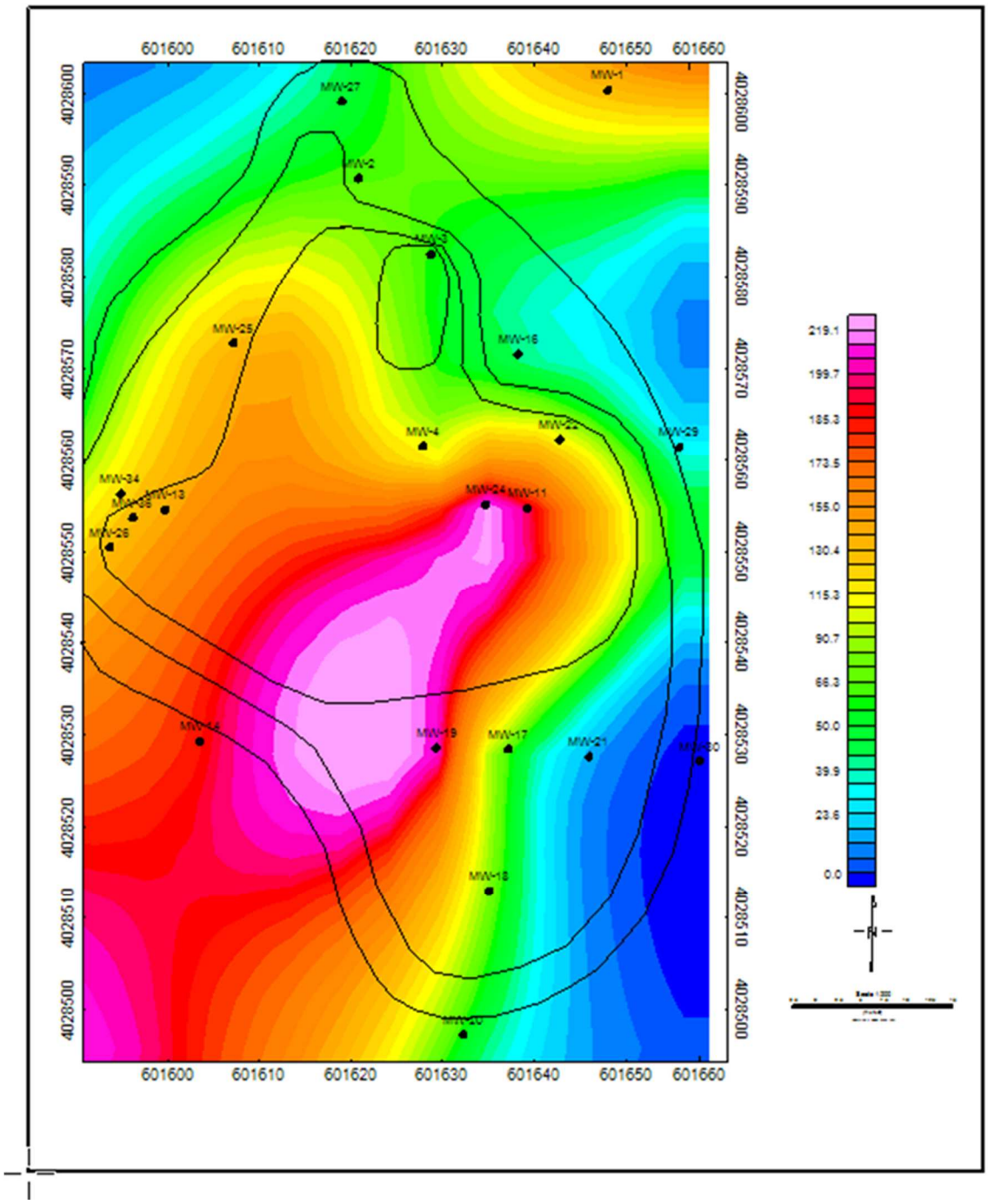

SO_4 (g/L), February 2012. Outline indicates plume boundary with 1ft contours.

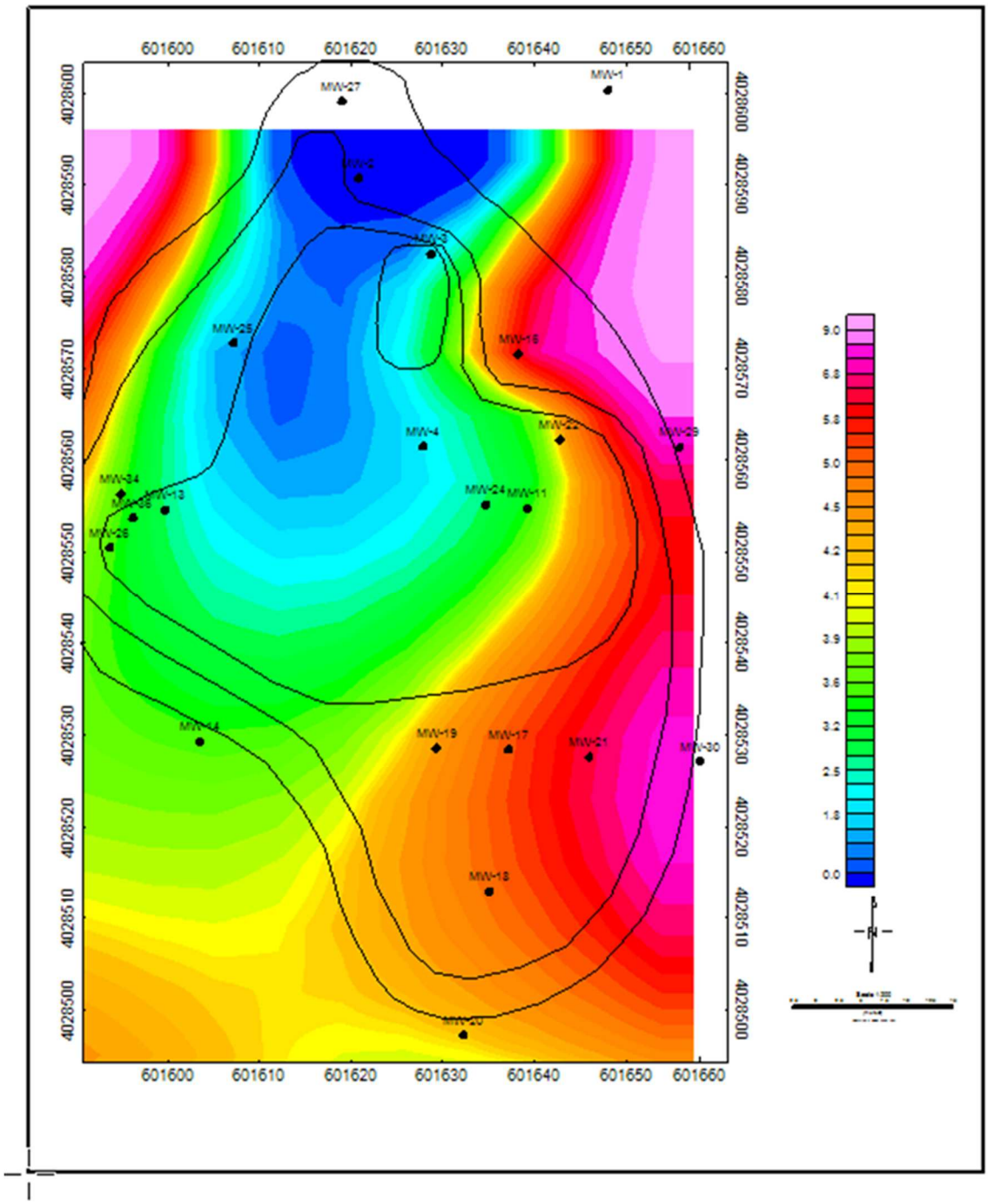

PO_4 (g/L), February 2012. Outline indicates plume boundary with 1ft contours.

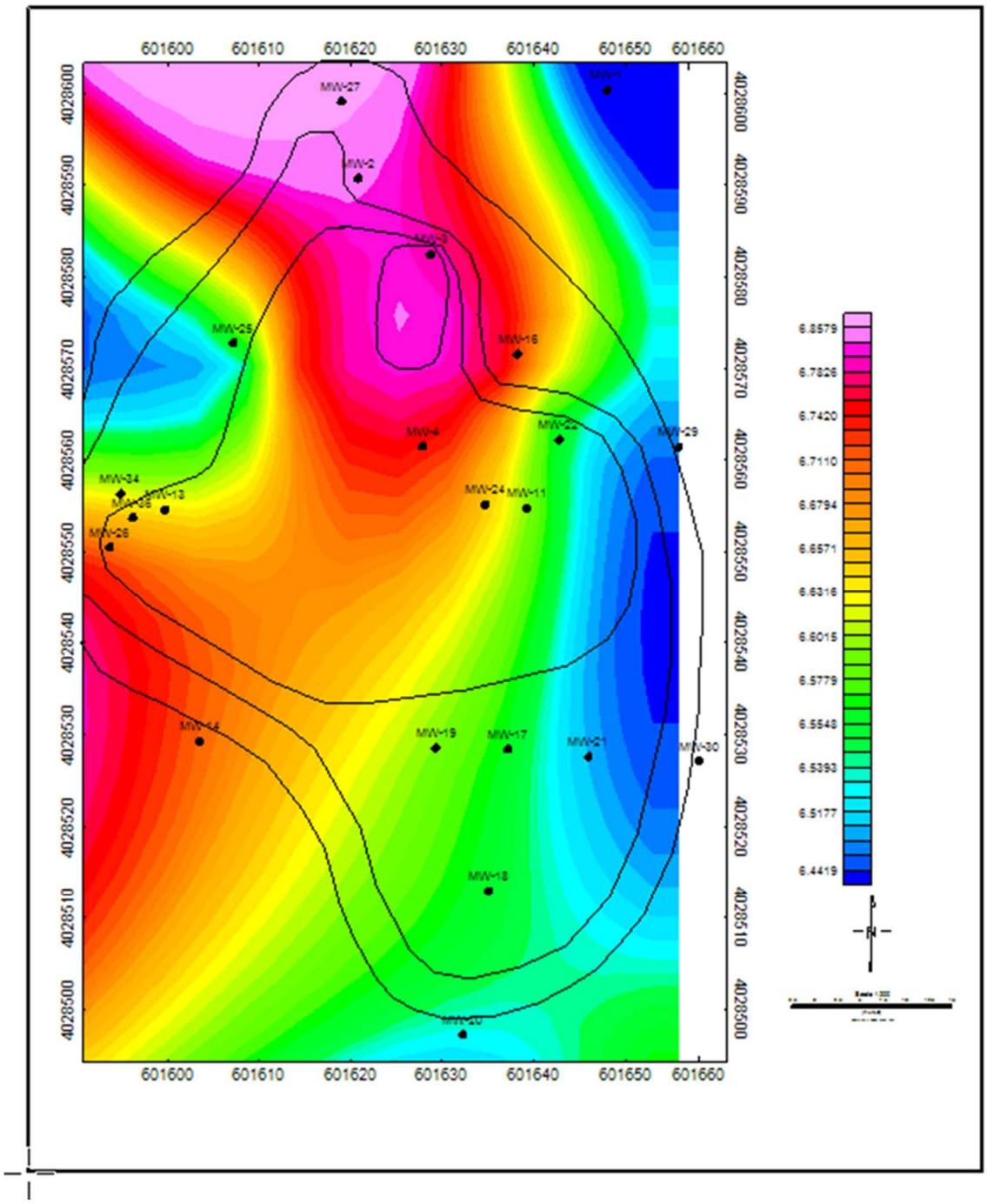

pH, February 2012. Outline indicates plume boundary with1ft contours.

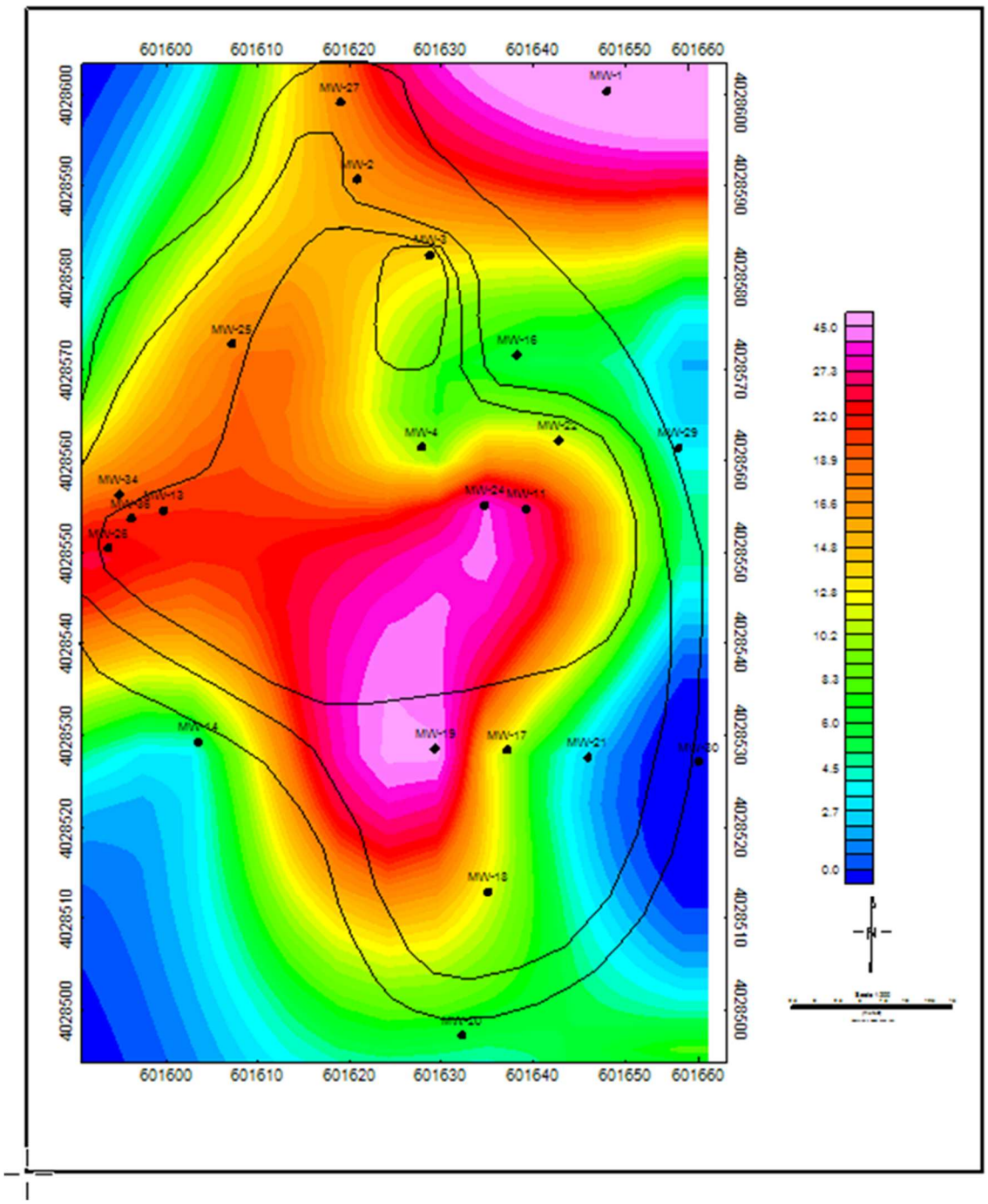

NO_3 (g/L), February 2012. Outline indicates plume boundary with1ft contours.

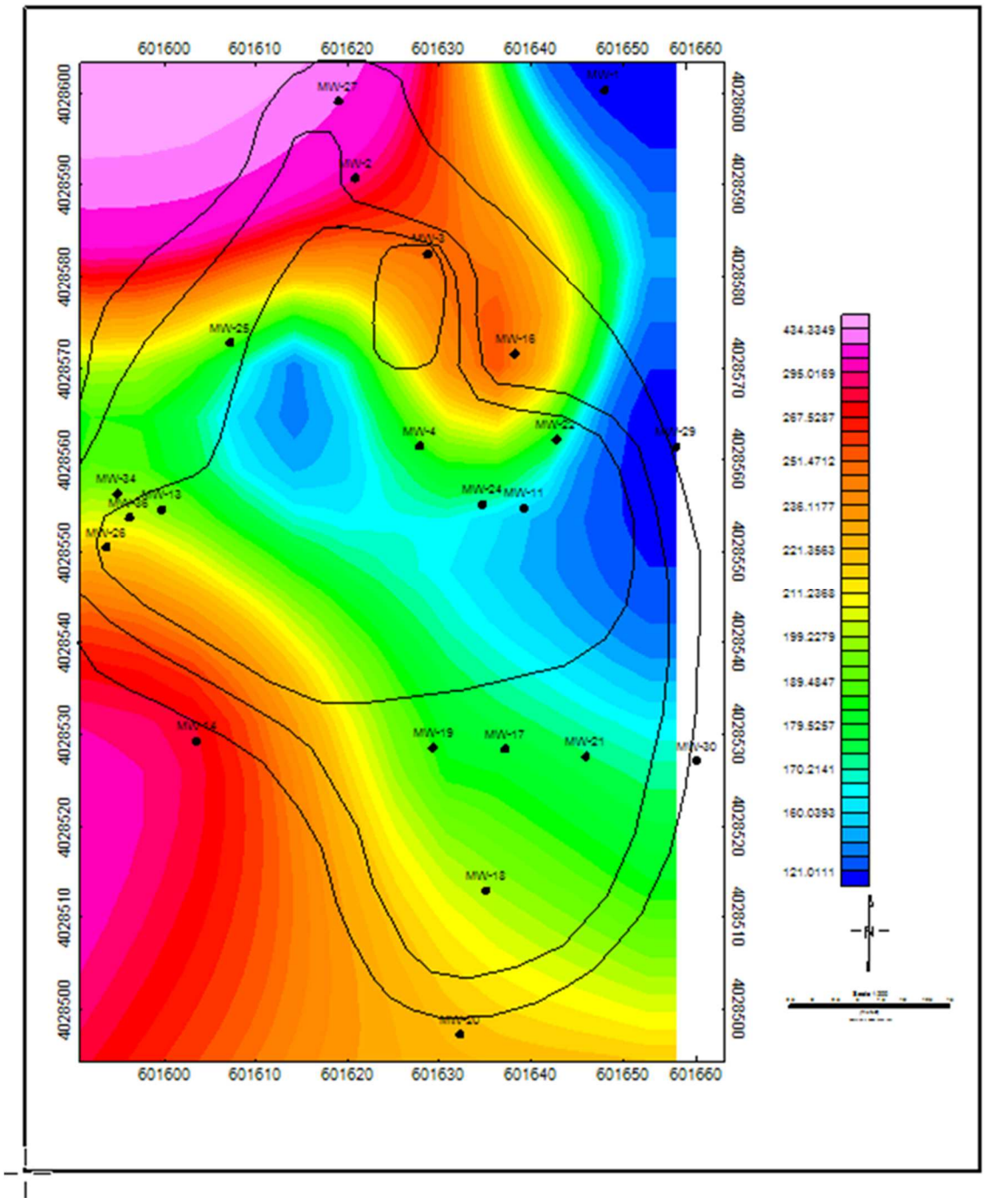

Na (g/L), February 2012. Outline indicates plume boundary with 1ft contours.

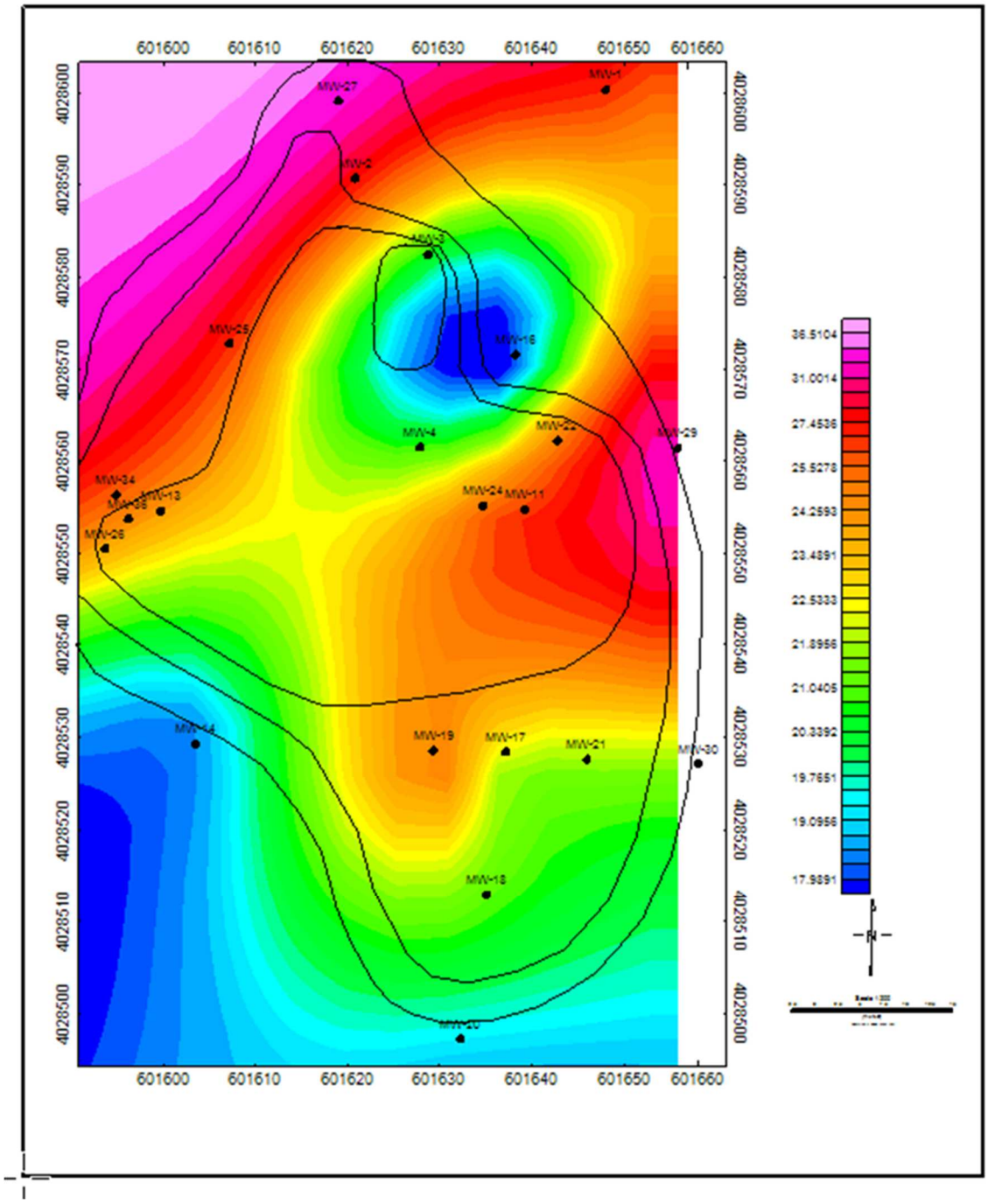

Mg (g/L), February 2012. Outline indicates plume boundary with 1ft contours.

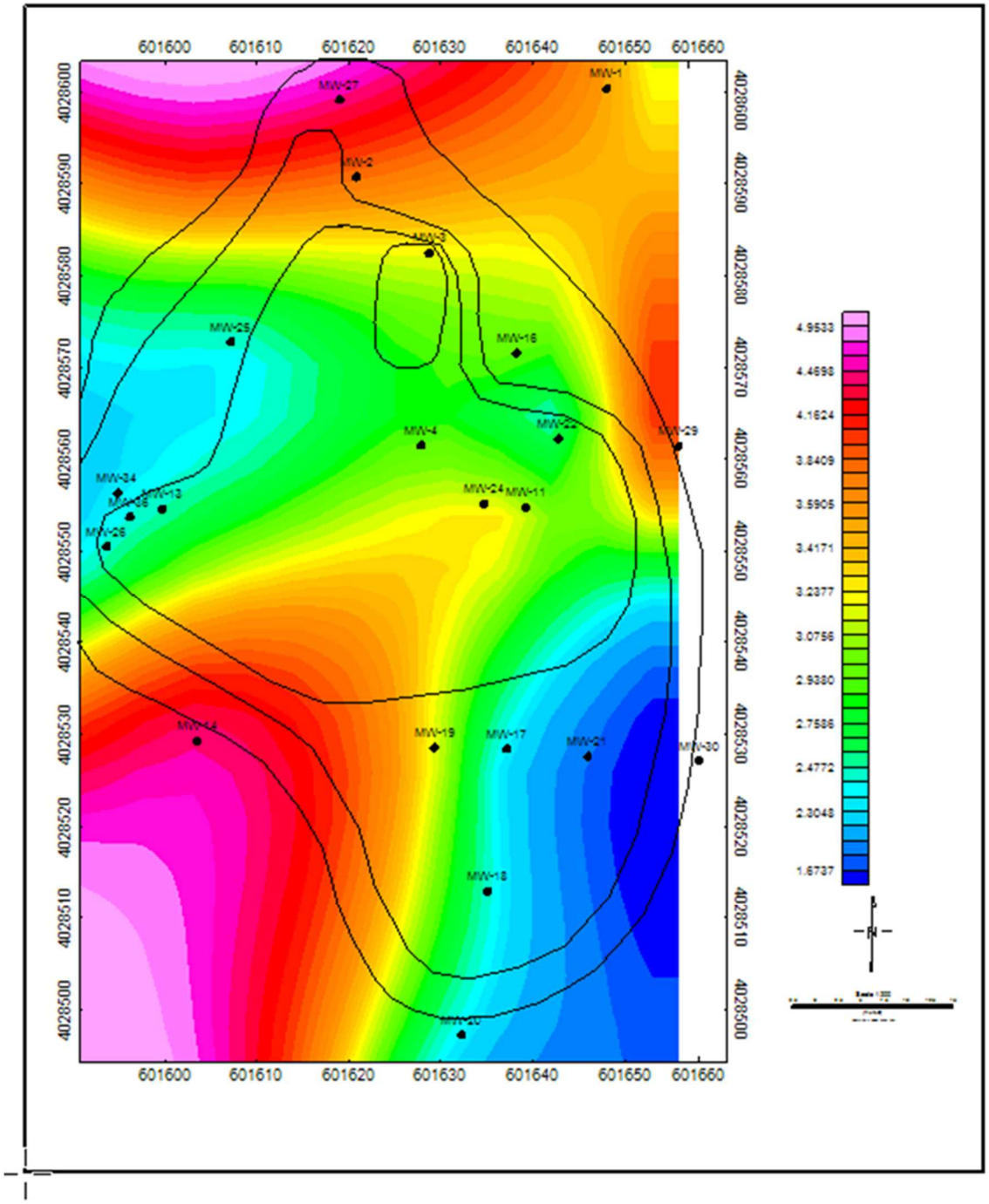

K (g/L), February 2012. Outline indicates plume boundary with 1ft contours.

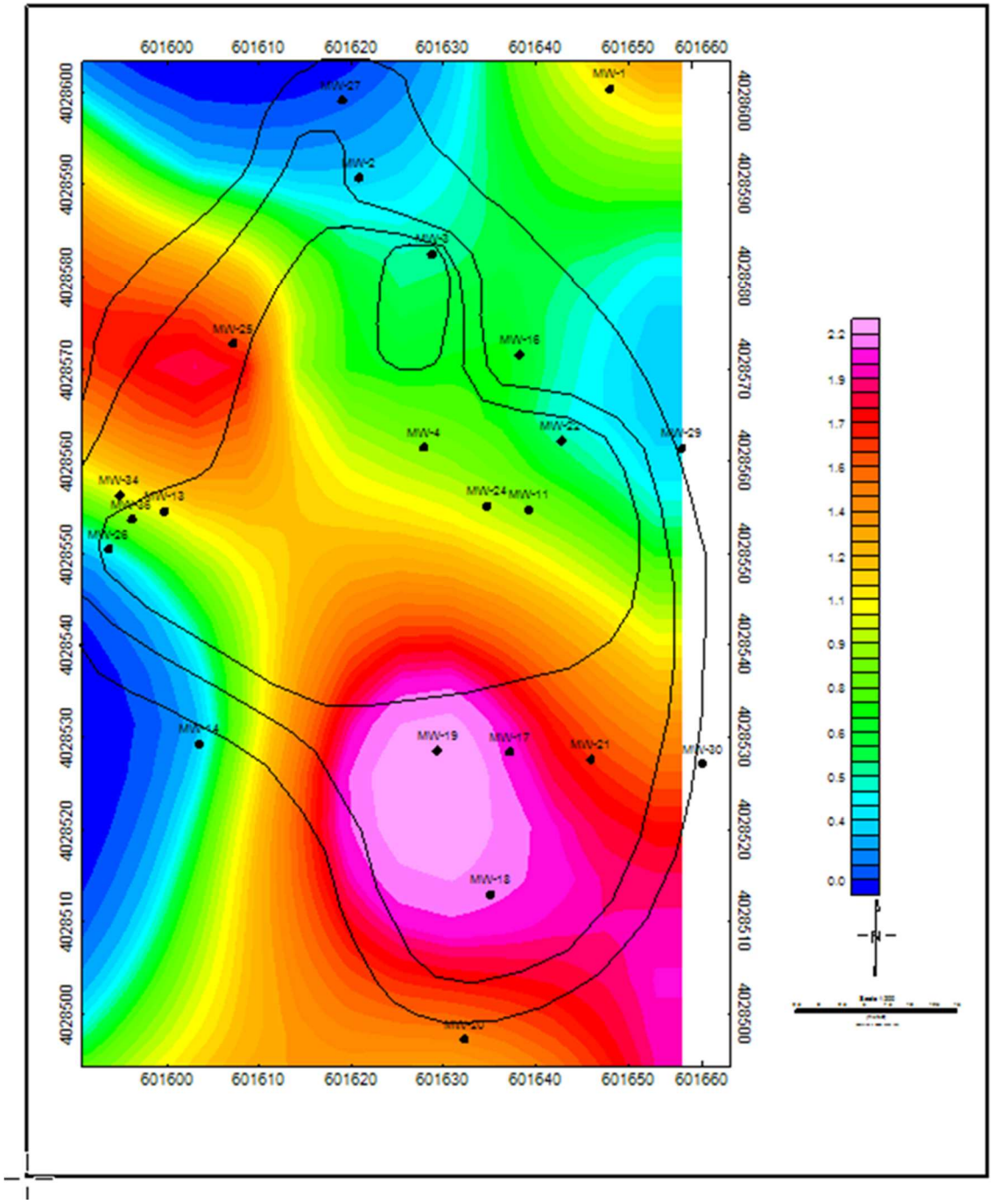

DO (mg/L), February 2012. Outline indicates plume boundary with 1ft contours.

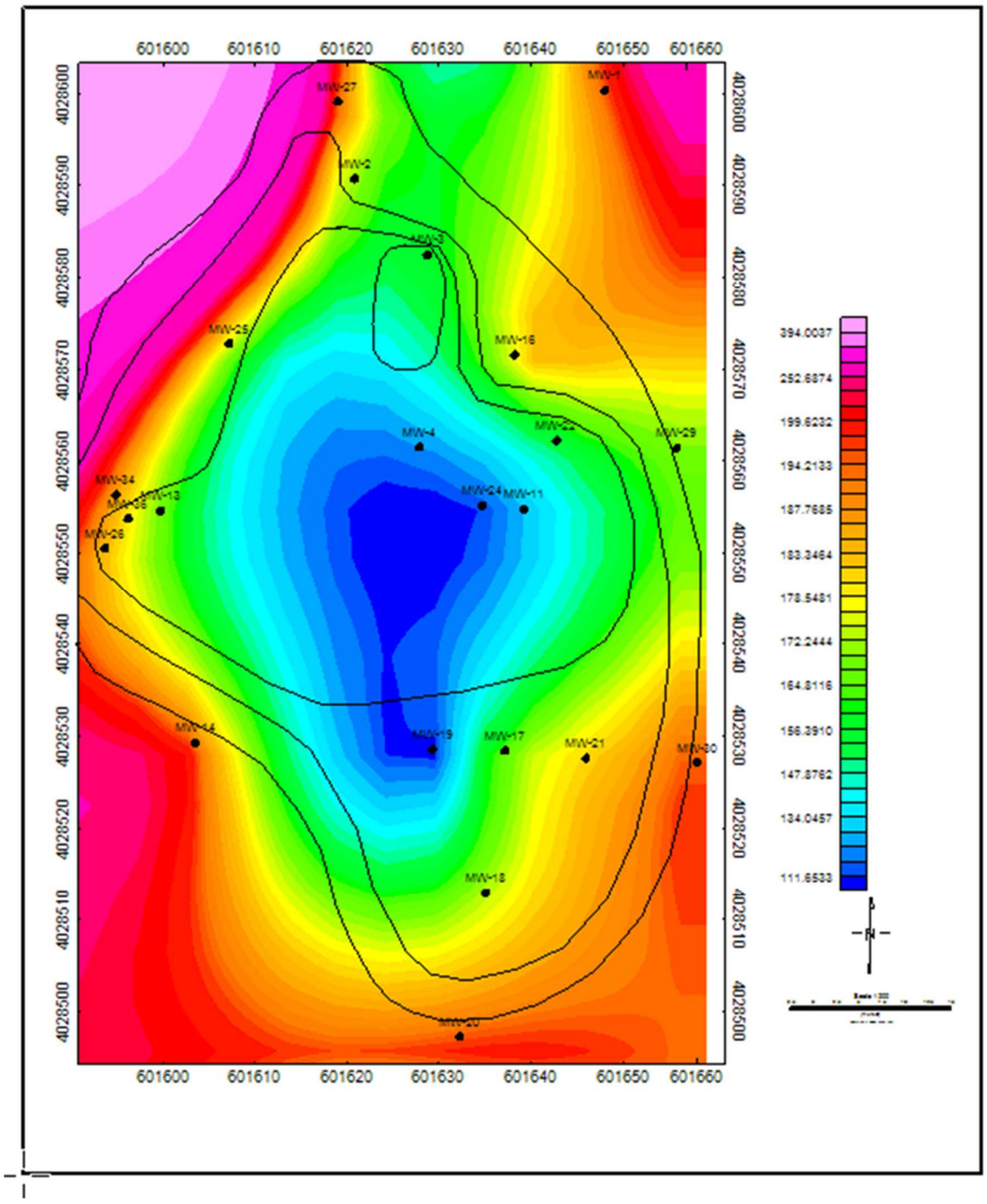

DIC (mg/L), February 2012. Outline indicates plume boundary with 1ft contours.

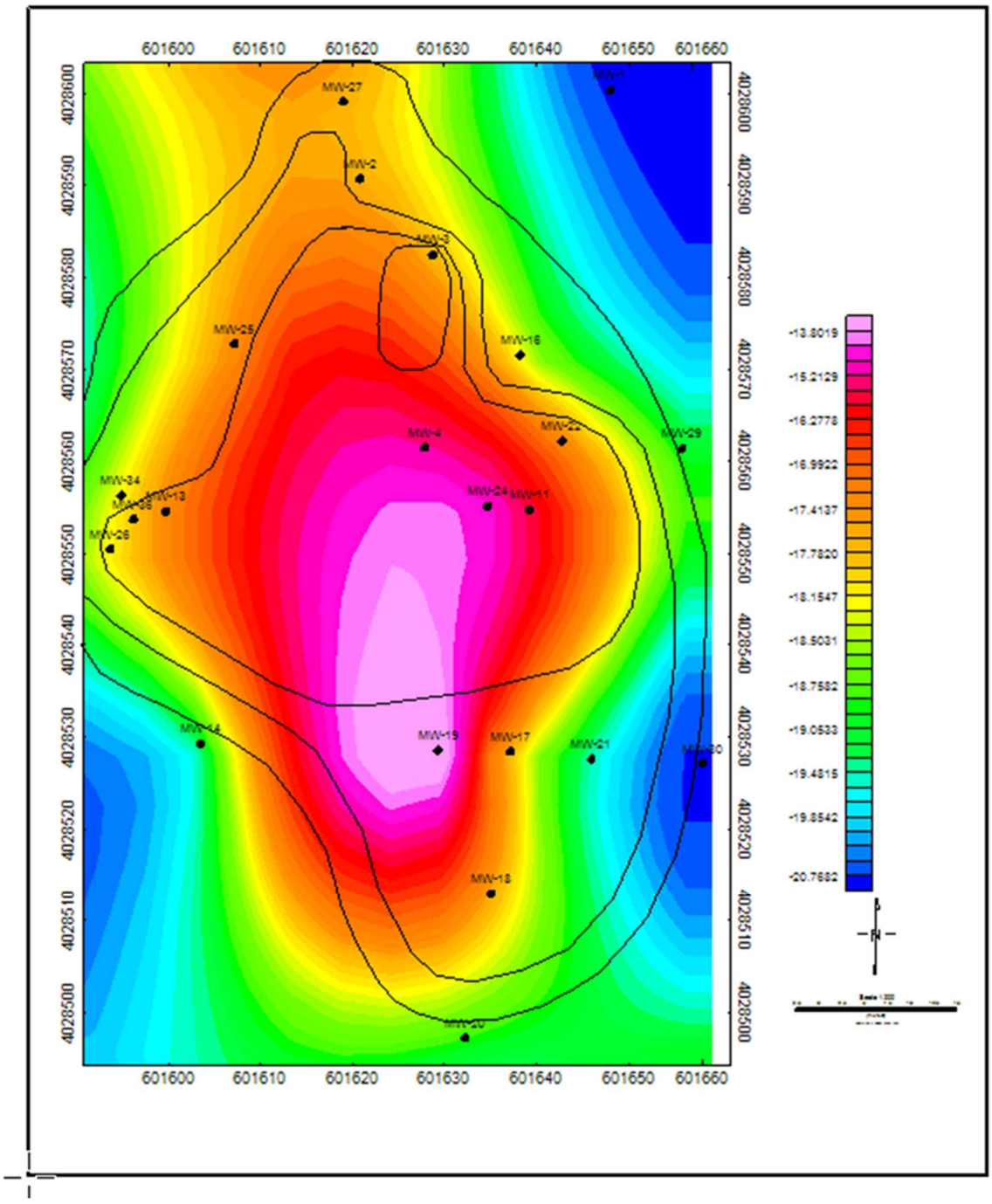

D13C/DIC (per mill), February 2012. Outline indicates plume boundary with 1ft contours.

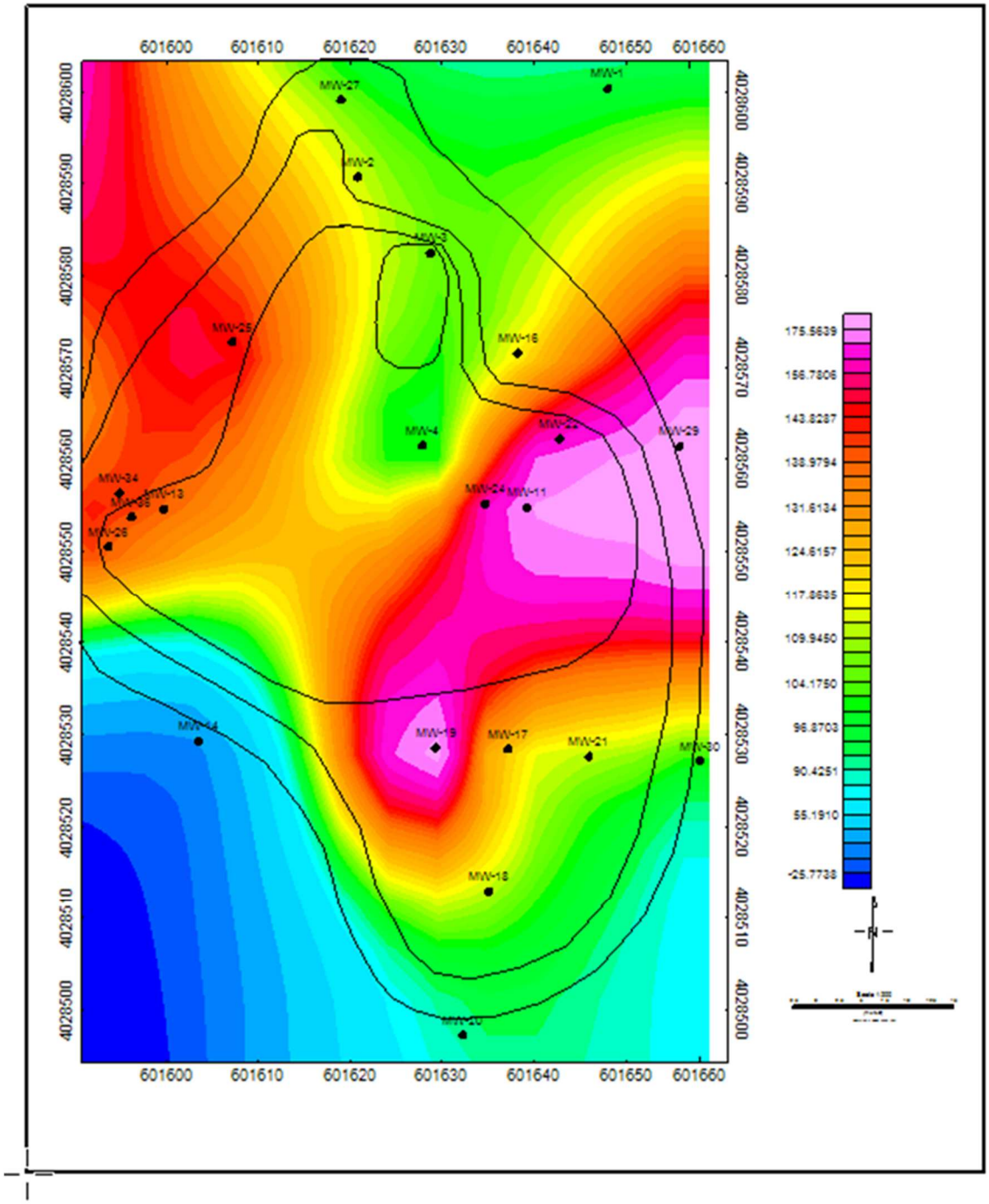

Cl (g/L), February 2012. Outline indicates plume boundary with 1ft contours.

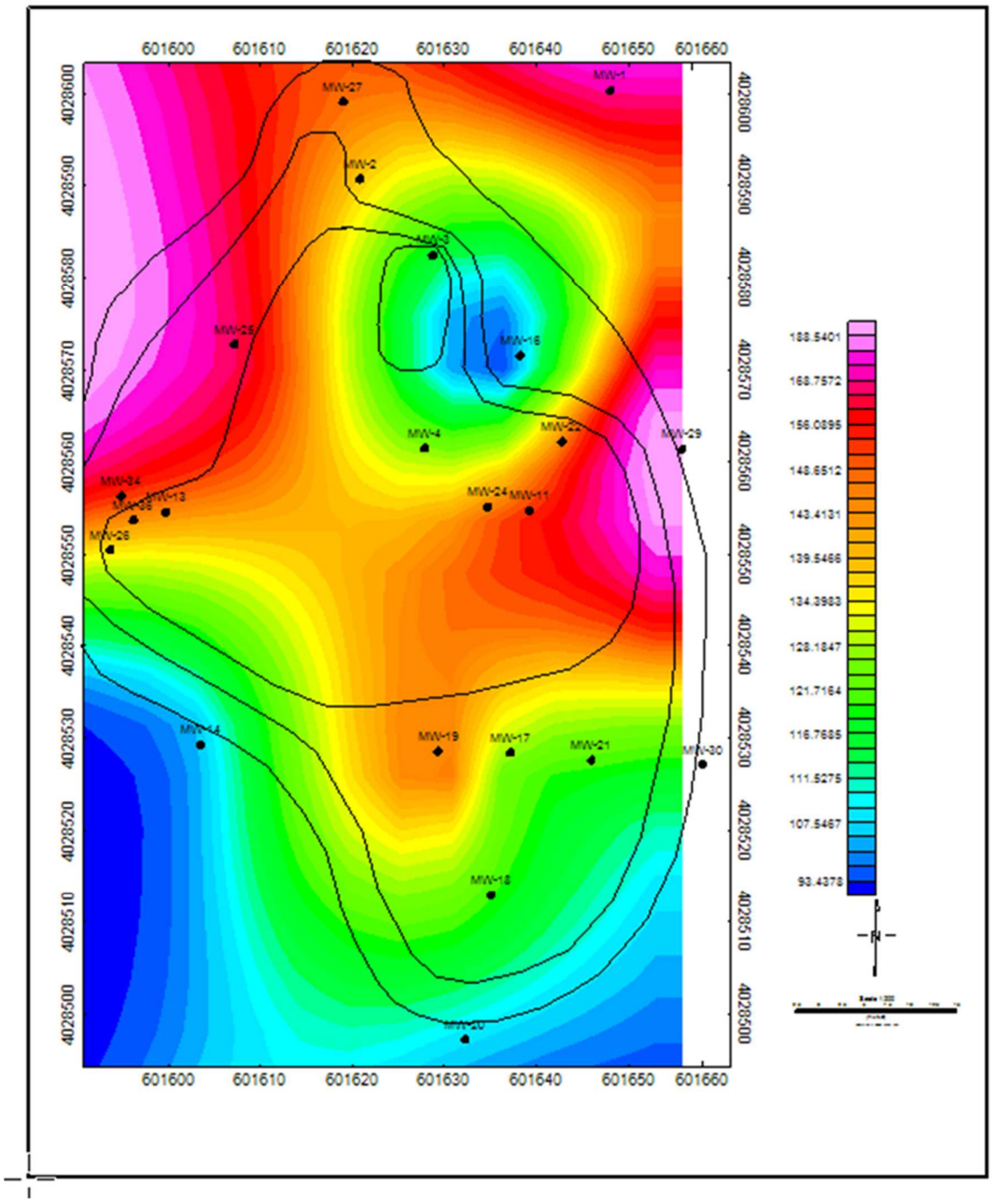

Ca (g/L), February, 2012. Outline indicates plume boundary with 1ft contours.

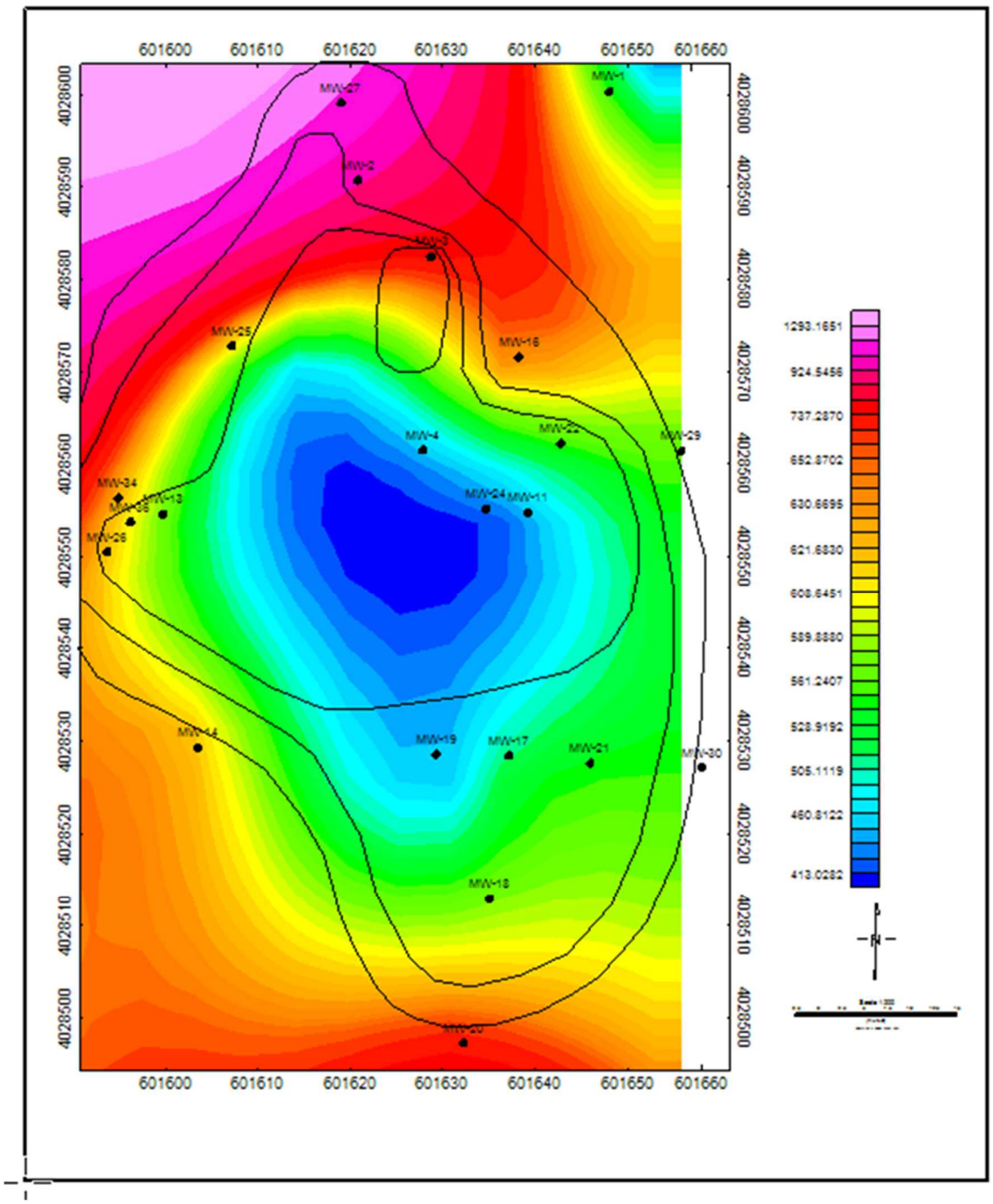

Alkalinity(mg/L), February 2012. Outline indicates plume boundary with 1ft contours.

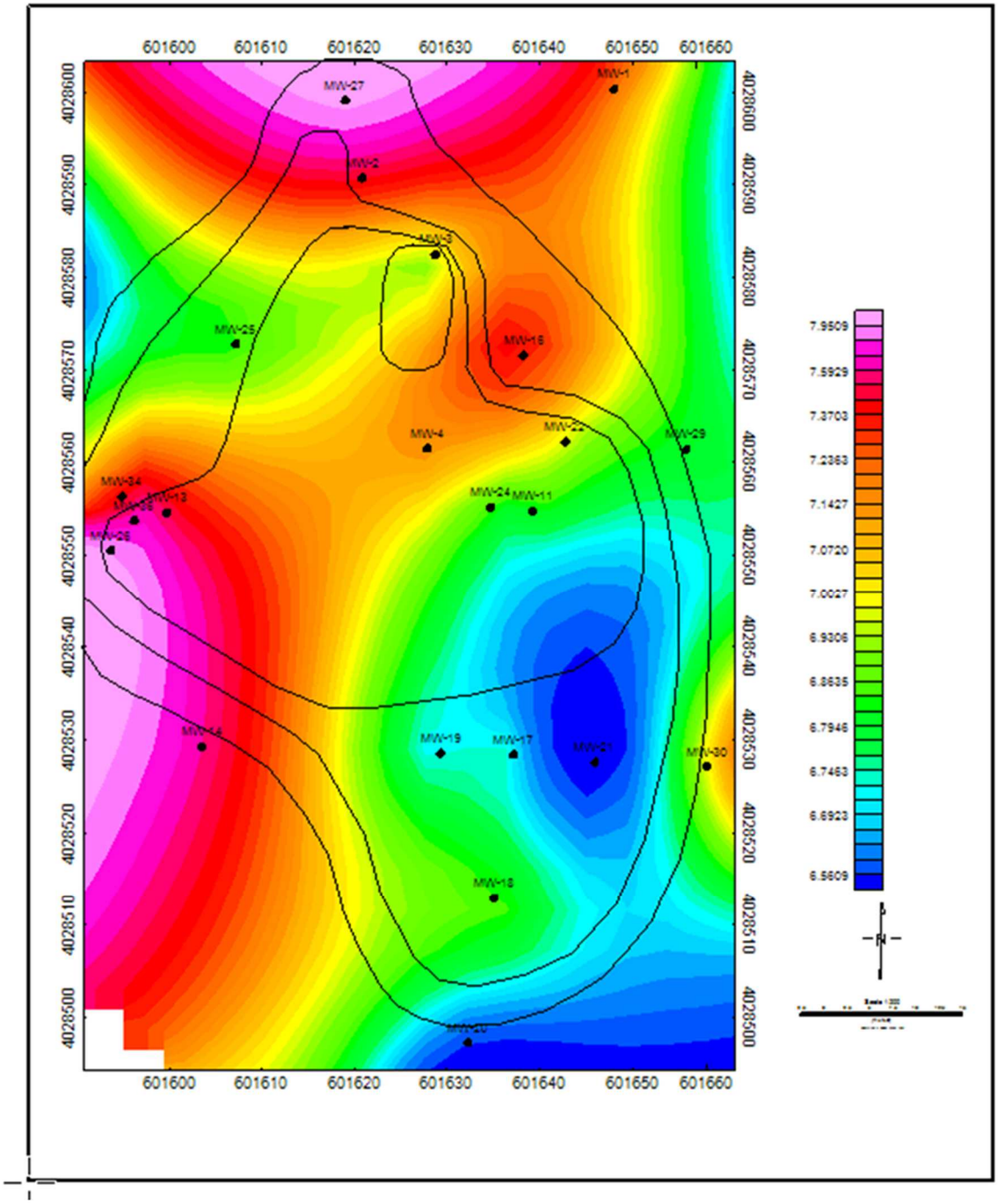

pH, February 2015. Outline indicates plume boundary with 1ft contours.

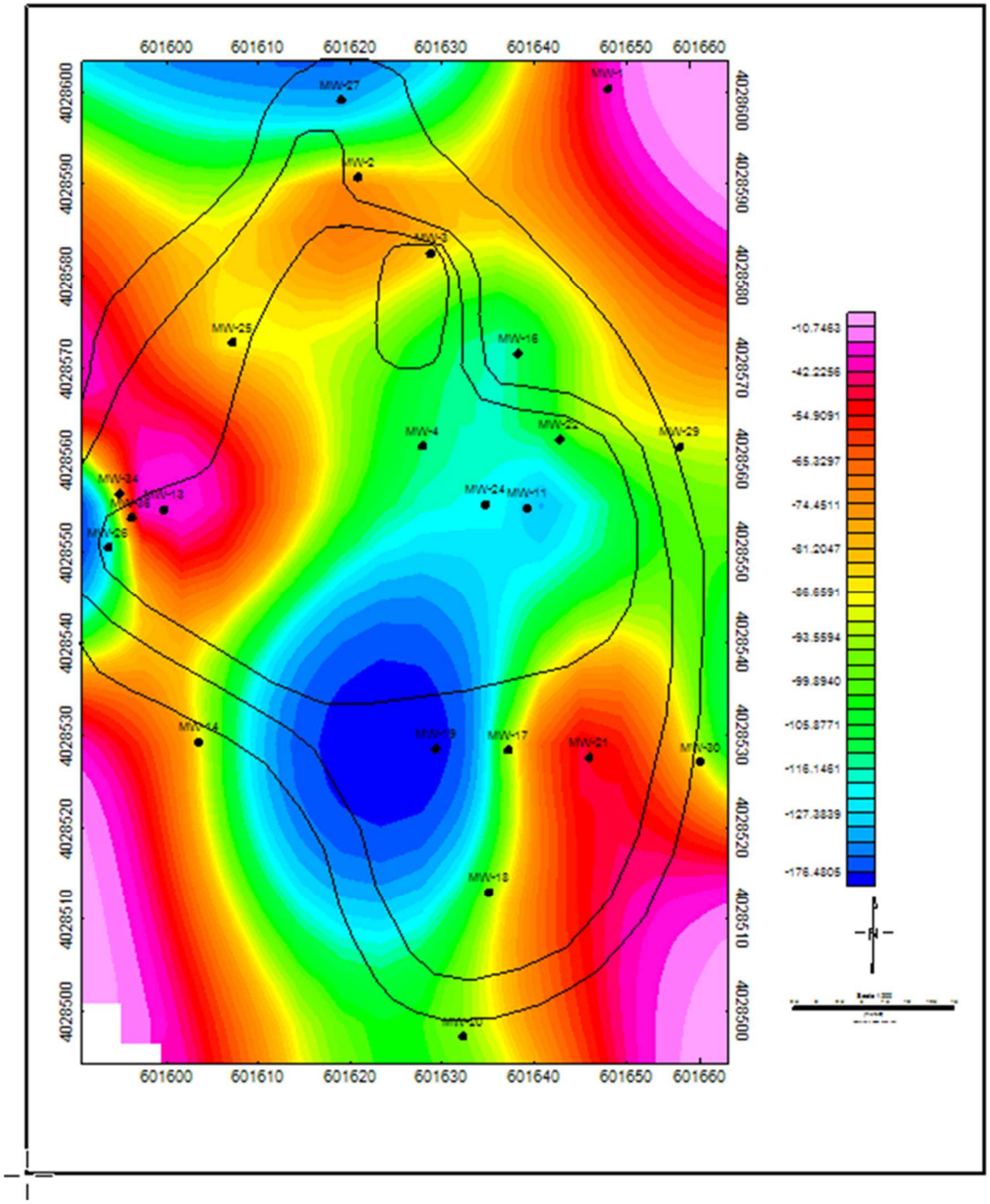

ORP (mV), February 2015. Outline indicates plume boundary with 1ft contours.

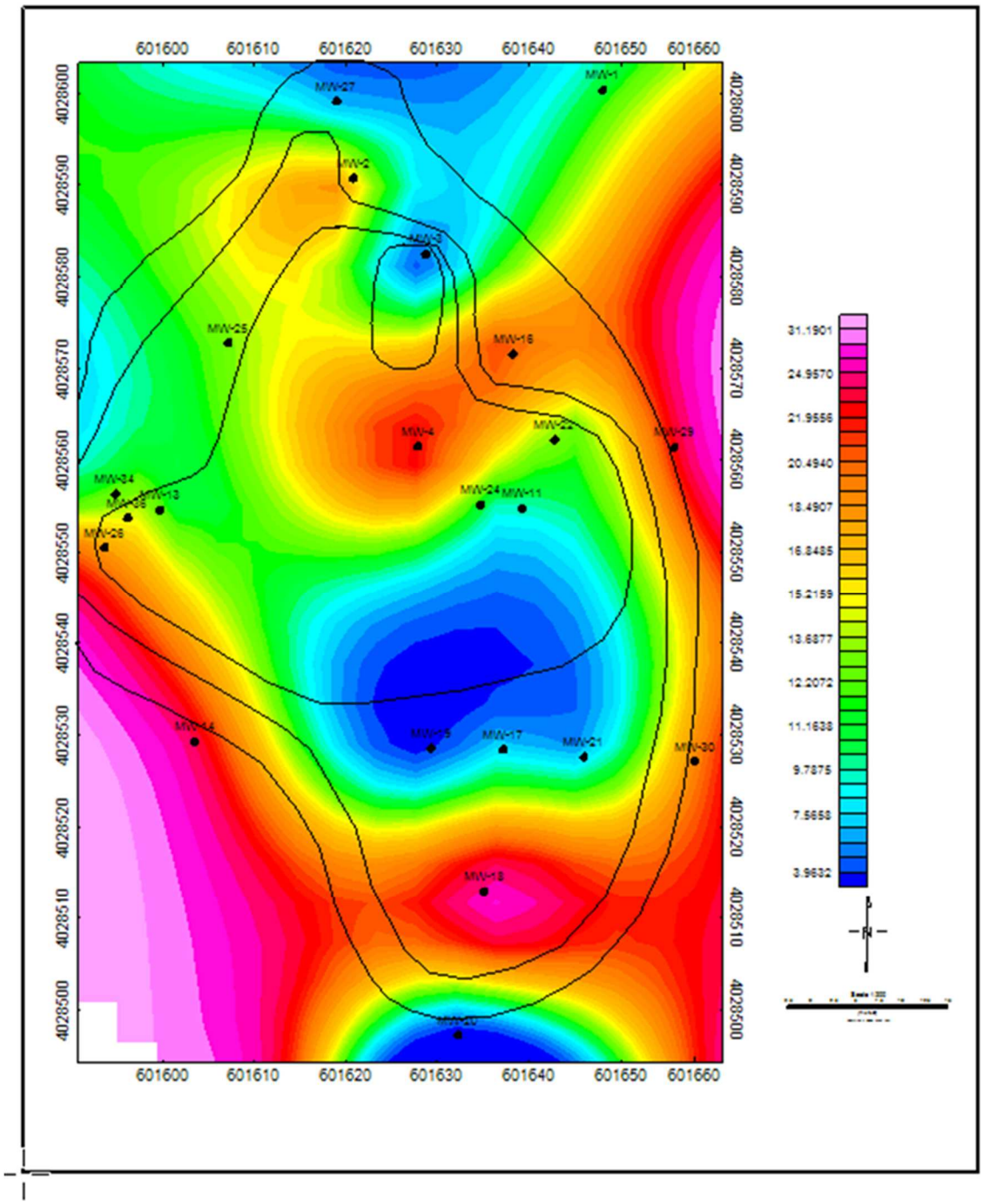

DO(mg/L), February 2015. Outline indicates plume boundary with 1ft contours.

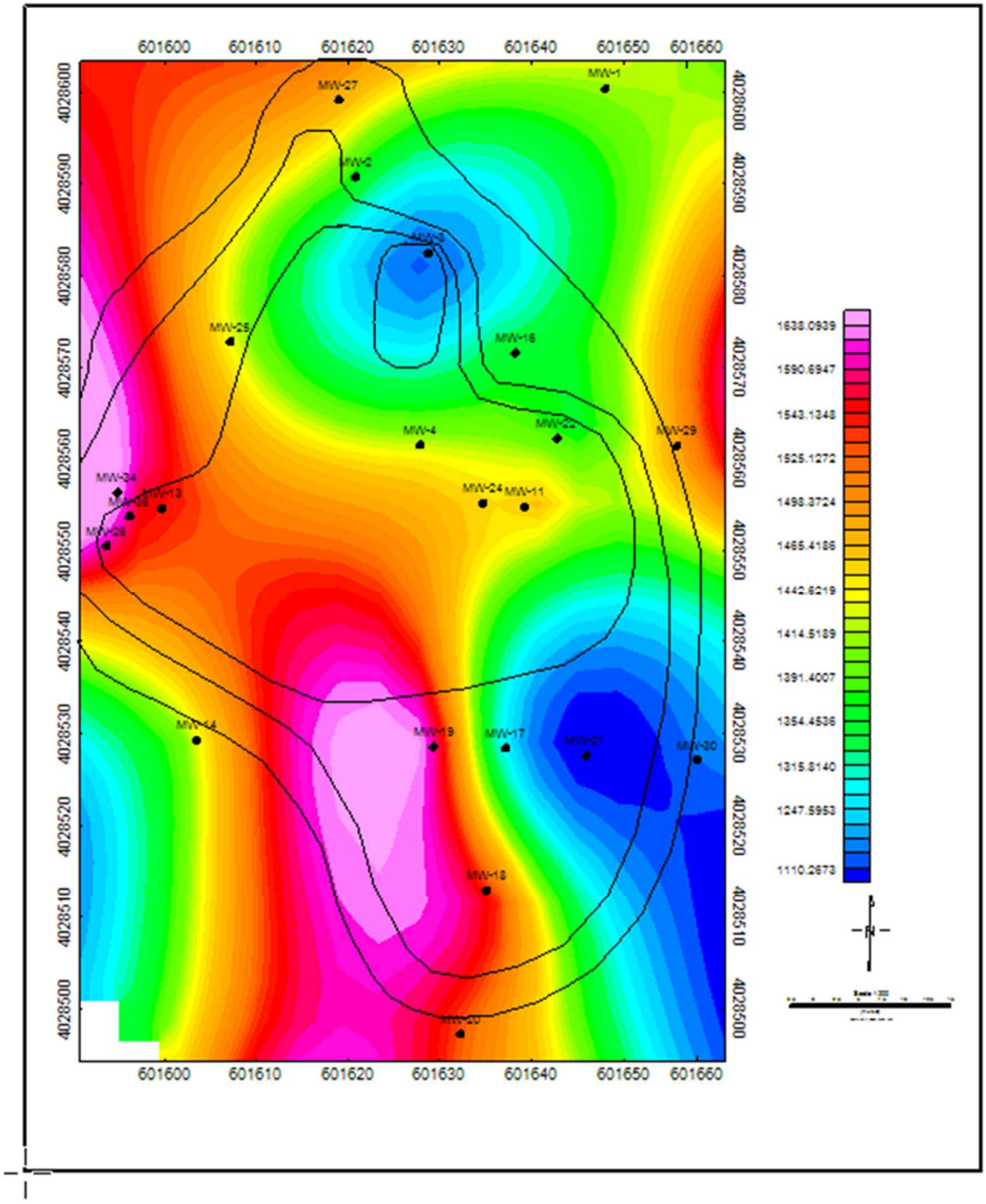

Conductivity (µS/m), February 2015. Outline indicates plume boundary with 1ft contours.

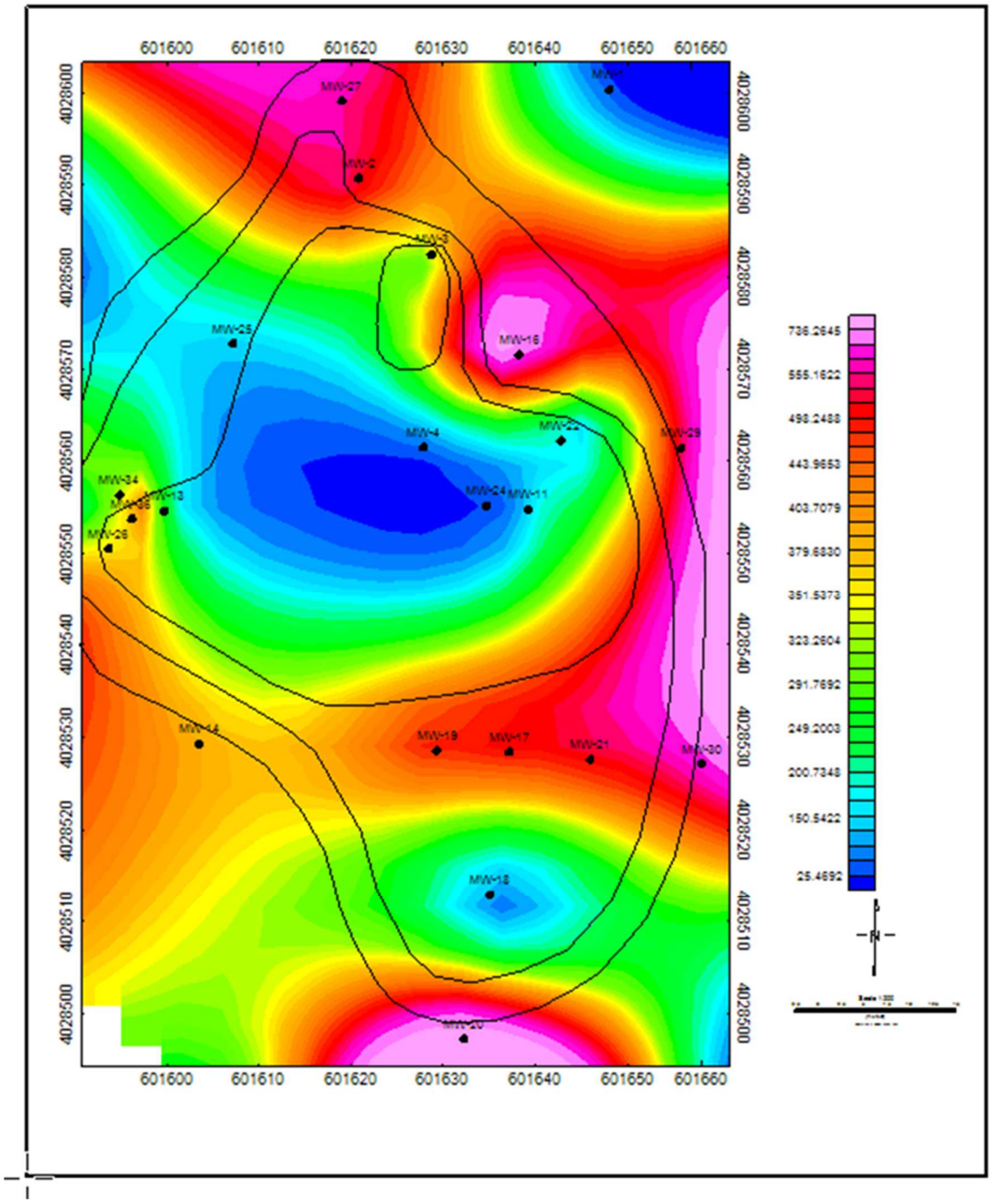

Alkalinity(mg/L), February 2015. Outline indicates plume boundary with 1ft contours.

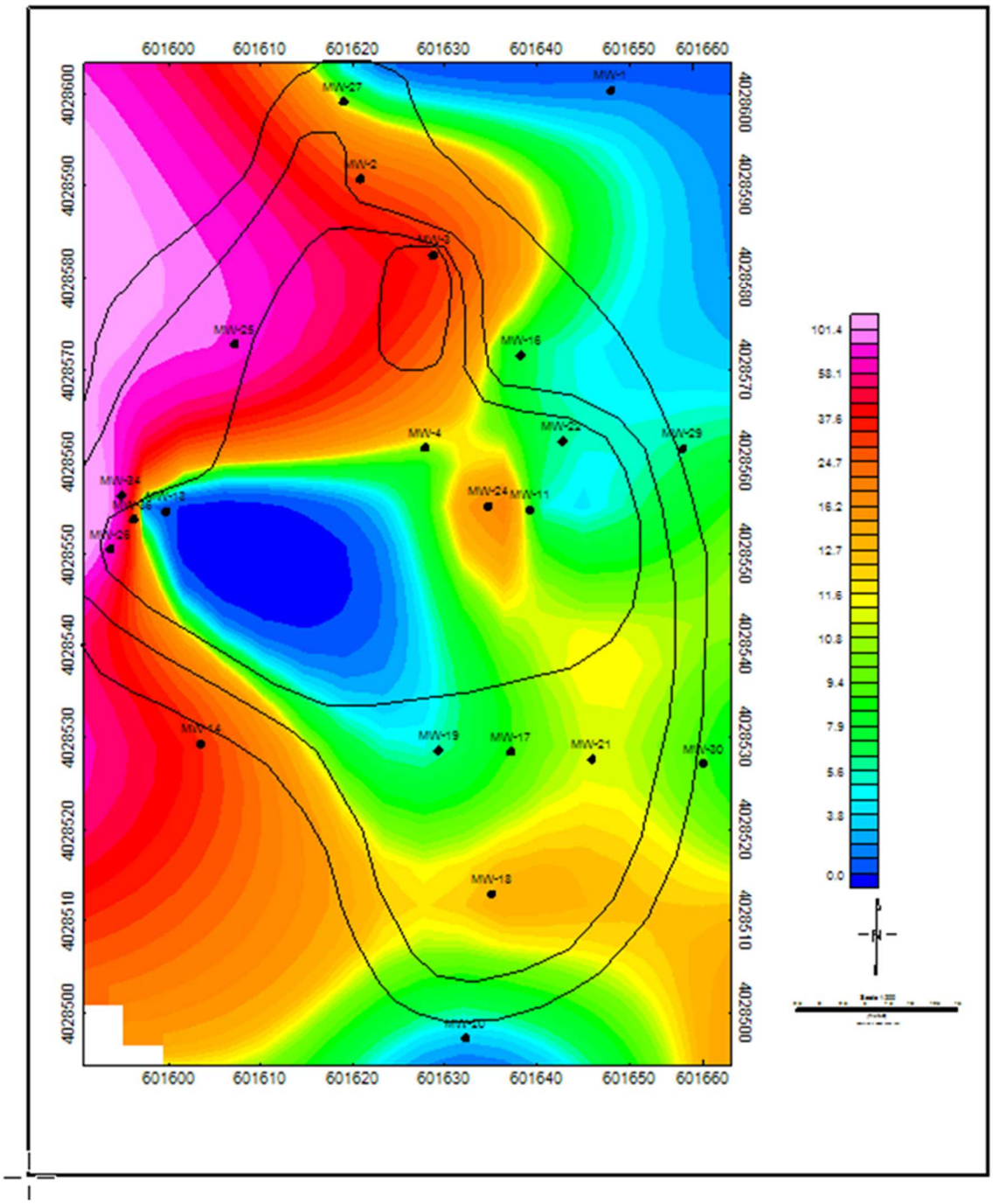

Fe total (ppm), February 2015. Outline indicates plume boundary with 1ft contours.

VITA

Daniel K. Morse

Candidate for the Degree of

Master of Science

Thesis: INVESTIGATING THE MAGNETIC SUCEPTIBILITY SIGNATURES OF A PARTIALLY REMEDIATED SITE CONTAMINATED BY GASOLINE IN ENID, OKLAHOMA.

Major Field: GEOLOGY

Biographical:

Education:

Completed the requirements for the Master of Science/Arts in Geology at Oklahoma State University, Stillwater, Oklahoma in May, 2015.

Completed the requirements for the Bachelor of Science/Arts in Geology at Oklahoma State University, Stillwater, Oklahoma in 2011.

Experience: Teaching Assistant for Oklahoma State University Fall 2010 and Spring 2011, Research Assistant Spring and Summer 2012,Internship with Newfield Exploration fall of 2012 and with Apache Corporation summer 2014.

Professional Memberships: American Association of Petroleum Geologist, Tulsa Geological Society